Dissertation zur Erlangung des naturwissenschaftlichen Doktorgrades (Dr. rer. nat.) an der Philosophischen Fakultät, Julius-Maximilians-Universität Würzburg

Bias correction of climate model output for Germany

vorgelegt von Chibuike Chiedozie Ibebuchi

aus Urualla

Würzburg 2022

Eingereicht am:

1. Gutachter:	Prof. Dr. Heiko Paeth
2. Gutachter:	Prof. Dr. Joaquim Pinto
der Dissertation	

Mentor*innen:	Prof. Dr. Heiko Paeth
	Prof. Dr. Barbara Sponholz
	Prof. Dr. Hartwig Frimmel

1. Prüfer:	Prof. Dr. Heiko Paeth
2. Prüfer:	Prof. Dr. Hartwig Frimmel
3. Prüferin:	Prof. Dr. Barbara Sponholz
der mündlichen Prüfung	

Tag der mündlichen Prüfung:	27. Februar 2023

Abstract

Regional climate models (RCMs) are tools used to project future climate change at a regional scale. Despite their high horizontal resolution, RCMs are characterized by systematic biases relative to observations, which can result in unrealistic interpretations of future climate change signals. On the other hand, bias correction (BC) is a popular statistical post-processing technique applied to improve the usability of output from climate models. Like every other statistical technique, BC has its strengths and weaknesses. Hence, within the regional context of Germany, and for temperature and precipitation, this study is dedicated to the assessment of the impact of different BC techniques on the RCM output. The focuses are on the impact of BC on the RCM's statistical characterization, and physical consistency defined as the spatiotemporal consistency between the bias-corrected variable and the simulated physical mechanisms governing the variable, as well as the correlations between the bias-corrected variable and other (simulated) climate variables. Five BC techniques were applied in adjusting the systematic biases in temperature and precipitation RCM outputs. The BC techniques are linear scaling, empirical quantile mapping, univariate quantile delta mapping, multivariate quantile delta mapping that considers inter-site dependencies, and multivariate quantile delta mapping that considers inter-variable dependencies (MBCn). The results show that each BC technique adds value in reducing the biases in the statistics of the RCM output, though the added value depends on several factors such as the temporal resolution of the data, choice of RCM, climate variable, region, and the metric used in evaluating the BC technique. Further, the raw RCMs reproduced portions of the observed modes of atmospheric circulation in Western Europe, and the observed temperature, and precipitation meteorological patterns in Germany. After the BC, generally, the spatiotemporal configurations of the simulated meteorological patterns as well as the governing large-scale mechanisms were reproduced.

However, at a more localized spatial scale for the individual meteorological patterns, the BC changed the simulated co-variability of some grids, especially for precipitation. Concerning the co-variability among the variables, a physically interpretable positive correlation was found between temperature and precipitation during boreal winter in both models and observations. For most grid boxes in the study domain and on average, the BC techniques that do not adjust inter-variable dependency did not notably change the simulated correlations between the climate variables. However, depending on the grid box, the (univariate) BC techniques tend to degrade the simulated temporal correlations between temperature and precipitation. Further, MBCn which adjusts biases in inter-variable dependency has the skill to improve the correlations between the simulated variables towards observations.

Zusammenfassung

Regionale Klimamodelle (RCMs) sind Werkzeuge, die verwendet werden, um den zukünftigen Klimawandel auf regionaler Ebene zu prognostizieren. Trotz ihrer hohen horizontalen Auflösung sind RCMs je nach Beobachtung durch systematische Verzerrungen gekennzeichnet, was zu unrealistischen Interpretationen zukünftiger Signale des Klimawandels führen kann. Andererseits ist die Bias-Korrektur (BC) eine beliebte statistische Nachbearbeitungstechnik, die angewendet wird, um die Nutzbarkeit der Ergebnisse von Klimamodellen zu verbessern. Wie jede andere statistische Technik hat BC seine Stärken und Schwächen. Daher widmet sich diese Studie im regionalen Kontext Deutschlands und für Temperatur und Niederschlag der Bewertung der Auswirkungen verschiedener BC-Techniken auf den das RCM-ErtragErgebnis. Die Schwerpunkte liegen auf der Auswirkung von BC auf die statistische Charakterisierung des RCM und auf der physikalischen Konsistenz. Letztere ist, definiert als die räumlich-zeitliche Konsistenz zwischen der systematisch korrigierten Variablen und den simulierten physikalischen Mechanismen, die diese Variable steuern, sowie auf den Korrelationen zwischen der systematisch korrigierten Variablen und anderen (simulierten) Klimavariablen. Fünf BC-Techniken wurden angewendet, um die systematischen Abweichungen in den Temperatur- und Niederschlags-RCM-Ausgaben Ergebnissen anzupassen. Die BC-Techniken sind lineare Skalierung, empirisches Quantil-Mapping, univariates Quantil-Delta-Mapping, sowie multivariates Quantil-Delta-Mapping, das Abhängigkeiten zwischen Standorten berücksichtigt, und multivariates Quantil-Delta-Mapping, das intervariable Abhängigkeiten (MBCn) berücksichtigt. Die Ergebnisse zeigen, dass jede BC-Technik einen Mehrwert bei der Reduzierung der Verzerrungen in den Statistiken der RCM-Ausgabe bringt, und dies, obwohl der Mehrwert von mehreren Faktoren abhängt, wie der zeitlichen Auflösung der Daten, der Wahl der RCM, der Klimavariable, der

Region und desr verwendeten Massstabsetrik zur Bewertung der BC-Technik verwendet. Darüber hinaus reproduzierten die rohen RCMs Teile der beobachteten Modi der atmosphärischen Zirkulation in Westeuropa und die beobachteten meteorologischen Temperatur- und Niederschlagsmuster in Deutschland. Nach der BC wurden im Allgemeinen die raumzeitlichen Konfigurationen der simulierten meteorologischen Muster sowie die maßgeblichen großräumigen Mechanismen reproduziert. Auf einer stärker lokalisierten räumlichen Skala änderte der BC jedoch für die einzelnen meteorologischen Muster die simulierte Kovariabilität einiger Gitter, insbesondere für Niederschlag. Bezüglich der Kovariabilität zwischen den Variablen wurde sowohl in Modellen als auch in Beobachtungen eine physikalisch interpretierbare positive Korrelation zwischen Temperatur und Niederschlag im borealen Winter gefunden. Für die meisten Gitterboxen Gitterfelder im Untersuchungsbereich und auch im Durchschnitt änderten die BC-Techniken, die die Abhängigkeit zwischen den Variablen nicht anpassen, die simulierten Korrelationen zwischen den Klimavariablen nicht merklich. Allerdings neigen die (univariaten) BC-Techniken je nach Gitterbox Gitterfeld dazu, die simulierten zeitlichen Korrelationen zwischen Temperatur und Niederschlag zu verschlechtern. Darüber hinaus hat MBCn, das Verzerrungen in der Abhängigkeit zwischen Variablen anpasst, die Fähigkeit, die Korrelationen zwischen den simulierten Variablen gegenüber den Beobachtungen zu verbessern.

Contents

List of Tables

List of Figures

List of acronyms

BC	Bias Correction
CMIP5	Coupled Model Intercomparison Project Phase 5
CNRM	Centre National de Recherches Météorologiques
CT	Circulation Type
EQM	Empirical Quantile Mapping
ERA5	European centre for medium-range weather forecasts Re-Analysis 5th Generation
EURO-CORDEX	European Coordinated Regional Climate Downscaling Experiment
GCM	General Circulation Model
KS	Kolmogorov Smirnov
LS	Linear Scaling
MAE	Mean Absolute Error
MBCn	Multivariate Quantile Delta Mapping (for inter-variable dependencies)
MPI-ESM-LR	Max-Plank Institute Earth System Model Lower Resolution
MQDM	Multivariate Quantile Delta Mapping (for inter-site dependencies)
NAO	North Atlantic Oscillation
PCA	Principal Component Analysis
PC	Principal Component
QDM	Quantile Delta Mapping
RCM	Regional Climate Model
RCP	Representative Concentration Pathway
S-MD	Spatial Mode
SD	Standard Deviation
SLP	Sea Level Pressure
T-MD	Temporal Mode

1. Introduction

1.1 Motivation and background

Climate change impact assessment is among the core interests of current climatological research. In this respect, climate models represent a key methodology since they are applicable for estimating projected changes in atmospheric and surface variables (Paeth et al. 2005, 2009) and for the analysis of processes (Abiodun et al. 2008; Druyan et al. 2008). Climate change signals are expected to occur at regional scales (Trenberth 2007) and hydrological hazards are often associated with local precipitation extremes (Olsson et al. 2012; Barros et al. 2014).

General circulation models (GCMs) are climate simulations that are applicable when studying the climate system on a global scale. GCMs have coarse horizontal resolutions (of about 100 to 500 km) that are typically not sufficient to study local and regional climates. Thus, the GCMs are downscaled to finer horizontal resolution either statistically or dynamically (Benestad 2016). The downscaled GCMs enable the understanding of local and regional climate responses to global change. In statistical downscaling, the empirical relationship between climate variables at smaller and larger scales (for example, precipitation and pressure) is used to downscale a climate variable (Wilby and Wigley 1997). In dynamical downscaling (that is the focus of this study) a GCM or reanalysis data provides the lateral boundary conditions for a regional climate model (RCM). The dynamical downscaling method incorporates both the physics and statistics of the climate system to obtain regional climate information. Thus, it is considered a better alternative to statistical downscaling (Rosen 2010). RCMs have higher horizontal resolutions (typically 50 km or less), and have relative advantages over GCMs, such as the provision of detailed features of a regional and local climate; provision of a more accurate projection of the future climate change; they

resolve vital parameterization schemes; have a better description of surface characteristics including topography, and also provide a better representation of the present-day climate. Thus, RCMs are often used when it comes to the assessment of local climate change signals and associated extremes (Paeth and Diederich 2011).

Despite the high horizontal resolution of RCMs and the relative advantages over GCMs, RCMs are still inapplicable for direct use in assessing the impact of climate change (Paeth et al. 2005; Fowler et al. 2007; Cannon et al. 2015) because they are often characterized by systematic biases against observations (Sillmann et al. 2013). The systematic biases can result from large-scale circulation biases from the GCM that provides the lateral boundary conditions (Ador et al. 2016; Maraun et al. 2017; Wu and Gao 2020), model parameterization, limited model complexity, and uncertain internal variability (Eden et al. 2012). For this reason, to improve the usability of RCMs for local impact modeling and navigate unrealistic interpretations of future climate change signals, bias correction (BC) is a commonly used statistical post-processing technique in reducing the systematic biases - to adjust model output towards observations (Dosio and Paruolo 2011; Hagemann et al. 2011; Paeth 2011; Cannon 2017; Maraun et al. 2019; Faghih et al. 2022). However, BC is not without critics as state-of-the-art BC techniques are mostly capable of improving some basic spatiotemporal statistical characteristics of individual output variables (Paeth 2011; Maraun 2016). There are still uncertainties on how BC impacts the spatiotemporal consistency of the bias-corrected variable and its co-variability with other climate variables (Maraun et al. 2010; Ehret et al. 2012). Thus, using temperature and precipitation that are most relevant for hydrological impact assessment (Bronstert et al. 2007) this study provides a process-based framework for evaluating the added value of distinct BC techniques by assessing their impact on the statistical characteristics and physical consistency of the bias-corrected variables.

1.2 Problem statement

Over different domains and time scales, several studies have reported that BC improves the usability of good-performing RCMs (Paeth and Diederich 2011; Berg et al. 2012; Widmann et al. 2019; Adakudlu et al. 2022). Nonetheless, the added value of BC techniques is mostly focused on the improved representation of the statistical distributions of RCM output (Vaittinada Ayar et al. 2021). Ehret et al. (2012) argued that BC techniques neglect feedback mechanisms and modify spatiotemporal field consistency. Ehret et al. (2012) further suggested that improved climate simulations can be expected by increasing the model resolution to the convection-permitting scale. Maraun and Widmann (2018) highlighted that state-of-the-art BC techniques do not improve circulation biases and the biases associated with the uncertainties in internal variability. Maraun (2016) noted that BC might alter the spatial dependency of the variables and so introduce inconsistencies with the driving model. Further, the stationarity assumption of the correction factor from the BC is questionable given the transient nature of the climate system (Bürger et al. 2011; Ehret et al. 2012; Cannon et al. 2015; Merkenschlager and Hertig 2020). After the BC, some aspects of the physical consistency in the corrected fields may be altered, which can affect the agreement between model dynamics and the correlation between different climatic variables (Bürger et al. 2011). Unlike the usual focus on how the BC adjusts the statistics of the RCM towards observations, the aforementioned shortcomings, that is, possible impact on the simulated meteorological patterns and coherency among climate variables, require to be considered equally as further evaluation metrics after the implementation of the BC approach. This will enhance the understanding of how the BC impacts the simulated underlying physics of the RCM.

1.3 Research objectives

Considering that BC does not improve circulation biases, before the application of the BC to the temperature and precipitation RCM outputs, this study aims to evaluate the representation of the reference large-scale atmospheric circulation patterns in the RCMs and to diagnose the misrepresentation of processes. Further, a process-based approach is applied to assess the added value of distinct BC techniques in reducing the systematic biases in the simulated precipitation and temperature output in Germany, as well as the impact of the BC techniques on the physical consistency of the RCM outputs. The impact of the BC on the physical consistency of the RCM is evaluated in two aspects, first, as the consistency between the bias-corrected climate variable and the simulated meteorological modes of variability that are associated with the variable at different spatial and time scales; second, as the consistency between temperature and precipitation at different spatial and time scales. Thus, in the regional context of Germany, given the plausible shortcomings of BC, the objectives of this study are:

(1) To evaluate the representation of large-scale atmospheric circulation modes in Western Europe, in the RCMs, using reanalysis data as the reference.

(2) To compare the performance of distinct BC techniques in improving the simulated statistics of temperature and precipitation towards observation.

(3) To evaluate the impact of the BC techniques on the simulated meteorological patterns of the climate variables and the governing mechanisms.

(4) To assess the impact of the BC techniques on the seasonal correlations between temperature and precipitation.

1.4 Structure of the thesis

This study is structured into ten chapters. In the first chapter, the motivation, background, and objectives of the research are presented. The second chapter describes the study region, its climate, and the patterns of atmospheric circulations in Western Europe that modulate the climate variability of the study region. The third chapter describes the data and methodology on which this study is based on. The fourth chapter presents the results on the capability of RCMs to capture the large-scale modes of atmospheric circulations in Western Europe. The fifth to eighth chapter presents the major results on the impact of different BC techniques on the statistics and physical consistency of RCMs. Discussion and recommendations are presented in the ninth chapter. Conclusions are drawn in the last chapter.

2. Study region

Germany is a country located in Central Europe. Figure 2.1 shows the geographical location of Germany. It borders the Baltic Sea to the northeast and the North Sea to the northwest. Starting from the north and moving clockwise, the countries sharing boarders with Germany are Denmark, Poland, Czech Republic, Austria, Switzerland, France, Luxembourg, Belgium, Netherlands

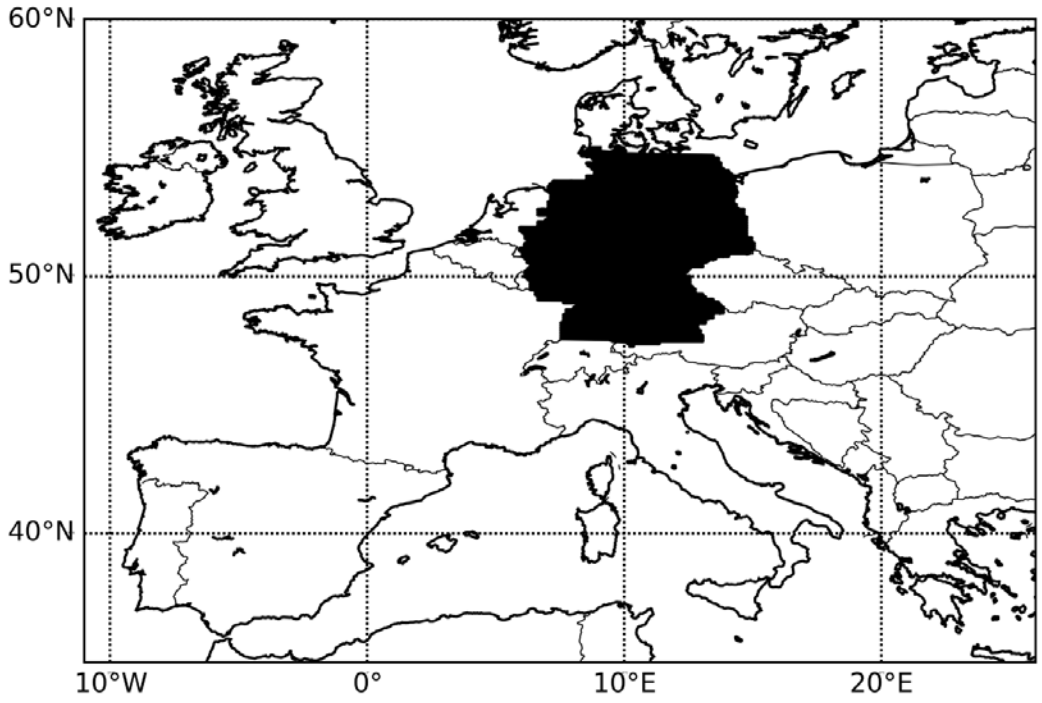

Figure 2.1: Geographical location of Germany in Europe. The black-shaded region shows the position of Germany in Central Europe

2.1 Climatology of precipitation and temperature in Germany

Germany is characterized by four seasons in a year. The seasons are boreal winter (typically from December to February, henceforth referred to as DJF); boreal spring (typically from March to May, henceforth referred to as MAM); boreal summer (typically from June to August, henceforth referred to as JJA), and boreal autumn (typically from September to

November, henceforth referred to as SON). Figure 2.2 and Figure 2.3 show the seasonal climatology and the annual cycle of precipitation and temperature, respectively, in Germany.

a)

b)

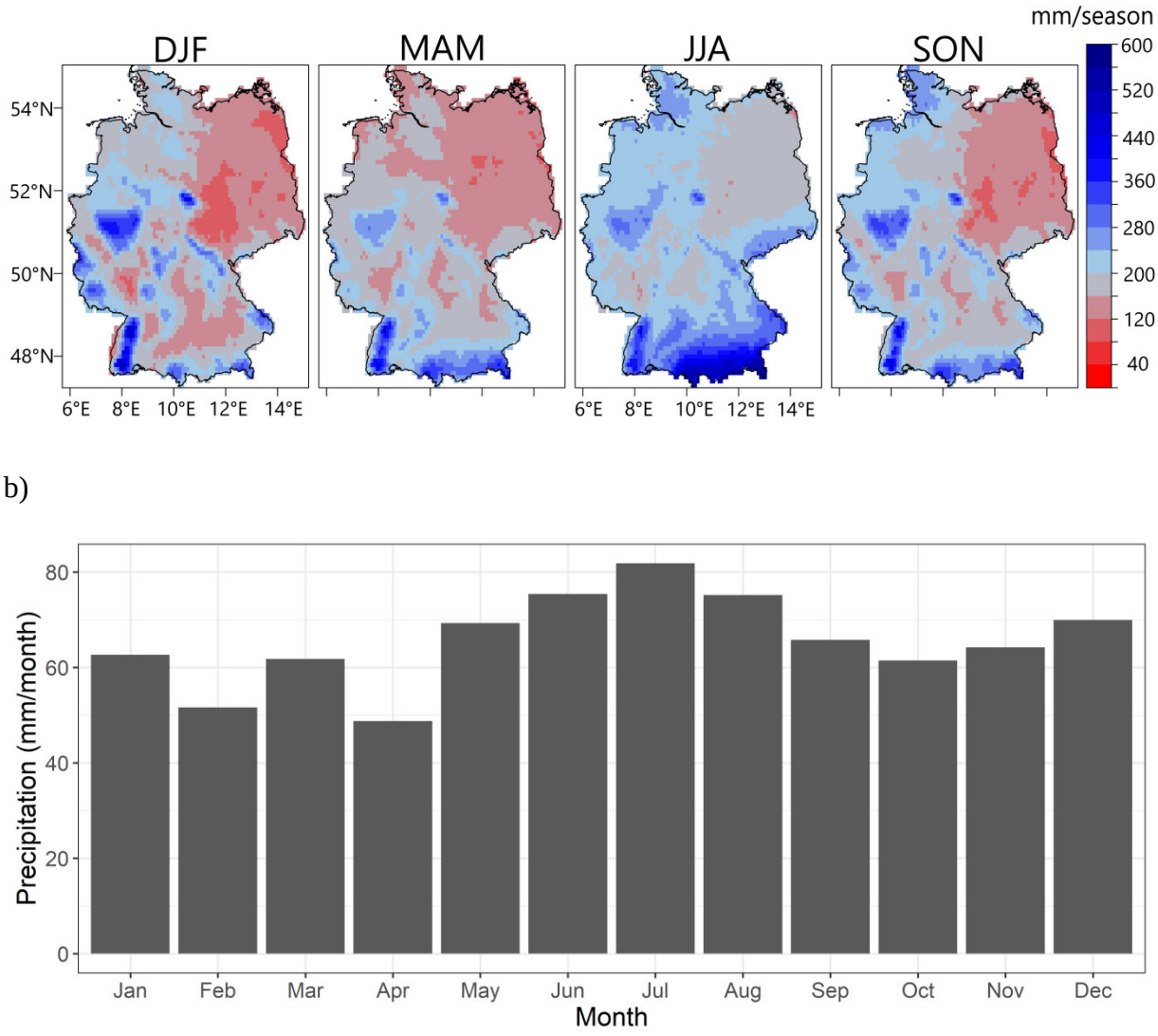

Figure 2.2: Seasonal climatology of precipitation (a), and the annual cycle of precipitation averaged over Germany (b). The climatology is calculated from the E-OBS data from 1981 to 2010

Based on Figure 2.2b, averaged over Germany, MJJA is the wettest period, and the months of February, March, April, and October are relatively drier. Also, some spatial differences become apparent: due to the proximity to the North Sea coast, the northwestern parts of Germany have an oceanic climate with more precipitation. The eastern parts of Germany are

relatively drier with a more continental climate because they are downstream with respect to the dominating (westerly) wind directions. The central parts can be classified as transition regions exhibiting both oceanic and continental climates with clearly visible windward and lee effects due to the low mountain ranges. The Alps, that is, the southernmost mountainous region, receive the highest precipitation, especially during the summer season.

a)

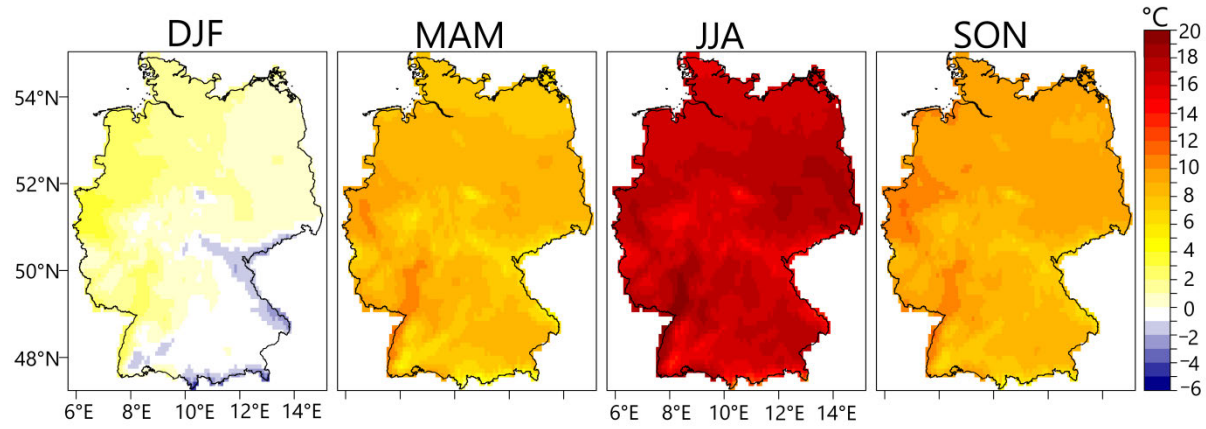

b)

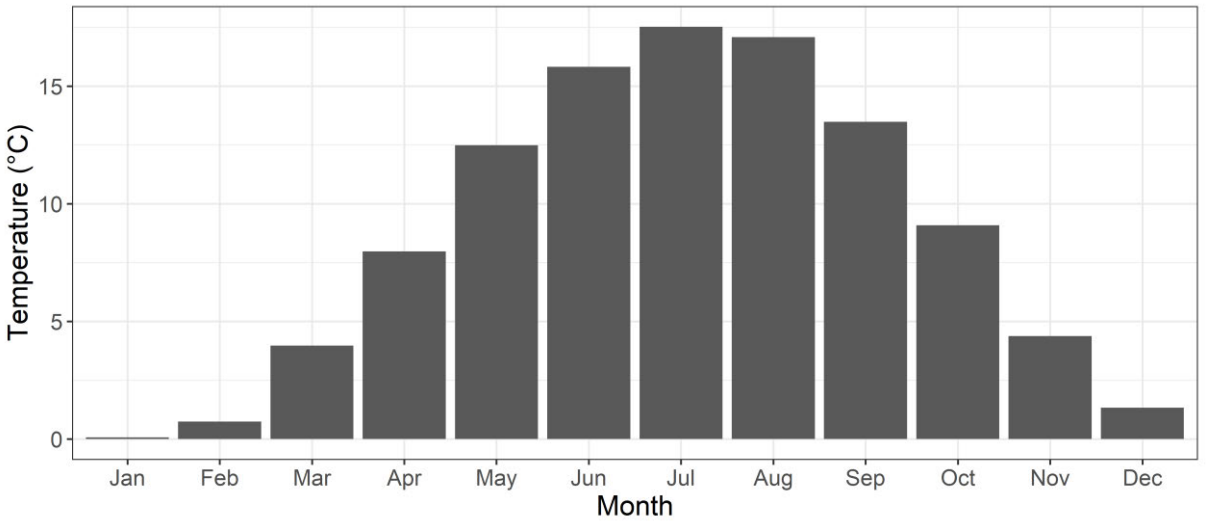

Figure 2.3: Seasonal climatology of temperature (a), and the annual cycle of temperature averaged over Germany (b). The climatology is calculated from the E-OBS data from 1981 to 2010

For temperature, JJA is relatively the hottest season and DJF is relatively the coldest season (Figure 2.3a). The transition seasons, MAM and SON, have relatively warmer (colder)

temperatures in months that are adjacent to the summer (winter) season. Figure 2.3b indicates that in Germany, there are spatial differences in temperature. For example, during DJF, the northern parts (specifically the northwestern parts) are warmer compared to the southern parts. Figure A1 indicates that the temporal variability of temperature, averaged over Germany is fairly related to temporal variations in solar radiation, especially during the summer and winter seasons.

2.2 Large-scale circulation patterns modulating the climate of Germany

Teleconnections such as the North Atlantic Oscillation (NAO) and the Arctic Oscillation that link variations in climate variables over long distances through the transport of energy and wave propagations in the ocean and atmosphere, significantly impact the climate of (Western) Europe. Hurrell (1995) noted that the NAO strongly impacts the mean winter climate of vast regions in the Northern Hemisphere. According to Ricardo et al. (2002), NAO influences precipitation rate and precipitable water in Europe. Scaife et al. (2008) highlighted that 90th percentile precipitation events over Europe are found from changes in the NAO. During the positive phase of the NAO, a strong subtropical anticyclone is situated over the central North Atlantic while a strong low-pressure system is centered over Iceland. Thus, the positive phase of the NAO is associated with the northward shift of the mid-latitude cyclone and enhanced westerly wind over the North Atlantic. During boreal winter, positive NAO corresponds with wet conditions in Northern Europe. During the negative phase of the NAO, dry condition is expected since westerly winds are weakened coupled with the intrusion of Arctic air into Europe. The NAO also influences storm tracks over the Atlantic region (Osborn et al. 1999). According to Mehta et al. (2000), North Atlantic sea surface temperature anomalies can modify the NAO. Towards the twenty-first century, Scaife et al. (2008) reported that changes in the frequency of NAO events might be linked to anthropogenic forcing. These teleconnections are the building blocks of atmospheric circulation patterns (Huth et al. 2008).

Further, anomalies of the NAO are also related to temperature variations in Germany. From Figure 2.4, anomalies of the NAO relate to the variations of the dominant mode of atmospheric circulation in Western Europe and temperature averaged over Germany, during the DJF season. This implies that during DJF, when the NAO oscillates to its negative phase, below-average temperature can be expected over large parts of Germany; on the other hand, when the NAO oscillates to its positive phase, during DJF, above-average temperature can be expected in large parts of Germany. Figure 2.5 shows that the fingerprint of the positive NAO in atmospheric circulations over Western Europe is characterized by westerly moisture fluxes and cyclonic activity over parts of Western Europe; this pattern brings wet and warmer conditions to Germany, during the DJF season (Figure 2.6). Conversely, the fingerprint of the negative NAO in atmospheric circulations over Western Europe is characterized by dry northerly fluxes and anti-cyclonic circulation over the mid-latitudes; this pattern brings dry and colder conditions to Germany, during the DJF season (Figure 2.6).

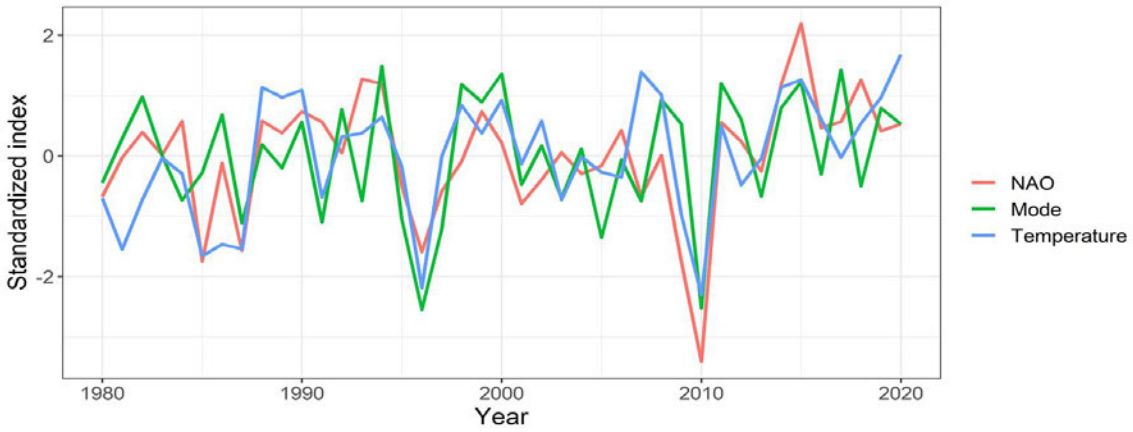

Figure 2.4: Time series of the NAO index, the temperature averaged over Germany and the amplitude of the dominant mode of atmospheric circulation in Western Europe. The classified circulation mode is the PC loadings of the dominant circulation mode over Western Europe classified in Ibebuchi (2022a). Temperature is obtained from E-OBS. The time series is for the boreal winter (DJF) season.

Figure 2.4 to Figure 2.6 show that at specific periods, large-scale climate drivers such as the NAO modulate synoptic-scale circulations (Ibebuchi and Paeth 2021), that is, circulation features typically at the spatial scale of 1000 to 5000 km. Also, the spatiotemporal variations of temperature and precipitation in Germany can be related to variations in the synoptic

circulations that modulate atmospheric transport and large-scale convection over Western Europe (Ibebuchi 2022a). A cursory investigation of Figure 2.6, shows that large-scale patterns associated with the NAO bring heterogeneous amounts of rainfall as well as different temperature values in Germany. The inference is that other localized factors such as orography, as well as the proximity of the landmasses to the adjacent oceans, and so forth, also play role in modifying the influence of synoptic circulations over different regions (Rebetez 1996).

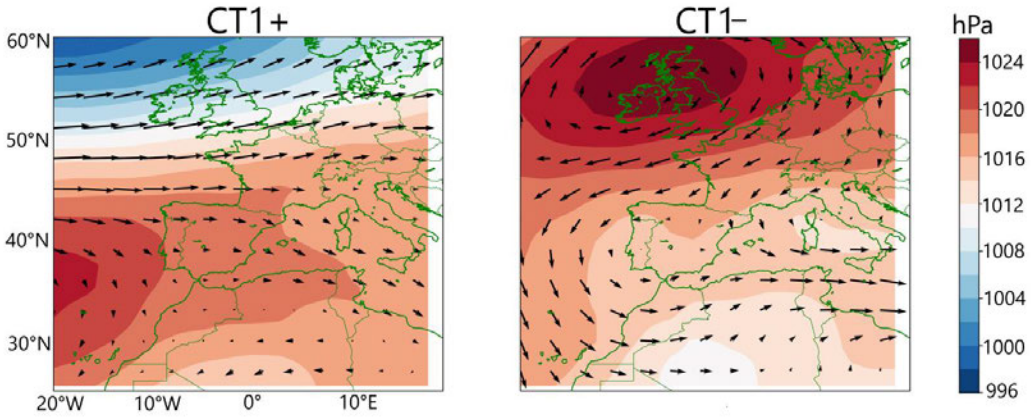

Figure 2.5: Asymmetry of the dominant circulations mode in Western Europe related to the North Atlantic Oscillation. CT1+ implies circulation type related to the positive NAO and CT1− implies circulation type related to the negative NAO. Vector is 850 hPa moisture flux composites and color is sea level pressure.

Indeed, climate extremes in Germany such as floods, drought and extreme temperatures can be related to variations in synoptic patterns in Western Europe and beyond. During boreal summer, omega blocking can be associated with positive temperature anomalies in Western Europe (Henley et al. 2019). Concerning controls of moisture transport, the major sources of moisture in Europe are the North Atlantic Ocean and the Mediterranean Sea (Craig et al. 2016; Volosciuk et al. 2016; Skliris et al. 2018; Vazquez et al. 2020). Though during boreal summer, the North Atlantic Ocean becomes the major source of moisture for Western Europe (Vazquez et al. 2020). Variations in the North Atlantic anticyclone (that is, the semi-

permanent high pressure over the North Atlantic in Figure 2.5), also impact moisture transport to Western Europe and significantly impact the weather and climate of Western Europe (Davis et al. 1997)

a)

b)

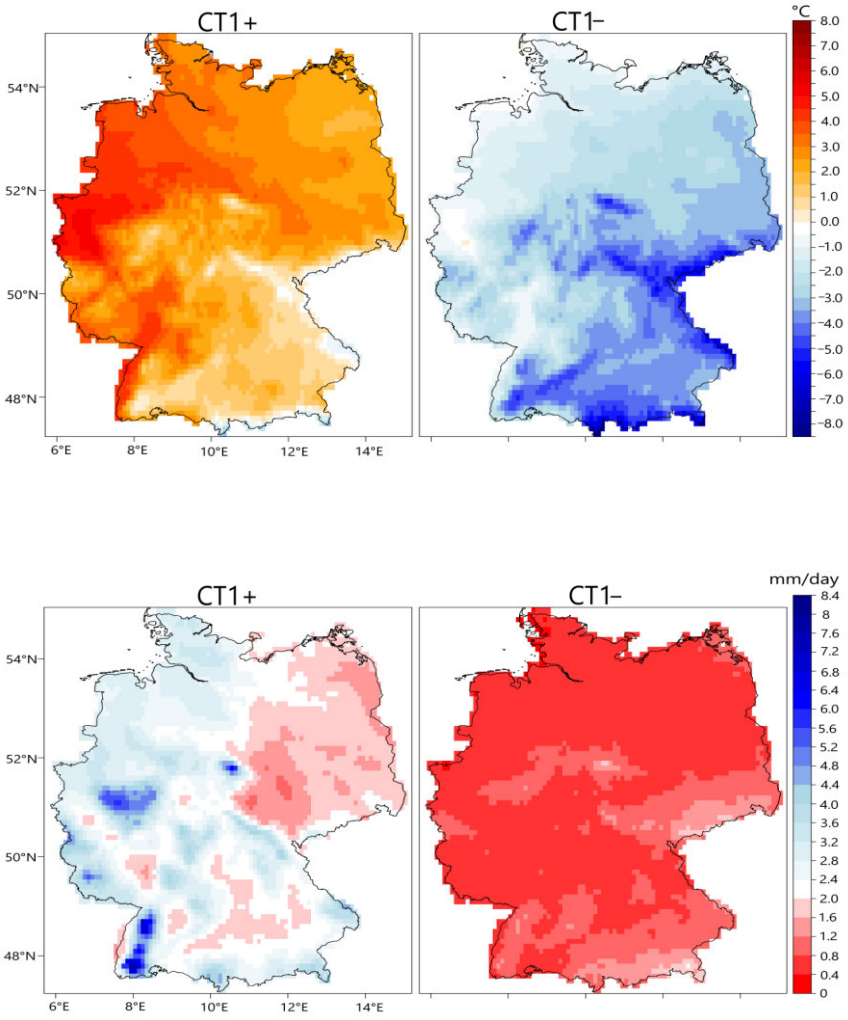

Figure 2.6: Composites of temperature (a), and precipitation (b) during the positive and negative phases of the circulation mode in Figure 2.5 that is related to the NAO. The composite maps are created for the DJF season.

Further, in the July 2021 flood episode in Germany, using circulation typing Ibebuchi (2022a) reproduced the spatiotemporal configuration of the synoptic circulations that contributed to the flood event. Among other factors, at the synoptic scale, the enhancement and northward track of the cyclonic system over the Mediterranean; northward track of the North Atlantic

anticyclone, further displacing poleward, the mid-latitude cyclone over the North Sea, enabling a band of westerly moisture fluxes to penetrate Germany; cyclonic system over the Baltic Sea coupled with northeast fluxes of moisture to Germany; and unstable atmospheric conditions over Germany, in addition to a cut-off low that formed over Central Europe were found to have contributed to the heavy rainfall event (Figure 2.7).

Given that large-scale patterns of atmospheric circulation contribute to climate extremes in Germany, in evaluating the capability of climate models to simulate the climate of Germany, it is useful to equally assess how the models represent the observed large-scale circulation patterns that influence the climate of Germany. Proper representation of the large-scale circulation patterns in the climate models will increase their credibility and the usability in projecting future climate extremes in Germany.

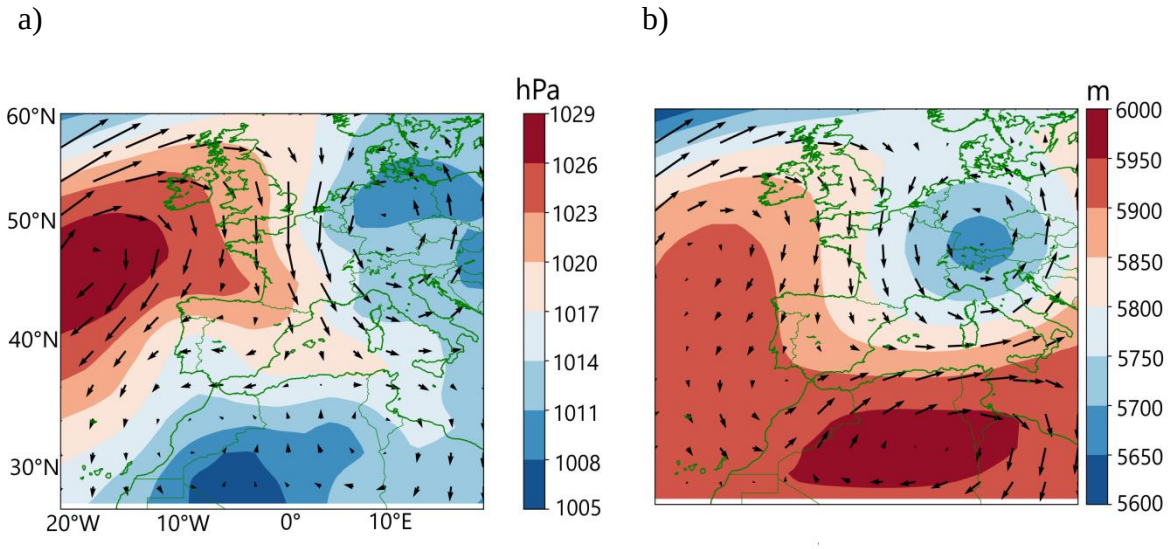

Figure 2.7: Synoptic circulations during the 14 July to 15 July flood episode in Germany. SLP (color) and 850 hPa moisture flux composites (black vectors) (a), and 500 hPa geopotential height (color) and 700 hPa moisture flux composites (black vectors) (b), for 14 July to 15 July 2021. The dates are when a classified circulation type associated with precipitation extremes in Germany persisted for at least a day.

3. Data and Methodology

3.1 Data

Simulated 2-meter temperature, precipitation, 10-meter wind vectors, and sea level pressure (SLP) are obtained from the European Coordinated Regional Climate Downscaling Experiment (EURO-CORDEX) Coupled Model Intercomparison Project Phase 5 (CMIP5) ensemble (Jacob et al. 2014). Table 3.1 contains an overview of the RCMs used in this study. The lateral boundary conditions for the RCMs are provided by ERA-Interim reanalysis, and two GCM data, respectively. ERA-Interim is based on the combination of different observations and numerical short-term weather forecasts. Conversely, GCMs are models without assimilation of observational data. Therefore, the RCMs driven by ERA-Interim are more consistent with the observed climate. Evaluating the quality of the RCMs when the lateral boundary condition is provided by ERA-Interim provides further information on whether the biases stem from the GCM or are due to the weaknesses of the RCM. Observed gridded precipitation and 2-meter temperature data are obtained from E-OBS (European daily high-resolution gridded dataset) version 23.1e (Cornes et al. 2018). SLP and 10-meter wind vectors data sets are obtained from ERA5 reanalysis (Hersbach et al. 2020), which is the 5th generation climate reanalysis product from the European Centre for Medium-Range Weather Forecasts. The NAO index is obtained from https://www.ncdc.noaa.gov/teleconnections/.

The RCMs that are driven by the GCMs are obtained under the historical experiment from 1950 to 2005 when they overlap with the E-OBS data and under the representative concentration pathway (RCP) 8.5 emission scenario (from 2070 to 2100). Depending on the time at which the data is available across the RCMs driven by ERA-Interim, the data sets are generally obtained from 1979 to 2005. Simulated precipitation and 2-meter temperature data sets are obtained at both daily and monthly original temporal resolutions. Simulated SLP is

obtained at daily temporal resolution. The E-OBS and ERA5 data sets are obtained at daily temporal resolution from 1950 to 2020, and 1979 to 2020, respectively. The horizontal resolution of the RCMs is 0.11°; 0.1° for E-OBS; and 0.25° for ERA5 reanalysis. The RCMs are further interpolated to the 0.1° longitude and latitude of the E-OBS data using first-order conservative remapping (Jones 1999) for precipitation and bilinear interpolation for temperature. The simulated SLP data sets are interpolated to the 0.25° resolution of the ERA5 data using the bilinear interpolation.

All analyses in this study are made for the RCMs in Table 3.1, but in evaluating the performance of the BC techniques, the results from CCLM4 and REMO model driven by the MPI-ESM-LR GCM will be mostly presented.

Table 3.1: Overview of the selected EURO-CORDEX RCMs. The references for each of the simulations are given in Jacob et al. (2014)

Institution	**RCM**	**Driving data**	**Ensemble-member under each driving model**
Royal Netherlands Meteorological Institute, Ministry of Infrastructure and the Environment	RACMO 2.2E	MPI-ESM-LR; CNRM-CM5;ERA-Interim	r1ip1; r1ip1; r1ip1
CLMcom (CLM Community with contributions by BTU, DWD, ETHZ, UCD, WEGC)	COSMO-crCLIM	MPI-ESM-LR; CNRM-CM5; ERA-Interim	r1ip1; r1ip1; r1ip1
Climate Service Center Germany, Hamburg, Germany	REMO2015	MPI-ESM-LR; CNRM-CM5; ERA-Interim	r3ip1;r1ip1; r1ip1
Danish Meteorological Institute, Copenhagen, Denmark	HIRHAM5	MPI-ESM-LR; CNRM-CM5	r1ip1; r1ip1
Rossby Centre, Swedish Meteorological and Hydrological Institute, Norrkoping Sweden	RCA4	MPI-ESM-LR; CNRM-CM5	r3ip1; r1ip1
CLMcom (CLM Community)	CCLM4	MPI-ESM-LR; CNRM-CM5; ERA-Interim	r1ip1; r1ip1; r1ip1

3.2 Methodology

3.2.1 Bias correction techniques

The performances of different BC techniques in reducing the systematic biases in simulated precipitation and temperature in Germany are evaluated, in addition to the impact of the BC techniques on the physical consistency of the bias-corrected variable. The BC techniques are linear scaling (LS) (Lenderink et al. 2007), empirical quantile mapping (EQM) (Panofsky and Brier 1968), univariate quantile delta mapping (QDM) (Cannon et al. 2015), multivariate quantile delta mapping using homogeneous grid points as related variables (MQDM) (Ibebuchi et al. 2022a), and multivariate quantile delta mapping using the individual climate variables (that is, temperature and precipitation) as related variables (MBCn) (Cannon 2017). The technique(s) is applied to the simulated precipitation and temperature RCM outputs both at daily and monthly resolutions to also assess the performance of the BC techniques as a function of the temporal resolution at which the BC is applied. The BC transfer functions are obtained at a seasonal time scale (that is, conditioning the data by seasons to account for the time dependency of the biases) for the four seasons in the study region. For the univariate techniques that assume a stationary correction factor (that is, LS and EQM), the transfer functions (that is, the correction factor) are obtained and applied at each grid box in Germany (Figure A2). The QDM is not based on a stationary correction factor but incorporates the change signal during the BC. For MQDM that is applied to a single variable, the spatial heterogeneity of the field is simplified to obtain a homogeneous region (generally characterized by a common climate for the climate variable); the homogeneous grids are treated as related variables. Hence, using the sub-grids as related variables, the MQDM is designed to improve the spatial dependency structure of the field (that is, inter-site correlations) during the BC. The rationale behind reducing the spatial complexity of

the field is that the consideration of all grid boxes over Germany implies an immense dimensionality of the spatiotemporal field and hence, might lead to overfitting in the statistical models. Similar to the MQDM, the MBCn also adjusts the simulated multivariate distribution towards the observed multivariate distribution, but in MBCn, the related variables are the individual climate variables (that is, temperature and precipitation) at each grid box. The general difference between MQDM and MBCn is that the former is designed to improve inter-site correlations and the latter is designed to improve inter-variable correlations, towards observations.

The analysis period, 1950 to 2005, is divided into two halves – 1950 to 1977 and 1978 to 2005. The first half is the training period for which the BC transfer function is obtained, and the second half is the validation period when the performance of the BC technique is evaluated, that is, the added value of the post-processing in reducing the systematic biases of the RCM output variable. When correcting projected future values, the historical period (1950 to 2005) is used as the training period when the correction factor is obtained and used to adjust the biases in the forecast period (that is, to adjust the biases in the projected simulated values). As earlier explained, the transfer function is assumed to be stationary for the LS and EQM techniques, but for QDM, MQDM, and MBCn, climate change signals are incorporated in the course of the BC. As a result, the stationarity assumption is not necessary under the QDM technique and its multivariate versions.

3.2.1.1 Linear scaling

The LS approach is among the simplest BC techniques. It adjusts the biases in the mean based on Equation (3.1):

$$\hat{x}_{m,f}(t) = x_{m,f}(t) \times \left(\frac{\bar{x}_{o,h}}{\bar{x}_{m,h}}\right) \qquad (3.1)$$

$x_{m,f}(t) =$ Raw modeled values, at time t in the validation or forecast period

$\hat{x}_{m,f}(t) =$ Corrected modeled values, at time t in the validation or forecast period

$\bar{x}_{o,h} =$ Seasonal mean of the observed values, during the training or historical period

$\bar{x}_{m,h} =$ Seasonal mean of the simulated values, during the training or historical period

For a non-zero bounded variable, like temperature in °C, Equation (3.1) becomes:

$$\hat{x}_{m,f}(t) = x_{m,f}(t) + (\bar{x}_{o,h} - \bar{x}_{m,h}) \qquad (3.2)$$

3.2.1.2 Empirical quantile mapping

In the EQM, the transfer function is based on the cumulative distribution function (CDF). The transfer function that is based on the historical CDF (or CDF obtained in the training period) is applied to the forecast (or validation) period by matching the quantiles of the simulated data to that of the observed data, according to Equation (3.3):

$$\hat{x}_{m,f}(t) = F_{o,h}^{-1}\{F_{m,h}[x_{m,f}(t)]\} \qquad (3.3)$$

$F_{o,h}^{-1} =$ Inverse CDF of observed values over the historical or training period

$F_{m,h} =$ Modelled CDF from the simulated data in the training or historical period

The major limitation of the EQM is the stationarity assumption of the CDF. Since the algorithm relies on the historical CDF to correct future projections, problems can be encountered when the forecast data is outside the range of the historical values, which is plausible when there is a strong climate change signal. As a consequence, projected trends can be affected in an undesirable way.

3.2.1.3 Quantile delta mapping

The QDM can be considered an improved version of the EQM. Instead of the stationarity assumption in the EQM, the QDM is designed to preserve the model's relative changes in the quantiles (Cannon et al. 2015). As outlined in Cannon et al. (2015), there are two steps

followed by the QDM to preserve the projected changes in the simulated quantiles: (1) before the quantile mapping, model outputs are detrended by quantile so that simulated historical and simulated projected values take the characteristics of the historical observations - without considering the change signal, and (2) projected relative (or absolute) changes in the simulated quantiles are incorporated in the corrected values. The aim of step (2) is to incorporate the climate change signal. These steps are described further in Equation (3.4) to Equation (3.6) as implemented in Cannon et al. (2015) from where the equations were adapted.

$$\Delta(t) = \frac{x_{m,f}(t)}{F_{m,h}^{-1}[\tau_{m,f}(t)]} \qquad (3.4)$$

$\tau_{m,f}(t) =$ The non-exceedance probability (ranging from 0 to 1) of the projected value at a given time in the validation or forecast period

$F_{m,h}^{-1} =$ Inverse CDF of the simulated value during the historical or training period for the original values

$\Delta(t) =$ Relative change signal in the simulated quantiles (for the precipitation variable)

$$\hat{x}_{o:m,h:p}(t) = F_{o,h}^{-1}\{\tau_{m,f}(t)\} \qquad (3.5)$$

$\hat{x}_{o:m,h:p}(t)$ is the corrected quantile in the forecast or validation period using the inverse CDF of observed values over the historical simulations. The final bias-corrected quantiles with climate change signal are obtained by:

$$\hat{x}_{m,p}(t) = \hat{x}_{o:m,h:p}(t)\Delta(t) \qquad (3.6)$$

For temperature, in °C $\Delta(t)$ is suited for an absolute change, and Equation (3.4) becomes:

$$\Delta(t) = x_{m,f}(t) - F_{m,h}^{-1}[\tau_{m,f}(t)] \qquad (3.7)$$

Also, Equation (3.6) becomes:

$$\hat{x}_{m,p}(t) = \hat{x}_{o:m,h:p}(t) + \Delta(t) \qquad (3.8)$$

3.2.1.4 Multivariate quantile delta mapping

Depending on what is treated as related variables, the QDM can be implemented as a multivariate BC technique, that is, the MQDM and the MBCn (Cannon 2017; Ibebuchi et al. 2022a). The methodological concepts are explained in detail in Cannon (2017). The multivariate versions of the QDM reorder the time series of ranks so that the empirical copula is adjusted; nevertheless, the marginal distributions are the same as QDM that is used in matching the simulated multivariate distribution to the observed multivariate distribution. Hence, the multivariate versions of the QDM transfer the full multivariate distribution and the empirical copula following these basic steps:

(1) Apply orthogonal rotation to the 3 sets of data sets respectively, that is, the set of related observed variables in the training period; the set of the same related simulated variables in the training period; and the set of the same related simulated variables in the validation period. The rotation in step (1) aims to (i) obtain a linear combination of the related variables and, (ii) a uniform multivariate distribution that allows convergence between the simulated and observed multivariate distributions. In this study, the set of related variables that are rotated to obtain the uniform multivariate distribution are either temperature and precipitation, or group observations at homogeneous grid boxes for a given variable.

(2) Match the simulated multivariate distribution (from the RCM) to fit the target multivariate distribution (from the observed data) using QDM.

(3) Apply inverse rotation to the matched multivariate distribution in step (2).

Iteratively repeat steps (1) to (3) until the multivariate distribution of the simulated data converges to the multivariate distribution of the observed data.

3.2.2 Classification of atmospheric circulation modes of variability and evaluation of the modes in climate models

Model-derived climate data are rooted in physical laws programmed in those models to approximate atmospheric processes. Therefore, model outputs are imperfect and can only reproduce a portion of the observed atmospheric circulation modes of variability. Model deficiencies in representing meteorological processes can be identified by spatiotemporal variability of the climate variable, and such deficiency is often a major cause of errors in model data output (Flato et al. 2013). Therefore, if reference modes of variability that govern a given climate variable are known for a given region, it is advantageous to document the correspondence between modes of variability from modeled data, and the reference modes of variability in hindcast experiments. Such diagnostic checks can be used to ascertain the physical processes that are misrepresented in the models, which can be improved as part of model developments.

In this study, two concepts are applied in evaluating the representation of the atmospheric circulation modes of variability in the RCMs: first, is the classification of circulation types (CTs) in Western Europe using the SLP data, which explains atmospheric circulation (Kidson 1999) and influences surface variables such as precipitation and temperature; second, is the regionalization of the temperature and precipitation data over Germany, to obtain individual meteorological patterns or climate regimes. The reference CTs and climate regimes are obtained from observational or reanalysis data. The portion of the reference CTs and climate regimes that are reproduced by the RCM output are documented. If a statistical post-processing technique such as BC is applied to an RCM output, it is not expected that the BC corrects the physical processes that are misrepresented in the RCM, but at least, upon reducing the systematic biases in the statistics of the RCM, significant portions of the simulated modes of variability should also be reproduced from the post-processed data.

The individual meteorological patterns of temperature and precipitation are defined using homogeneous regions of temperature and precipitation anomalies, respectively. Given the high spatiotemporal variability of climate fields such as precipitation, regionalization of the field helps in simplifying the spatial heterogeneity and identifying a set of homogeneous regions that covary over time. The co-variability of the precipitation regions can arise from the variability that can be resolved by the grid network. Thus, depending on factors such as the grid resolution, typical mesoscale variability (that is, features that are between about 2 km and 1000 km) to synoptic- and larger-scale variability (that is, features that are about 1000 km and above) can be captured in the classified meteorological patterns.

Among the multivariate techniques used to study the spatiotemporal characteristics of climatic modes of variability, the rotated principal component analysis (PCA) is popular and commonly applied (White et al. 1991). In this study, the rotated PCA is applied not just to reduce the dimensionality of the data (that is, removal of the noise portion), but basically as a classification tool, following the logic outlined in Richman (1981, 1986) that ensures that the rotated PC patterns have a physical foundation. Hence rotated PCA is applied as a time decomposition technique to obtain a group of time series with a similar spatial pattern of a field that explains atmospheric circulation (that is, CTs); and as a spatial decomposition technique to obtain a group of grid boxes that covary over time (that is, homogeneous regions for a climate variable).

3.2.2.1 Modes of matrix decomposition

The general idea behind the different modes to represent a data matrix is that in a climatological field there are three underlying entities:

(1) The (meteorological) field: a field can be described as a spatial array of the variable(s) such as temperature, precipitation, SLP, and so forth, with observations (mostly) in form of time series.

(2) Time: time series at which the field observations were made.

(3) Location: stations or grid points at which the field was observed at a given time.

The application of PCA to a meteorological field has the flexibility of holding one of the three entities constant while varying the others. The entity held constant and the one that is varied depends on the (matrix) mode in which the data is represented. Richman (1986) listed six (matrix) modes of decomposing a meteorological field. However, in this work, the focus will be on the T-mode (T-MD) matrix and the S-mode (S-MD) matrix. The common characteristic between both is that the field is fixed whereas either time or location is varied. Therefore, an S-MD matrix is simply the matrix transpose of the T-MD matrix. Figure 3.1 shows the respective structures of both matrices. In the S-MD, variable or column matrix is grid points, and the observations or row matrix is time series. In T-MD, the variable or column matrix is time series, and the observations or row matrix is grid points.

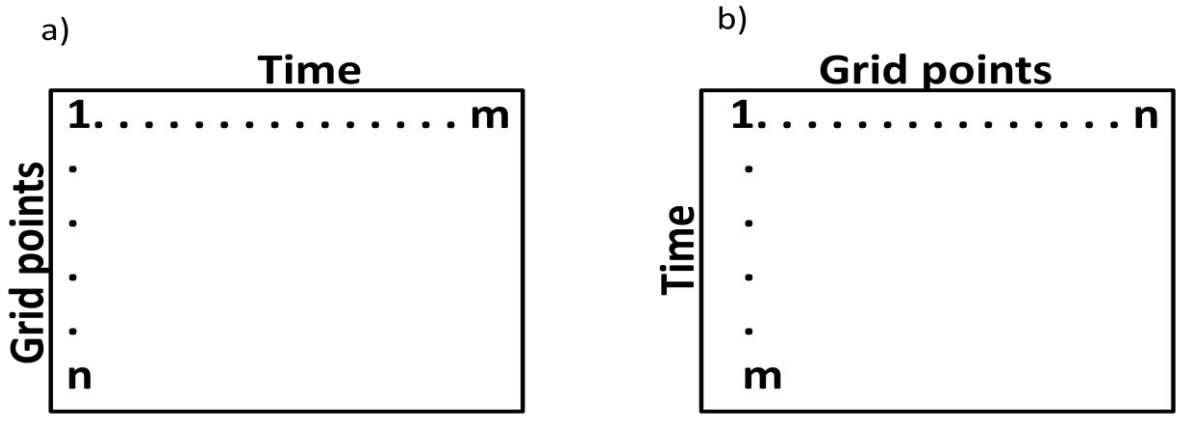

Figure 3.1: Structures of the T-MD matrix (a), and the S-MD matrix (b). For the T-MD matrix: the column or variables contains m number of time series in the study period, and the rows contain n number of grid points in the study region. For the S-MD matrix: the column or variables contain n number of grid points in the study region, and the rows contain m number of time series in the study period

3.2.2.2 Precipitation regionalization with rotated S-MD PCA

The rotated S-MD PCA is a spatial decomposition technique that is applied to denoise, and regionalize a climate variable (Richman and Lamb 1985). The denoising aspect is based on

the variance maximization property of the PCA. The regionalization aspect follows the rotation of the PC loadings to obtain a simple structure that can be physically interpreted. The standard methods that are applied to select an appropriate number of PCs to retain, for example, the scree test (Cattell 1966), are applicable for unrotated PCs because the eigenvalues or variances are characteristics of unrotated PCs. However, rotated PC analysis redistributes the variance among individual PCs, so eigenvalues are no longer defined and are not applicable in deciding the number of rotated PCs to be analyzed (Richman 1981, 1986). The first unrotated PC usually merges multiple unique sources of pattern variability that results in an inflated eigenvalue of the first PC (Karl and Koscielny 1982). When PCA is applied as a classification tool, the rotation is aimed at making the PC loadings resemble the patterns embedded in the correlation matrix (Richman 1986). Therefore, in deciding the optimal number of rotated PC patterns, only the solution where every rotated PC loading vector contains valid (physically interpretable) signals that match well quantitatively to those signals in the correlation patterns are retained and interpreted. This is based on the assumption that in climate science, correlations can be physically interpreted.

The rotated S-MD PCA is applied in this study to obtain homogenous regions of precipitation and temperature, respectively. In the process, the correlation matrix is used to relate the grid boxes in Figure A2. The correlation matrix containing the Pearson's correlation between the grid boxes is decomposed with singular value decomposition to obtain the PC scores, eigenvectors, and eigenvalues. The eigenvectors are multiplied by the square root of the corresponding eigenvalues to obtain the PC loadings that can be longer than a unit length and are more responsive to simple structure rotation (Richman and Lamb 1985). PC loadings are in units of Pearson's correlation coefficients that relate the standardized data with the PC scores. Equation (3.9) shows the PC model equation linking the PC loadings to the PC scores. In an S-MD analysis, the PC loadings summarize the spatial patterns of variability in the

correlation matrix and the PC scores are time series that designate the amplitude of the spatial variability patterns for each of the time steps. The simple structure rotation of the PC loadings using Equation (3.10), aims at simplifying the patterns in the PC loadings as much as the data allow by finding a position of the PC axes that provide a maximum count of near-zero loadings, and a smaller number of salient magnitude loadings, thereby creating a homogeneous pattern representing a region of precipitation anomalies (Richman 1986).

$$Z = FA^T \qquad (3.9)$$

Z = original standardized matrix of the field

F = matrix of PC scores

A^T = Transpose of the PC loadings

$$B = AT \qquad (3.10)$$

B = rotated loading vector (using a simple structure rotation method)

T = (linear) transformation matrix

When PCA is applied as a classification tool aiming to group similar variables, for example, homogeneous grid boxes for a given climate data, the similarity matrix that decides the efficacy of the grouping is the correlation (or covariance) matrix; and the simple structure rotation as previously noted aims to make the PC loadings reflect the patterns in the similarity matrix from where they are drawn (Richman 1981, 1986). The resemblance of the rotated PC loadings with the correlation patterns is used as a test for the physical interpretability of the PCs.

To determine the number of PCs to retain and rotate, the PCs are retained and rotated iteratively (that is, keeping and rotating two components, then three, four...), and then

matched to the correlation vector that indexes the highest loading magnitude on that PC vector using the congruence coefficient in Equation (3.11). A congruence coefficient magnitude ≥0.92 (Richman 1986) is required as an arbiter to assess if the PC pattern is sufficiently similar to the correlation pattern to be considered free of artifacts arising from the PCA process. Considering that congruence matches can be biased high, compared to correlations, following Richman (1986), the congruence matches are defined as follows: 0.98 ≤ excellent match ≤ 1.00; 0.92 ≤ good match < 0.98; 0.82 ≤ borderline match < 0.92; 0.68 ≤ poor match < 0.82; terrible match < 0.68.

$$I_{XY} = \frac{\sum XY}{\sqrt{\sum X^2 \sum Y^2}} \qquad (3.11)$$

I_{XY} is the congruence coefficient; X and Y are two distinct (PC loading) vectors.

The decision of the optimal number of components to retain is made by identifying the largest set of components where all rotated PC loadings match the correlation patterns with a congruence coefficient magnitude of ≥0.92 (Ibebuchi 2022b). Because the observational data (that is, E-OBS) or ERA5 reanalysis are the most reliable data sets that provide the most realistic representation of the variability patterns, they are used as a reference in determining the optimal number of PC patterns to rotate. Oblique rotation is used in this study as that relaxes the orthogonality in the PC scores and adds additional information on the correlation among the PC scores. Hence the Promax oblique rotation algorithm (Hendrickson and White 1964) is applied at integer powers of two to four (that is, the power at which the Varimax rotation is raised). The Promax solution at which all rotated PC loadings have the highest congruence match with the correlation patterns is deemed optimal in rotating the PC patterns to reflect the correlation patterns. Also, the data sets that are regionalized were first detrended as the analysis is not interested in the trend component of temporal variability. Hence each rotated PC loading pattern is designated as a homogeneous region of rainfall or temperature

anomaly (or referred to as variability pattern or meteorological pattern). The Promax solution and the number of components to retain and rotate that are determined from the observational data, are also used when the same algorithm is applied to climate models.

For precipitation, the physical interpretability of the observed variability patterns is further diagnosed by analyzing the precipitation, 10-meter wind, and SLP composite anomaly maps associated with the time development of the variability patterns. The PC scores designate the time development of the classified homogeneous regions. To cluster dates when a given classified homogeneous region has dominant signals, a PC Score threshold at which the PC loading pattern matches the associating precipitation composite anomaly pattern with a congruence match of at least 0.92 is required. Thus, the PC loading vectors are matched iteratively with the composite anomaly precipitation pattern arising from a given PC score threshold and seeking a PC score threshold that gives a congruence match of at least 0.92. When the required threshold is established, for a given PC, the composite anomaly patterns of the aforementioned climate variables (that is, precipitation, 10-meter wind, and SLP) are created from a group of dates that have PC score magnitudes above the required threshold. The anomaly patterns are created with respect to the seasonal climatology. Given the continuous nature of atmospheric processes, this steps aid in reducing noise to signal ratio, by enabling the creation of composite patterns that reflects the precipitation variability pattern strongly and so enhance the robust diagnosis of the physical processes associated with the time development of the respective homogeneous regions. The variability patterns are tested for robustness, by first applying the classification scheme to the E-OBS and reanalysis data set from 1979 to 2020, and then from 1979 to 2005, for which the RCMs driven by ERA-Interim and the GCMs are available.

3.2.2.3 Classification of circulation types with rotated T-MD PCA

The rotated T-MD PCA analysis is a time decomposition technique. The time-scale decomposition associated with this technique, when applied meticulously as a fuzzy classification tool (for example, Ibebuchi and Richman 2022) can capture the three aspects of time-scale variability comprising trends (that is, variations due to an anthropogenic influence), low-frequency, and high-frequency variability (Compagnucci et al. 2001). The classification procedure is the T-MD analysis is the same as the S-MD analysis. The major differences are that the standardized SLP field (the standardization is to give equal weight to all dates) is used for the classification and the correlation matrix contains the correlation between the times series. Hence the PC loadings are time series that localize in time the spatial patterns captured by the PC scores (Compagnucci and Richman 2008). Similar to the S-MD analysis, the largest number of components to retain and the most optimal Promax power to use in rotating the PCs is that at which all the rotated PCs have the largest congruence match with the correlation patterns. Again, PCs are expected to resemble the correlation patterns to pass the test for physical interpretability (Richman 1981).

PCA being a linear multivariate tool does not explore the non-linearity of the rotated PC loadings in the T-MD analysis (or PC scores in the S-MD analysis). Basically, in the T-MD analysis, post-processing the loadings with a simple structure rotation simplifies those PC loadings (time series) as much as the data allow into groups of dates that have similar spatial patterns (and their inverse) for subsets of the analyzed dates, simultaneously finding the configuration where most dates have near-zero loadings, ensuring unique patterns. Hence, unique CTs are obtained when a simple structure rotation is applied to the SLP data. To explore the non-linearity of the rotated and retained PC loadings, a threshold of ± 0.2 (Richman and Gong 1999; Ibebuchi 2022b) is used to separate loadings within the zero-interval from the signal, implying that only loading magnitudes greater than $|0.2|$ are

considered signals. Hence, each retained component forms two classes, CTK+ and CTK− (K is the PC number), with loadings above and below the ± 0.2 threshold. The two CTs from each PC have asymmetric spatiotemporal characteristics that are common for atmospheric modes of variability (Ibebuchi 2022b). A PC comprising both the positive and negative phase of the loadings is defined as the mode whereas the SLP composite of the days assigned to a given phase of the mode is defined as the CT. A day can also be grouped under more than one CT, using the $|0.2|$ threshold width to define the signal and the probability of group membership. Thus, an overlapping solution is possible, implying that a day can be assigned to more than one CT insofar as the loadings under the CT in question are associated with the signal. The preference for an overlapping solution is due to the continuous nature of atmospheric circulation patterns.

3.2.2.4 Physical consistency evaluations for temperature and precipitation

Climate variables are commonly correlated due to the continuous nature of the atmospheric system. There are continuous interactions and feedbacks among atmospheric signals at various spatiotemporal scales. Large-scale signals, such as the NAO modulate synoptic-scale signals, which are also modulated by other atmospheric processes and features at smaller scales. Therefore, mesoscale to microscale variability contains synoptic to large-scale signals, and so forth. Hence, any statistical processing technique applied to modeled climate data is expected not to notably change the physical consistency of the data. This implies that the simulated portion of the atmospheric signals that govern the climate variable and the simulated correlation between the variable and other climate variables should not be notably changed. There is no guarantee that a post-processing technique such as BC, applied to a model data will not change some aspects of the physical consistency. Discrepancies can arise as the post-processed simulated data may not capture the same variability as the raw simulated data, which can lead to differences in the respective PC patterns. Most important,

the spatiotemporal scale and the extent to which the change in simulated pattern variability occurred, after the BC, can be documented to inform end users of the post-processed data. In this study, the model data is first decomposed spatially, and the portion of the reference modes that are simulated by the data is documented. After the BC, the bias-corrected data is decomposed again spatially, and then it is evaluated if the documented portion of the simulated modes of variability was preserved or changed at certain spatiotemporal scales.

If during model evaluations, it is diagnosed that some meteorological processes that can enhance the physical consistency of the model data are misrepresented relative to observations, such errors can be qualitatively corrected as part of climate model development and not during statistical post-processing that neglects feedback mechanisms. For a targeted impact assessment requiring that a specific set of simulations have statistical characterizations that are comparable with observations, BC is indeed a suitable approach to reducing the systematic biases in the statistical characterizations of RCMs. Nonetheless, it is an arbiter for success that any set of statistical post-processing techniques applied to climate model data (1) reduces uncertainty in the data, relative to a reference, without changing the simulated meteorological processes that govern the data, and the correlation between the data and other climate variables, and (2) if possible, can be used to diagnose the source of model error, which can be improved as part of climate model developments.

To assess physical relationships between climate variables, multivariate analysis such as PCA can be applied to a single variable to obtain modes of variability, and composite maps of distinct climate variables can be used to diagnose the meteorological processes that are associated with the variability pattern (Ibebuchi 2022a). For example, Behera et al. (2003) applied rotated PCA to obtain the Indian Ocean dipole mode, and the physical and dynamical understanding of the mode was enhanced through composites of ocean-atmosphere parameters. Alternatively, multivariate analysis can be applied to obtain coupled modes of

variability from distinct fields by using the singular value decomposition (SVD) (Prohaska 1976), canonical correlation analysis (CCA) (Rencher 1992), or combined PCA, that is, applying eigenanalysis on multiple variables at the same time; or other advanced methods such as the maximum covariance analysis (MCA) (An 2003). Cherry (1996) made a detailed comparison of SVD and CCA and found that both methods can generate spurious spatial patterns and highly correlated maps that are due to mathematics but have no physical justification. The major issue with the SVD, when applied in geosciences, is the orthogonality constraint placed on the coupled modes; nonetheless, the actual climatic modes are not orthogonal. Further, a combined PCA will not necessarily show shared patterns unless cases are discovered when the maps of both fields analyzed have large loading magnitudes over a set of PC scores with large magnitudes; and since such a scenario is rare, combined PCA is not guaranteed to reveal much about the coupling of the fields. The MCA tends to generate coupled patterns that are not due to physical interaction between the climate variables but due to the influence of external factors (An 2003).

As explained in section 3.2.2.2, unrotated vectors whether in PCA, MCA, CCA, or SVD can be post-processed with a rotation to obtain physically interpretable patterns. Nonetheless, Cherry (1997) argued that when the goal is to obtain coupled modes, simultaneously rotating two distinct fields is not physically justifiable. Cherry (1997) suggested, that separate PCA analysis can be carried out in distinct meteorological fields. According to Cherry (1997), if there are set of rotated PC patterns from each of the distinct fields that are strongly correlated, and if the rotated PC patterns are physically interpretable, then evidence of coupling that has not been mathematically forced can be established. Such an approach suggested by Cherry (1997) was applied by Ibebuchi (2022c) to successfully uncover physically interpretable coupled atmospheric patterns (from the time decomposition of SLP and spatial decomposition of precipitation, with rotated PCA), through which the Subtropical Indian Ocean dipole

influence summer rainfall variability of the central parts of Africa, south of the equator. Moreover, a more optimal method (referred to as Procrustes target analysis) of applying rotated PCA on the individual fields and then matching the respective PC patterns, to seek coupled modes was introduced by Richman and Easterling (1988). Hence, to navigate analyzing spurious coherent patterns, evidence of coupling between the variability patterns of temperature and precipitation will be investigated by correlating the respective PCs that have passed the test for physical interpretability. If a post-processing technique such as BC does not notably change the temporal variability of the mode (that is, the time series), then the coupling (or correlations between distinct modes) will not be notably affected, since it is the time series of the coupled modes that are correlated before and after BC.

Further, in addition to assessing the consistency of a climate variable with the governing mechanisms, this study aims to also evaluate how statistical post-processing with BC impacts the coherency between specific climate variables (that is, temperature and precipitation) that are relevant for certain impact studies. In assessing such relationships, calculating and plotting spatial correlation maps to uncover physically important mechanisms between two variables have long been found useful to advance the science of the climate since Walker (1904) applied correlation maps to discover the Walker Oscillation. Pearson's correlations, presented in Equation (3.12), can be deemed physically interpretable due to their cohesiveness and magnitude.

$$r_{XY} = \frac{n(\sum XY) - (\sum X)(\sum Y)}{\sqrt{(n\sum X^2 - (\sum X)^2)\,(n\sum Y^2 - (\sum Y)^2)}} \qquad (3.12)$$

r_{XY} is the Pearson's correlation coefficient. The correlation coefficient of -1 indicates a strong negative correlation and the correlation coefficient of +1 indicates a strong positive correlation. 0 indicates no correlation.

n is the sample size

Hence Pearson's correlation is used to relate temperature and precipitation with a focus on the magnitude, sign, and large-scale mechanisms driving the correlations. The statistical significance of the correlations is tested using the non-parametric Kendall Tau-b (Kendall 1938) at a 95% confidence level.

3.2.3 Metrics used to validate the bias correction techniques

A process-based approach is developed in this study for evaluating the performance of the BC techniques. The assessment of the added value of the BC techniques includes their relative impacts on the model's (1) statistical characterization, (2) simulated meteorological patterns and, (3) the correlation between the bias-corrected variable and other output variables, relative to the reference.

3.2.3.1 Impact on the statistical characterizations

To assess how the BC techniques impact the statistics of precipitation and temperature, the first to fourth statistical moments of the raw and bias-corrected climate variables, averaged over Germany, are compared with the observed values at a seasonal time scale. Also, the mean absolute error (MAE) presented in Equation (3.13) is used to evaluate the performance of the BC techniques in adjusting the biases at the grid box level, for spatial mean and spatial variability (that is, the standard deviation) of precipitation and temperature, respectively.

$$MAE = \frac{1}{n}\sum_{j=1}^{n}\left|y_j - y\right| \qquad (3.13)$$

y_j are the simulated values and y is the reference values

To assess the performance of the BC techniques concerning extreme values, which are of importance in modeling climate extremes, return value calculations are used during JJA when Germany receives on average the highest precipitation (and temperature in absolute values). To optimize the fit of the extreme value distribution on the data values, the extreme value

theoretical distribution that fits relatively best on the data values and the technique that best fits the distribution on the data are adopted. The peak over threshold method was prioritised so that more representative data values are obtained compared to the annual maxima approach. For estimating the parameters of the distributions, the maximum likelihood estimation and method of moments are also compared. Return values between 2 and 150 years are calculated and the simulated results from the bias-corrected output are compared to observed values using MAE.

3.2.3.2 Impact on the simulated meteorological patterns

Unlike the Pearson's correlation, which assumes normality of the data, the congruence match from Equation (3.11) has no statistical assumptions and is insensitive to scalar multiplication of the (PC loading) vectors, X and Y. The congruence match is commonly applied in assessing the closeness of eigenpatterns (Lorenzo-Seva and ten Berge 2006; Dholakia and Bhavasar 2017). Therefore, given its advantages, the simulated meteorological patterns, before and after bias correction, are matched with the reference patterns using the congruence match. The aim is to assess if the BC techniques alter the spatiotemporal structure of the simulated meteorological patterns. For coupled variability patterns of temperature and precipitation (that is, the respective individual PC patterns that are strongly correlated), it is investigated if BC impacts the coupling or correlation between the variability patterns. Also, in addition to the congruence matches, by further visual examination of the isopleths of the variability patterns (before and after BC), the assessment explores the possible spatial scale at which a notable change was made to the pattern configuration.

Further, the PC scores that are the amplitude of the variability patterns at a given time are used to find dates when the patterns occurred with strong signal, that is, dates with high PC score magnitudes above a pre-selected threshold. After BC, a physically consistent eigenpattern should have PC scores that find the correct periods or representative dates when

the composites of SLP, wind, precipitation, and so forth, give physically interpretable composite patterns that are comparable with the reference. Therefore, when the raw simulated data reproduced a portion of governing mechanisms associated with a mode, if the PC scores are comparable before and after BC, then it is suggested that the BC has not notably changed the simulated physical consistency of the field.

3.2.3.3 Impact on the correlations between the simulated variables

It is investigated if the observed statistical correlation between temperature and precipitation is replicated by the raw RCMs and how the BC techniques affect the simulated seasonal coherency between temperature and precipitation. The correlations between temperature and precipitation at the grid box level results in 4840 correlation coefficients (that is, the number of grid boxes in the study domain at which temperature and precipitation time series are related, in a specific season). The empirical distribution of the correlation coefficients from the simulated data sets is compared to the reference using the Kolmogorov-Smirnov (KS) two-sample test (Massey 1951). The KS test is non-parametric and assumes the distribution of the data is continuous. The null hypothesis is that the two data values are from the same distribution. The null hypothesis is tested at a 95% confidence level. Also, the test provides a KS statistic value (that is, the D statistic). The KS D statistic quantifies the distance between the empirical distribution functions of the two samples that are compared. Thus, the KS D statistic is used to evaluate how close the distribution of the correlation coefficients from the (un)corrected data sets are to the correlation coefficients from the reference. Since the KS test does not indicate the aspect of the statistical distributions that are changing, the summary statistics of the respective distributions are also computed and compared among the data sets. Also, correlation maps are computed from the observed data and simulated data before and after BC. The changes in the magnitude and sign of correlations at the grid box level are

equally assessed to establish the effect of the BC techniques on the simulated correlations between temperature and precipitation in Germany.

For the season(s) that the correlations are statistically significant at a 95% confidence level, based on the non-parametric Kendall Tau-b, the possible underlying (large-scale) atmospheric mechanism(s) that control the correlations is investigated. This will enhance the physical interpretations of the statistical correlations. Further, when the large-scale mechanism that governs the seasonal correlation between temperature and precipitation in the study region is simulated by the raw RCMs, the effect of BC on the mechanism is investigated.

4. Representation of atmospheric circulation modes in regional climate models

A major source of model biases stems from the limitations in representing meteorological processes. In Europe, biases associated with the misrepresentation of processes have been reported to include blocking frequency biases, sea surface temperature biases, representation of teleconnections such as the NAO, orographic effects, and cloud parameterizations (Feldmann et al. 2008; Muller et al. 2018). The circulation biases in the GCMs are propagated into the RCMs used to downscale them, which can result in the misrepresentation of surface variables, such as precipitation and temperature (Teichmann et al. 2013).

Further, the representation of atmospheric circulation modes in RCMs can enhance the credibility of regional climate projections. Circulation biases are regional constraints in studying and projecting changes in dynamically downscaled surface variables such as precipitation (Zhang and Soden 2019; Fernandez-Granja et al. 2021). A good representation of large-scale atmospheric circulation modes in Western Europe in the RCMs will enhance the accuracy of the future projections of temperature and precipitation changes over Germany. Though the added value of dynamical downscaling towards a better representation of large-scale circulation features is unclear (Prein et al. 2019), through better representation of smaller-scale processes such as orography, improvements, for example, in rains shadow effects have been reported (Clark et al. 2010). However, there are also concerns that RCMs might not be physically consistent with the driving GCM because increasing resolution might alter the structure of climate parameters such as wind field (Benestad 2016). For that reason, it is crucial to examine how the RCM ensemble simulates the observed CTs under different constraints. Moreover, BC techniques do not improve circulation biases and biases associated

with the misrepresentation of processes (Maraun et al. 2021). Therefore, it is important that the RCMs faithfully simulate the observed large-scale circulation modes.

4.1 The capability of the climate models to replicate the observed circulation types

The reference large-scale atmospheric circulation modes are represented by the classified ERA5 CTs in Figure 4.1. The CTs are classified using SLP data from 1979 to 2005, which is the longest period that all data sets are available. Also, when ERA-Interim provides the lateral boundary conditions, HIRHAM and RCA4 RCMs are not available from 1979; hence in the CT analysis, HIRHAM and RCA4 were not included for the RCMs driven by ERA-Interim. The ERA5 CTs are more consistent with the observed climate. Moreover, external validation of the ERA5 CTs in Western Europe has been made using other reanalysis products (Ibebuchi 2022a). The same rotated T-MD PCA classification scheme that is used to classify the ERA5 CTs is applied to the individual RCMs aiming to reproduce the reference CTs. Hence the reference CTs from ERA5 are matched with their counterparts as classified from the individual RCMs using the congruence coefficient as a measure of goodness-of-match. The ERA5 CTs are compared with the same CTs from (1) the individual RCMs driven by ERA-Interim, (2) individual RCMs driven by MPI-ESM and CNRM, respectively and, (3) the multi-model ensemble mean of the RCMs driven by reanalysis and by the GCMs, respectively. Thus, the analysis aims to measure the sensitivity of the results to (1) the choice and quality of the RCM, (2) the choice of GCM and, (3) the reduction of inter-model uncertainties using the multi-model ensemble mean.

By matching the rotated PC loadings from the ERA5 and the climate simulations, respectively, to the correlation vectors that they are indexed to, the first four Promax rotated components all have congruence coefficients greater than 0.92. At a Promax power of 2, the highest magnitude of congruence matches (with the correlation patterns) for all the four

components were attained. Thus, the four components rotated at a Promax power of 2 are analyzed. Figure 4.1 to Figure 4.4 show the classified CTs when the classification is applied to the RCMs driven by ERA-Interim, the GCMs (that is, MPI-ESM and CNRM), and the multi-model ensemble mean of the RCMs, respectively. The simulated CTs are compared to the same ERA5 CTs, and the CTs (that is, the SLP composite patterns) were replicated in each case with one-to-one correspondence. There are biases (that is, mismatch in the isopleths of the composite patterns) specific to both the choice of RCM and the GCM-RCM combination. To quantify these biases, that is, how well the simulated CTs match with the observed CTs, Table 4.1 contains the congruence coefficients between the observed SLP composite anomaly patterns from ERA5 and the same simulated SLP composite anomaly patterns from the climate models. First, the congruence match is highest for the CTs classified from the RCMs driven by ERA-Interim compared to when the GCMs provide the lateral boundary condition. This is an indication that the RCMs can capture the atmospheric circulation modes as obtained from ERA5 and the major biases that constrain the model chain in replicating the CTs stem from the driving GCM. Also, the explained variance of the simulated modes is quite comparable with the modes from ERA5 (Table 4.2). The major uncertainty in the explained variance arises when the data driving the RCM is changed, mostly for the first retained component that explains most of the variability.

Further, in Table 4.1 and Figure 4.2 to Figure 4.4, it can be inferred that when the RCMs are driven by GCM, the biases associated with the representation of the CTs depend on the choice of RCM and the quality of the data providing the lateral boundary conditions. Further, the results show that GCMs have large deficits in simulating large-scale atmospheric circulation compared to ERA-Interim. On average, the multi-model ensemble mean of the analyzed RCMs slightly improved the representation of the large-scale atmospheric circulation modes

when the RCMs are driven by ERA-Interim. No improvement was attained in the ensemble mean of the five RCMs driven by the GCMs. But a slight improvement was attained if only the ensemble mean of the best performed RCMs (that is, RACMO and COSMO driven by CNRM) were considered (Table 4.1). Thus, there is no guarantee that multi-model ensemble mean will improve the skill of the RCMs in simulating the large-scale atmospheric circulation modes. Only with careful consideration of the ensemble members, a benefit might be obtained. From Table 4.1, when the RCMs are driven by reanalysis, the lowest congruence match with the reference is in CT4− associated with anticyclonic circulation over Western Europe. In the ensemble mean of the five RCMs driven by GCM data, CT2+ and CT4− that are associated with anticyclonic circulations have the lowest congruence matches with the reference CT, respectively. Thus, the models indicate deficiencies in simulating anticyclonic circulations over Western Europe.

From Table 4.3, for the RCMs driven by reanalysis, the loadings (amplitude) of mode 1 and mode 2 match mostly in the good range with ERA5 loadings. The accuracy relatively drops under mode 3 and mode 4. The plausible reason can be that the first two modes (and their temporal evolution), which explain ~56% of the variability in the SLP field (Table 4.2) are well represented in the climate models, compared to modes that explain lesser variability. Figure 4.5 shows that the inter-annual variability of the amplitude of the modes from ERA5 is in phase with the simulated modes when ERA-Interim provides the lateral boundary condition. From Table 4.3, on average, the multi-model ensemble mean helps in reducing the model uncertainties in the temporal variations of the amplitudes of the simulated modes when reanalysis provides the lateral boundary condition. However, when the GCMs provide the lateral boundary conditions, the match between the PC loadings of the simulated modes and the ERA5 modes is in the terrible range (Table 4.3). Thus, while the GCM-RCM chain can

4.1 - The capability of the climate models to replicate the observed circulation types

reproduce the climatological mean of circulation patterns, there is nearly no skill in reproducing the temporal sequence of circulation patterns.

Table 4.1: Congruence match between the anomaly maps from ERA5 CTs and the same CTs from the RCMs.

Data	**CT1+**	**CT1−**	**CT2+**	**CT2−**	**CT3+**	**CT3−**	**CT4+**	**CT4−**	**Average**
			ERA-Interim (RCM)						
COSMO	0.99	1.00	0.99	0.99	0.95	0.99	0.94	0.85	0.96
RACMO	1.00	1.00	0.98	0.98	0.94	0.98	0.95	0.92	0.97
REMO	1.00	0.99	0.98	0.99	0.96	0.98	0.94	0.94	0.97
			MPI-ESM (RCM)						
COSMO	0.97	0.91	0.79	0.78	0.88	0.97	0.91	0.84	0.88
RACMO	0.98	0.95	0.82	0.89	0.85	0.97	0.92	0.81	0.90
REMO	0.96	0.84	0.63	0.63	0.85	0.81	0.95	0.92	0.82
RCA4	0.96	0.77	0.60	0.61	0.79	0.79	0.95	0.88	0.79
HIRHAM	0.97	0.89	0.76	0.85	0.76	0.89	0.88	0.74	0.84
			CNRM (RCM)						
COSMO	0.97	0.95	0.90	0.97	0.94	0.87	0.90	0.83	0.92
RACMO	0.98	0.98	0.87	0.98	0.91	0.86	0.83	0.86	0.91
REMO	0.97	0.97	0.79	0.96	0.88	0.81	0.74	0.74	0.86
RCA4	0.96	0.98	0.81	0.98	0.86	0.79	0.82	0.86	0.88
HIRHAM	0.98	0.96	0.78	0.94	0.94	0.91	0.75	0.80	0.88
			ENSEMBLE (RCM)						
ERA-Interim	1.00	1.00	1.00	1.00	0.99	1.00	0.96	0.94	0.99
MPI-ESM	0.98	0.80	0.72	0.91	0.99	0.77	0.92	0.77	0.86
CNRM	0.97	0.92	0.77	0.98	0.87	0.86	0.81	0.77	0.87
CNRM (COSMO, RACMO)	0.99	0.98	0.92	0.98	0.90	0.82	0.85	0.88	0.92

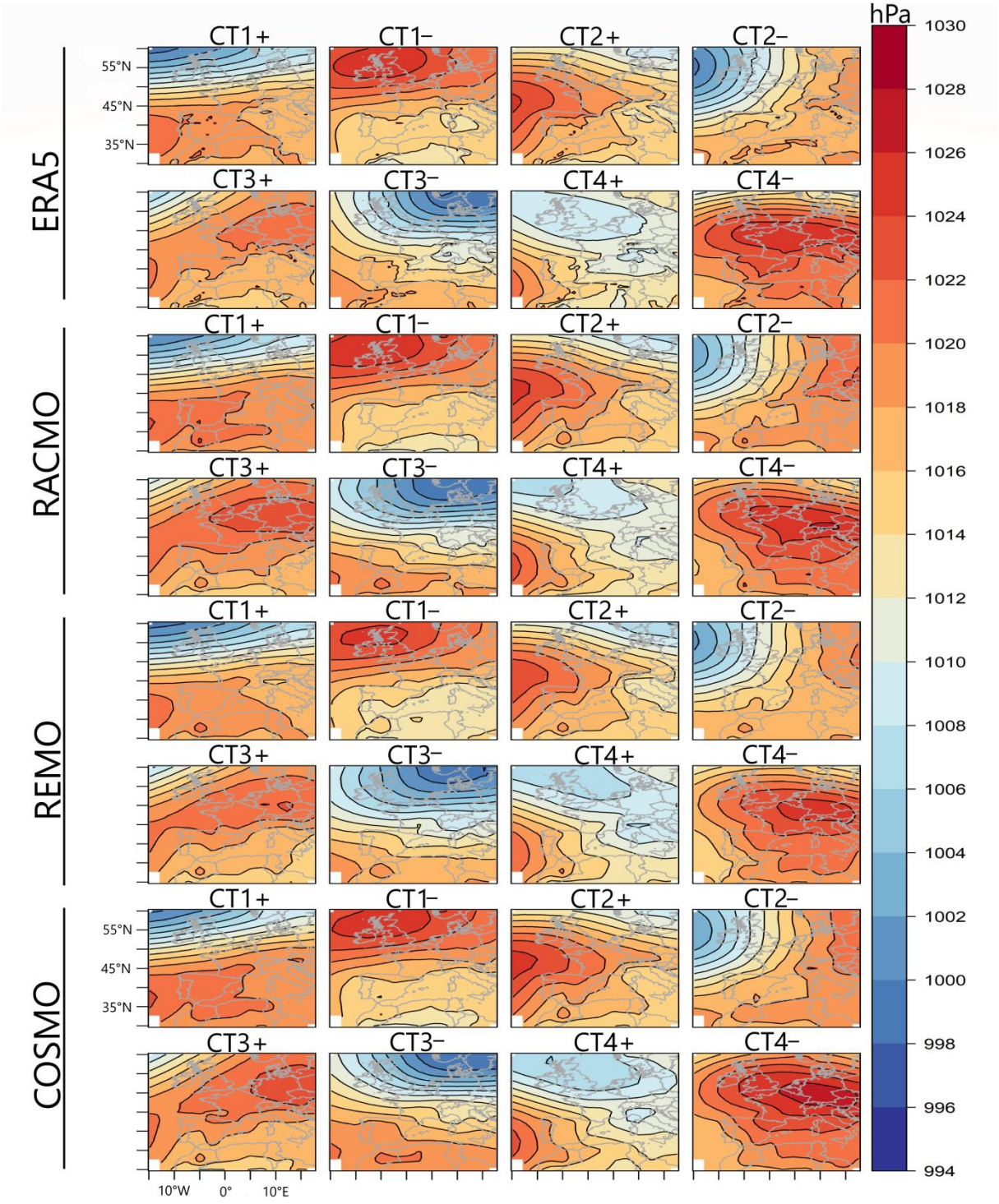

Figure 4.1: Circulation types from ERA5 and the regional climate models, driven by the ERA-Interim. The circulation types are the SLP composites of the days grouped under a given class.

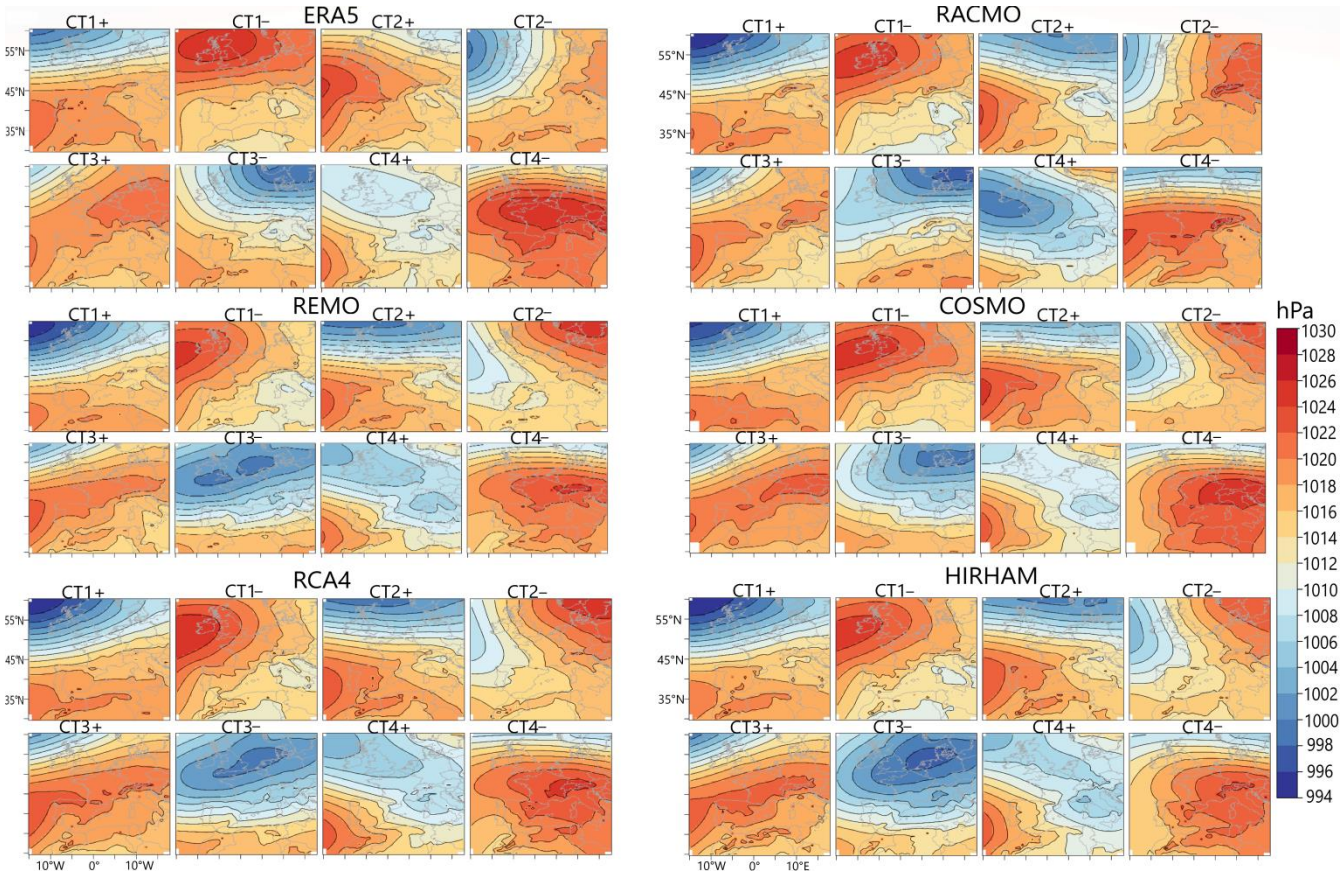

Figure 4.2: Circulation types from ERA5 and the regional climate models, driven by the MPI-ESM-LR GCM. The circulation types are the SLP composites of the days grouped under a given class.

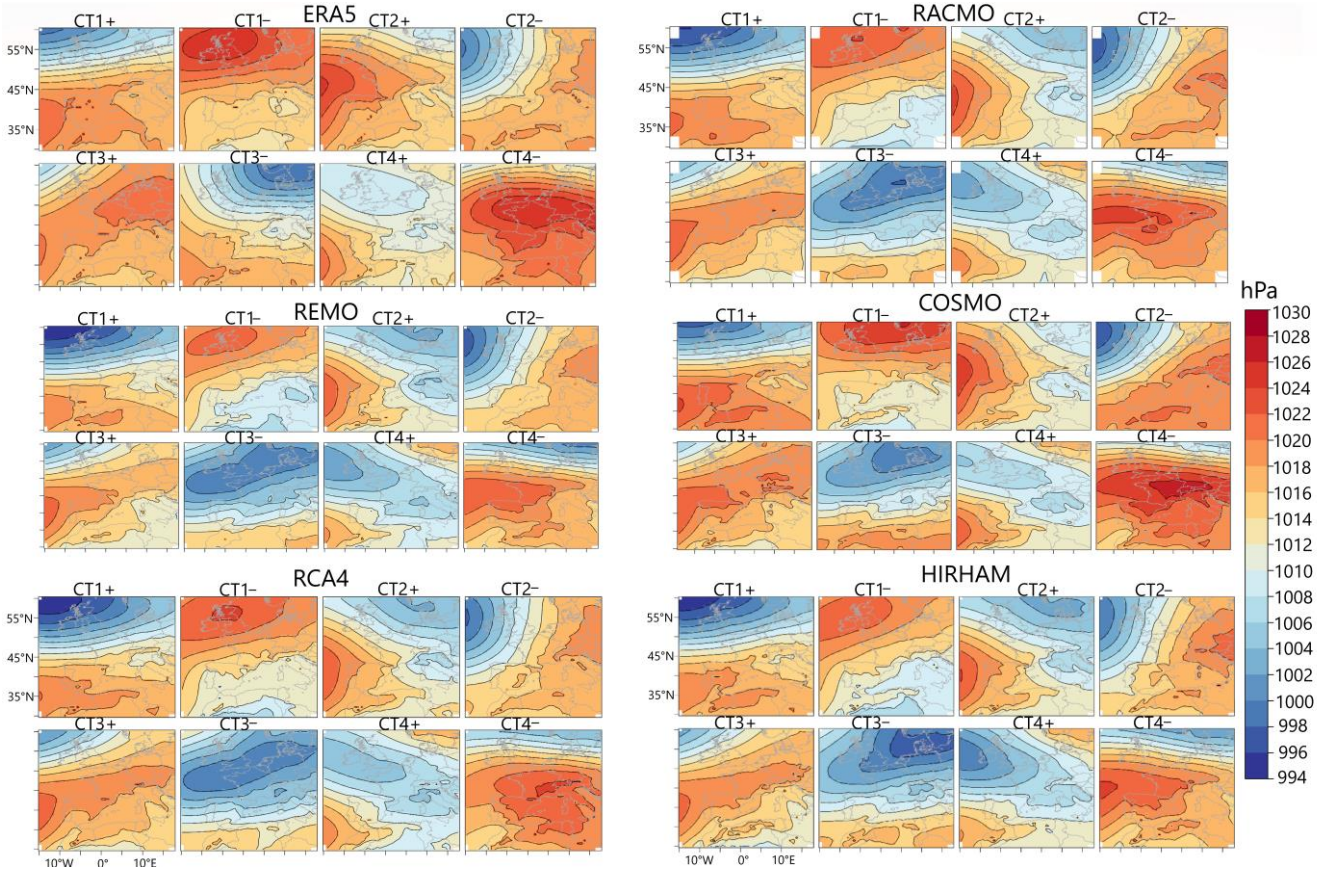

Figure 4.3: Circulation types from ERA5 and the regional climate models, driven by the CNRM GCM. The circulation types are the SLP composites of the days grouped under a given class.

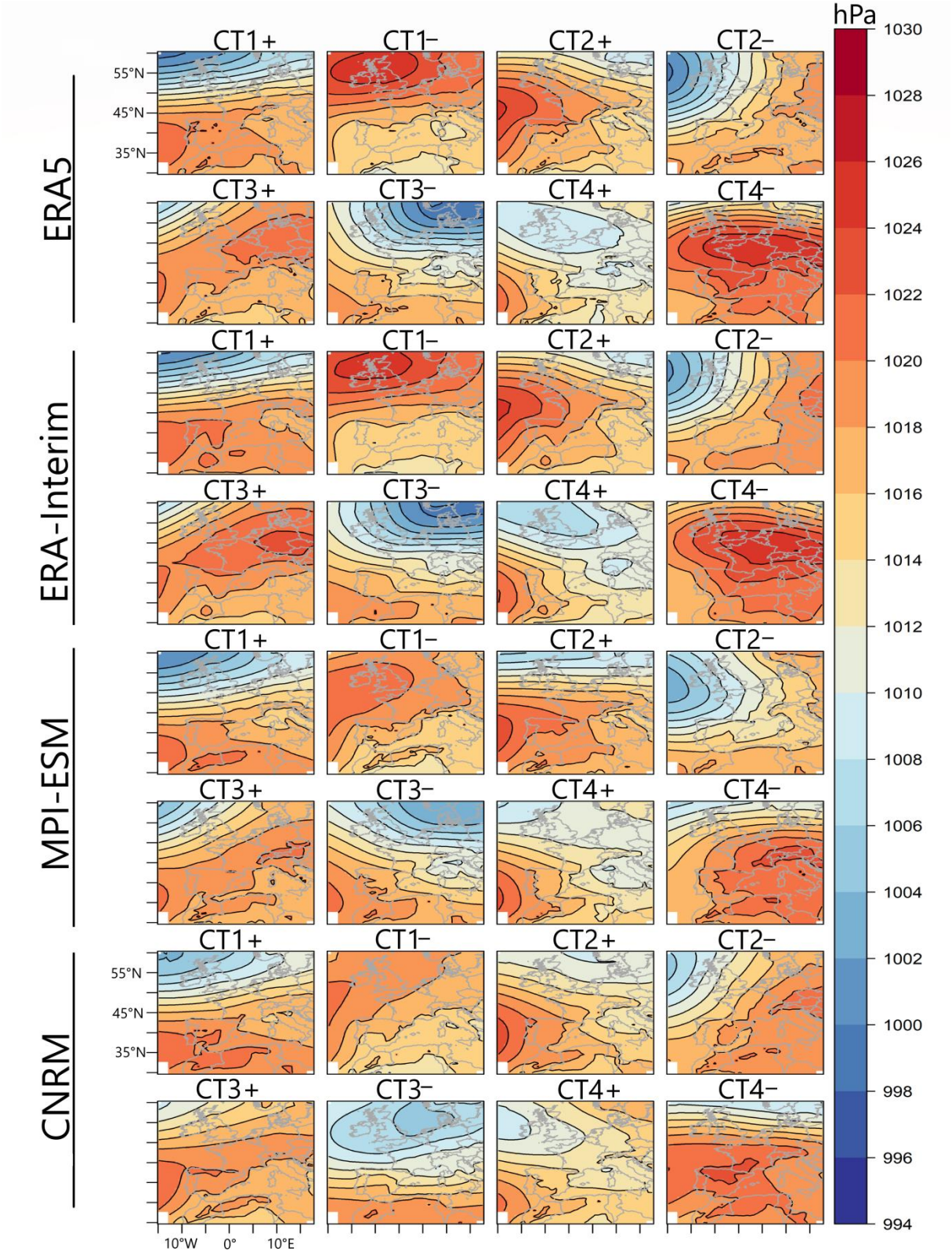

Figure 4.4: Circulation types from ERA5 and the multi-model ensemble mean output of the regional climate models driven by ERA-Interim, MPI-ESM-LR and CNRM GCMs.

Table 4.2: Explained variance (in %) of the PC patterns from ERA5 and the RCMs when driven by ERA-Interim, MPI-ESM-LR, and CNRM; and for the multi-model ensemble mean of the RCMs under each of the driving data.

Component	ERA5	RACMO	COSMO	REMO	HIRHAM	RCA4	ENSEMBLE
			ERA-Interim				
1	34.22	33.92	33.30	35.31	-	-	34.57
2	21.31	21.74	20.948	21.78	-	-	22.10
3	16.49	17.42	18.882	16.28	-	-	17.63
4	8.78	8.00	8.295	8.13	-	-	8.05
Total	80.80	81.08	81.429	81.51			82.34
			MPI-ESM				
1	-	37.63	37.39	39.72	38.11	39.99	44.79
2	-	20.77	20.34	20.07	20.25	19.90	19.94
3	-	15.95	16.47	14.50	15.78	15.25	13.20
4	-	7.97	8.14	8.19	8.11	7.67	7.05
Total	80.80	82.32	82.35	82.48	82.25	82.80	84.99
			CNRM				
1	-	32.94	33.01	34.18	33.35	34.84	35.47
2	-	21.41	20.85	21.10	20.88	18.86	22.45
3	-	15.53	15.91	15.22	15.66	16.78	14.97
4		9.18	9.69	9.06	9.06	9.05	8.85
Total	80.80	79.05	79.47	80.05	78.95	79.53	81.74

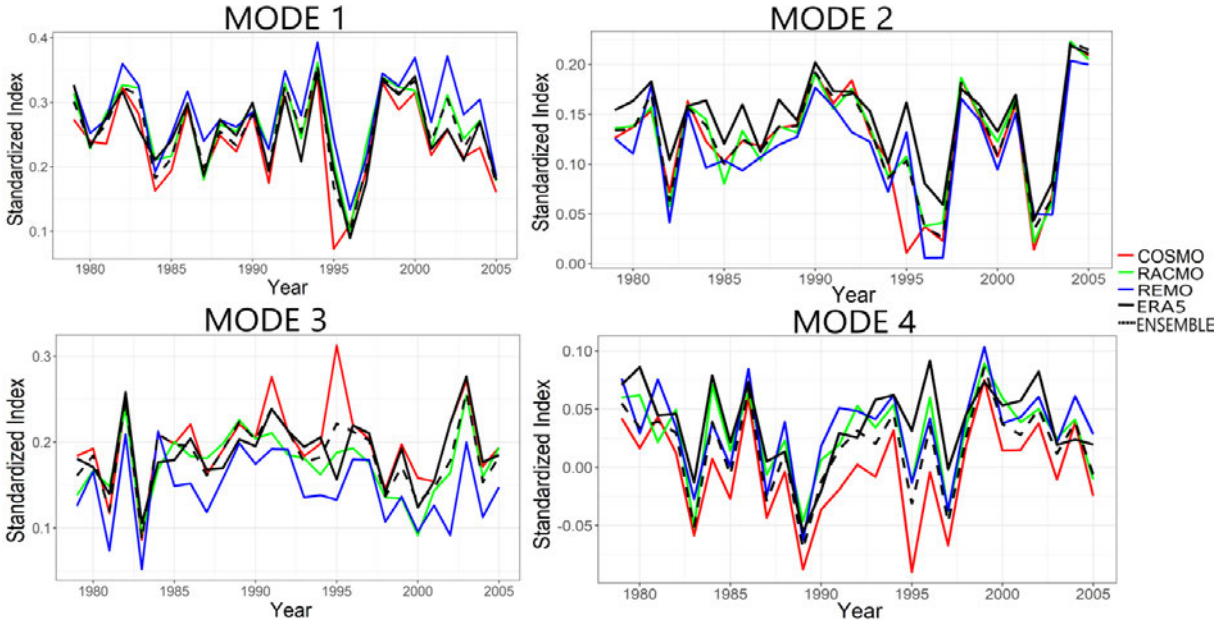

Figure 4.5: Annual mean loadings from classified ERA5 modes and the RCMs driven by ERA-Interim. The annual mean loading summarizes the inter-annual variability in the amplitude of the modes. Thick (dotted) lines represent the loadings from ERA5 (RCM ensemble mean). The time series is for the 1979 to 2005 period.

Table 4.3: Congruence match between the loadings of the modes from ERA5 and the same modes from the RCMs.

Data	**Mode 1**	**Mode 2**	**Mode 3**	**Mode 4**	**Average**
		ERA-Interim (RCM)			
COSMO	0.92	0.94	0.91	0.81	0.90
RACMO	0.94	0.95	0.90	0.82	0.90
REMO	0.93	0.94	0.90	0.83	0.90
		MPI-ESM (RCM)			
COSMO	0.24	0.21	0.28	0.08	0.20
RACMO	0.26	0.20	0.27	0.07	0.20
REMO	0.25	0.14	0.26	0.00	0.16
HIRHAM	0.27	0.21	0.28	0.06	0.21
RCA4	0.24	0.27	0.28	0.04	0.21
		CNRM (RCM)			
COSMO	0.26	0.15	0.20	0.06	0.17
RACMO	0.27	0.26	0.31	0.14	0.25
REMO	0.26	0.24	0.30	0.07	0.22
HIRHAM	0.28	0.25	0.30	0.06	0.22
RCA4	0.24	0.27	0.27	0.07	0.21
		ENSEMBLE (RCM)			
ERA-Interim	0.95	0.97	0.94	0.87	0.93
MPI-ESM	0.30	0.29	0.23	0.11	0.23
CNRM	0.32	0.30	0.34	0.08	0.26

5. Impact of the linear scaling bias correction technique on regional climate models

The LS technique is the simplest BC technique designed to adjust systematic biases in the mean statistic of the data. Shrestha et al. (2017) reported that the LS technique can be sufficient to adjust systematic biases in model output at a monthly resolution. However, there are speculations that for a highly variable parameter like precipitation, such a scaling technique that changes how much precipitation is allowed in each grid box can alter some aspects of the physical consistency in the field; for example, the variability in the simulated meteorological patterns, and the effects of microphysical and dynamical cloud processes on precipitation might be altered (Maraun 2016). In this chapter, the impact of the LS technique on the statistical characterization and the simulated meteorological patterns of monthly precipitation are examined. The results are exemplified during the MJJA season when Germany averages the highest rainfall (Figure 2.2). Also, considering the availability period of the RCMs driven by ERA-Interim that is used to evaluate the quality of the RCMs, against when the same RCMs are driven by GCM data, the analysis period is 1979 to 2005. The analysis period is divided into 1979 to 1992, and 1993 to 2005. The BC transfer function is obtained for each period (that is, the training period), and then applied to the other period (that is, the validation period). Thus, the complete analysis period is bias-corrected based on Equation (3.1). The correction factor is obtained and applied at each grid point in the study region to address the spatial heterogeneity of precipitation.

5.1 Impact of the linear scaling technique on the statistics of monthly precipitation

The performance of the LS bias correction approach in reducing the precipitation biases at each grid point in Germany is shown in Figure 5.1 and Table 5.1. During MJJA, the raw RCMs simulated the monthly precipitation estimates in Germany with some biases.

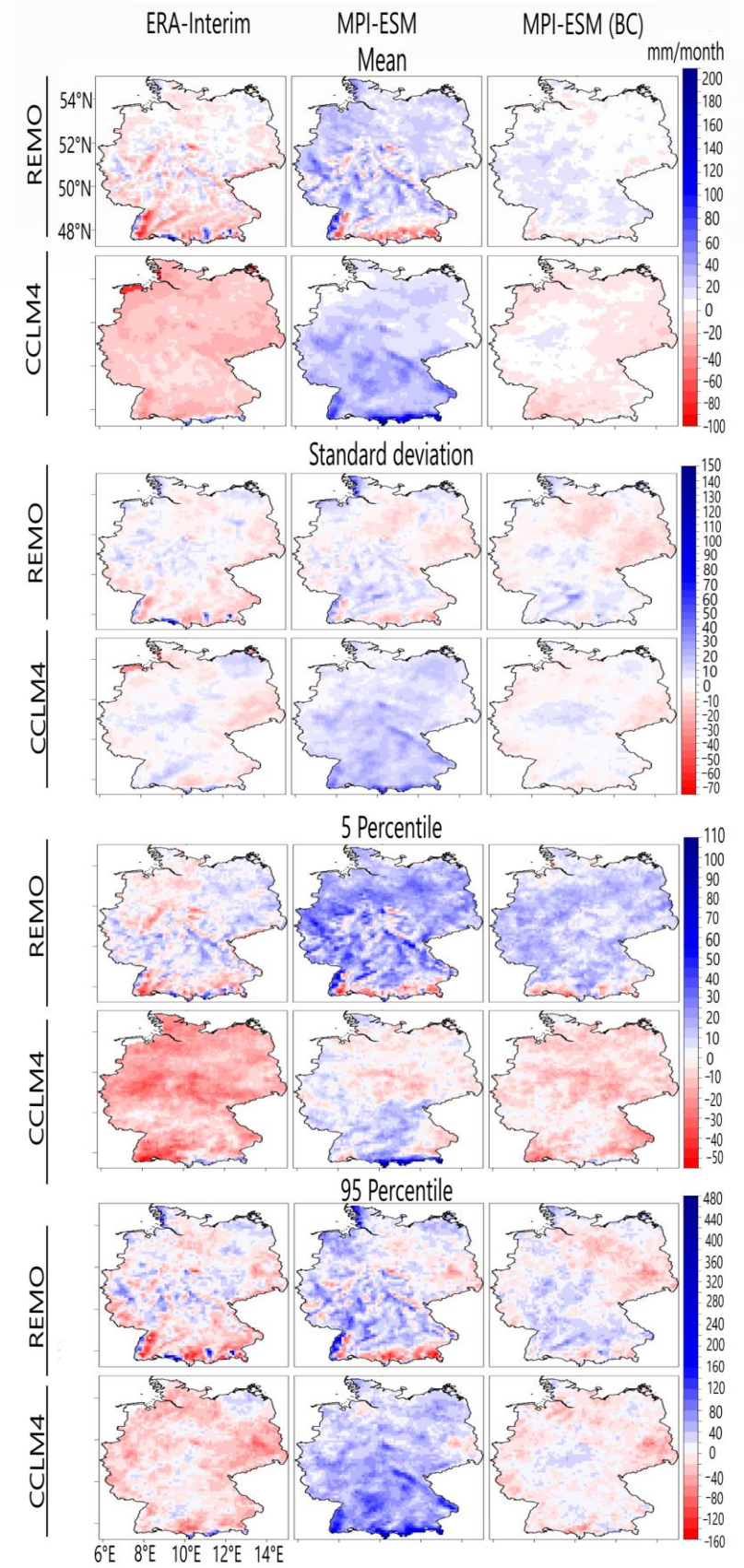

Figure 5.1: Validation of the linear scaling technique for the 1993 to 2005 period. Biases are computed as precipitation estimates from RCM minus observed values from E-OBS. Copyright © [2022b] [Ibebuchi et al.]. All rights reserved.

Table 5.1: Spatial correlation coefficient (r), and mean absolute error (MAE), in mm/month, for the basic spatial statistics of the RCMs compared to E-OBS before and after bias correction of the RCMs driven by MPI-ESM-LR, for the 1993 to 2005 validation period. The bias correction is based on linear scaling. SD implies standard deviation.

Data	**MAE**	**r**
	Mean	
REMO (ERA-Interim)	10.86	0.66
REMO (MPI-ESM RAW)	21.5	0.52
REMO (MPI-ESM BC)	8.63	0.97
CCLM4 (ERA-Interim)	14.4	0.93
CCLM4 (MPI-ESM RAW)	28.3	0.90
CCLM4 (MPI-ESM BC)	3.17	0.98
	SD	
REMO (ERA-Interim)	5.21	0.43
REMO (MPI-ESM RAW)	5.43	0.42
REMO (MPI-ESM BC)	4.72	0.81
CCLM4 (ERA-Interim)	4.20	0.63
CCLM4 (MPI-ESM RAW)	10.6	0.80
CCLM4 (MPI-ESM BC)	2.53	0.87
	5 percentile	
REMO (ERA-Interim)	6.47	0.71
REMO (MPI-ESM RAW)	21.09	0.41
REMO (MPI-ESM BC)	14.4	0.79
CCLM4 (ERA-Interim)	10.12	0.88
CCLM4 (MPI-ESM RAW)	11.2	0.88
CCLM4 (MPI-ESM BC)	3.62	0.90
	95 percentile	
REMO (ERA-Interim)	21.82	0.53
REMO (MPI-ESM RAW)	25.75	0.50
REMO (MPI-ESM BC)	11.38	0.90
CCLM4 (ERA-Interim)	16.01	0.85
CCLM4 (MPI-ESM RAW)	45.23	0.84
CCLM4 (MPI-ESM BC)	10.04	0.91

Figure 5.1 and Table 5.1 show that when the RCMs are driven by ERA-Interim, the precipitation estimates are closer to observed values, compared to when they are driven by MPI-ESM. Moreover, the MPI-ESM has been reported to be characterized by wet bias over Europe (Teichmann et al. 2013), and in chapter 4, it was found that the MPI-ESM model has a deficiency in simulating anticyclonic circulations (that is, the synoptic pattern associated with dryness) over Western Europe. The wet bias is evident from the mean precipitation values in Figure 5.1 from both the REMO and CCLM4 RCMs. This follows the result from chapter 4 that the GCMs are characterized by circulation biases that are propagated in the RCMs used to downscale the GCMs. The stronger biases in REMO might be due to challenges in simulating orographically induced precipitation over the Rhine valley and Black Forest region (Feldmann et al. 2008). Also, compared to CCLM4, REMO has a low spatial correlation, probably due to the missing precipitation advection (Table 5.1). Further, Table 5.1 and Figure 5.1 suggest that the biases for REMO and CCLM4 have different causes.

The results from Table 5.1 and Figure 5.1 indicate that the systematic biases in the statistics of simulated precipitation were reduced by the LS technique. The LS technique improved the spatial variation of precipitation, measured by the spatial correlation coefficient between simulated and observed values in Germany during MJJA. Also, the mean values and extreme value statistics (that is, the 5 and 95 percentile precipitation values) of the simulated precipitation were brought closer to the observed by the LS. The added value of the LS is relatively less for the standard deviation of precipitation, especially for the REMO model. From Figure 5.1, there are few grid boxes where the LS increased the biases in the standard deviations. Nonetheless, Table 5.1 contains that when the spatial average is computed, improvement in the simulated standard deviation, following LS, can be inferred since the grid boxes where the LS technique increased the biases are relatively few. The results equally indicate that the BC performance can be dependent on the choice of RCM.

For example, under CCLM4, the largest contribution to the overall bias (that is, the MAE) is coming from a few isolated grid points, mostly in the southernmost parts of Germany, and when these biases are reduced, the precipitation estimates from the RCM become quite closer to the observed.

The results in this section, concerning the capability of the LS technique to improve the basic statistics of the simulated precipitation estimates over Germany, are not limited to the analyzed RCMs, the analyzed period, and the analyzed variable. Figure A3 and Figure A4 show that for an ensemble of RCMs, there are marked improvements from the LS technique in adjusting the systematic biases for all seasons, in a longer time frame, both for monthly precipitation and temperature, respectively.

5.2 Precipitation variability patterns in Germany and the associating mechanisms

Figure 5.2 shows the spatial patterns of the homogeneous regions of MJJA precipitation anomalies in Germany from ERA5 and E-OBS. Following the application of the rotated S-MD PCA, only rotated PCs that match the correlation patterns with a minimum congruence coefficient of 0.92 are retained. Hence following this criterion that ensures that the retained modes can be physically interpreted, four regions are classified which represent the western part of Germany (R1), the southeastern part including the Bavarian Alps (R2), the eastern part (R3), and the northern and northwestern parts that are close to the North Sea and the Baltic Sea (R4). The central part of Germany is characterized by an overlap of these four regions and hence, indicates the fuzziness of precipitation and its governing processes, supporting the idea of a transition zone with varying rain-producing or inhibiting influences. Based on the E-OBS data, those four retained PCs explain ~75% of the variance of MJJA precipitation in Germany. From Figure 5.2, though the loading magnitudes appear to differ, E-OBS and ERA5 have comparable patterns. The precipitation data from ERA5 is a product of data

assimilation that can be biased because of systematic and random errors from the observations, the forecast model, and the observation operator when converting model fields to equivalent precipitation observation (Janjic et al. 2017). The differences in isopleths of the observed and assimilated patterns in Figure 5.2 reflect the basic differences in precipitation between the models and observations Nonetheless, Table 5.2 shows that there is a good congruence match between the variability patterns as obtained from the ERA5 and E-OBS data. Thus, the E-OBS patterns are externally validated using ERA5 reanalysis data, and in subsequent analysis, the focus will be on the precipitation variability patterns observed from E-OBS.

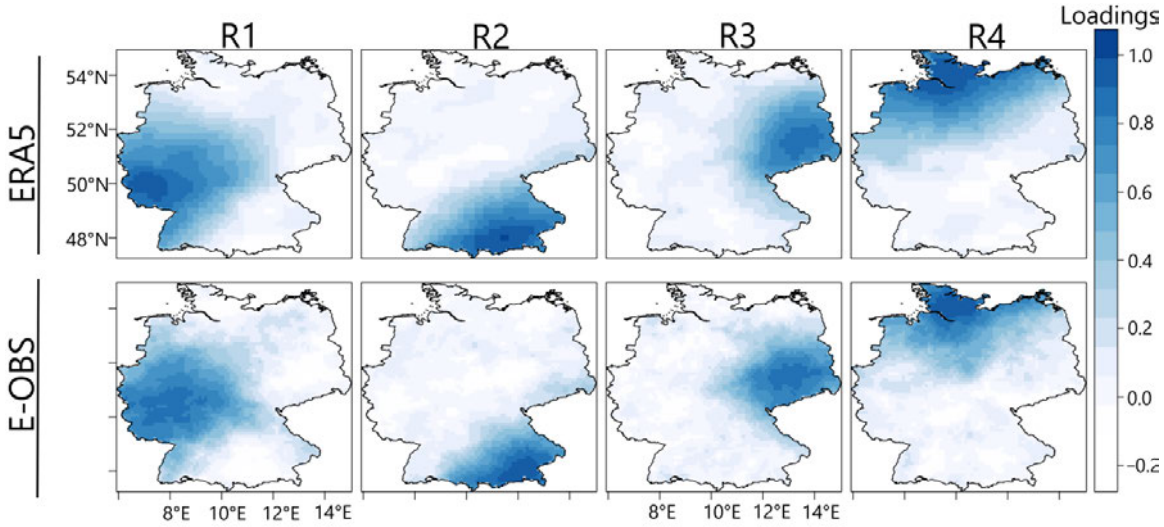

Figure 5.2: Variability patterns of MJJA precipitation anomalies in Germany from E-OBS and ERA5 for the 1979 to 2020 period.

Figure 5.2 shows that some precipitation regions have varying loading magnitudes, for example in the western region (R1), the loadings for the southwest are lower than in other domains in R1. The heterogeneity of the loading magnitudes in each region can be an indication that the co-variability of the grids has different extents. Even though a significant effort is made by the classification to simplify the spatial complexity of the precipitation field, the imprecise nature of the processes leading to the development of the regions can imply also that the governing mechanism of precipitation is expected to be generally homogeneous for a

given region (at least at the synoptic scale), nonetheless, spatial heterogeneity of precipitation can still be expected within a classified homogeneous region. This can be because of the local effects that modify the synoptic processes, which can translate, for example, to different precipitation amounts in each homogeneous region.

Table 5.2: Congruence coefficient between the variability patterns of MJJA precipitation anomalies in Germany from E-OBS and ERA5 for the 1979 to 2020 period.

Region	**Congruence coefficient**
R1	0.97
R2	0.95
R3	0.96
R4	0.97

To diagnose the physical processes associated with the time development of the precipitation regions in Figure 5.2, Figure 5.3 shows the spatial patterns of wind and SLP anomalies during the positive and negative phases of the homogeneous precipitation regions. For diagnosis of which phase in Figure 5.3 is dry or wet concerning the region in question, the associating precipitation composite anomaly maps are created in Figure 5.4. In the western region (R1), the positive phase indicates a widespread cyclonic anomaly over Germany and the maritime regions. The wind anomalies are mostly southwest over the western domains. Figure 5.4 indicates that the positive phase of the western region is wet in the domains classified under it, whereas the negative phase comes along with dry conditions. From Figure 5.3, an anticyclonic anomaly dominates over Germany and the North Sea during the negative phase of the western region. The wind anomaly is dominantly northerly in the negative phase. The anticyclonic anomaly over the North Sea is equally an indication of suppressed convection.

Under the R2 regime (that is, the southeastern region), Figure 5.3 shows a weak pressure gradient between the North Sea and the southeastern parts of Germany. During the positive (negative) phase, a positive (negative) SLP anomaly is evident over the North Sea; as a result, the wind patterns are northwest (southerly) towards the regions of a relative enhanced cyclonic anomaly. In combination with orographic effects along the northern Alps, these patterns associated with the positive (negative) phase of R2 bring wet (dry) conditions over southern Germany. A further reason for the difference between the precipitation in the positive and negative phase includes that the lower pressure over southern Germany (in the positive phase of the southeastern region) steers moist air from the surrounding oceans into southeastern Germany.

Under the positive (negative) phase of the eastern region (R3), the pressure gradient indicates a cyclonic anomaly, situated at the south (widespread) over the landmasses in Germany; this results in maritime northeast winds from the Baltic Sea (dry continental easterly winds) over the landmasses in the eastern region (Figure 5.3). Thus, from Figure 5.4, the positive (negative) phase of the eastern region is wet (dry).

Under the positive (negative) phase of the northern/northwestern region (R4), a strong cyclonic (anticyclonic) anomaly dominates from the central to the northern parts of Germany. The wind patterns are dominantly southwest (northwest) towards the domains under the northern/northwestern region, resulting in wet (dry) conditions in the northern/northwestern region. The northerly wind anomaly during the negative phase is dry since it could be related to the anticyclone that develops over Scandinavia.

In summary, the positive (negative) phases of all four MJJA precipitation variability patterns denote wet (dry) conditions. The associated wind and SLP anomalies are in line with the basic understanding of rain-bearing (rain-suppressing) meteorological situations over Central Europe.

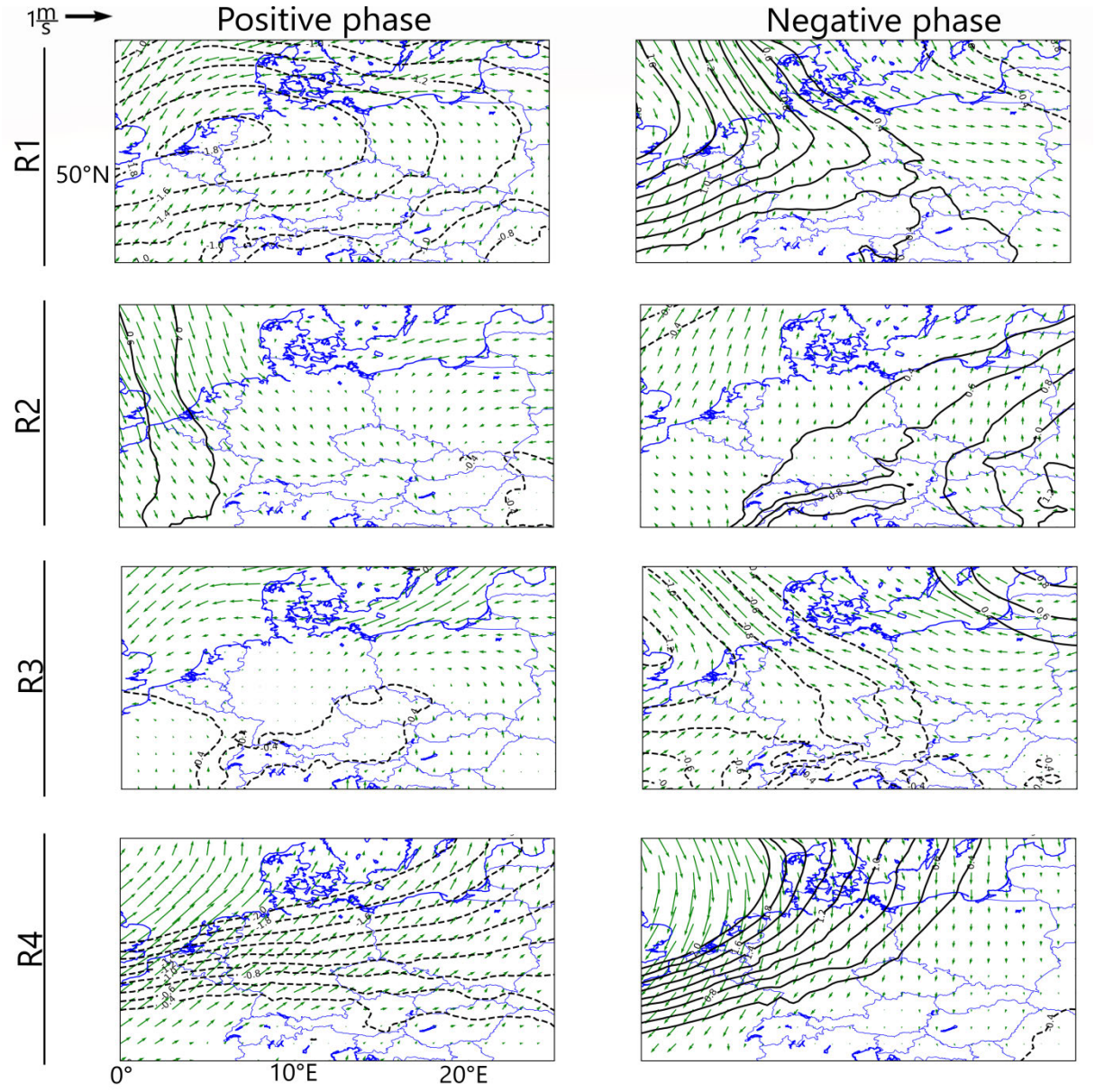

Figure 5.3: SLP and 10-meter wind anomalies during the positive and negative phases of the precipitation variability patterns in Figure 5.2. The green vectors denote wind anomalies, and the black contours indicate SLP in hPa. Contour interval is 0.2 hPa. Only values exceeding the 95% confidence limit based on the permutation test are plotted. Dashed (thick) contour lines indicate negative (positive) SLP anomalies. Anomalies are created with respect to the MJJA climatology.

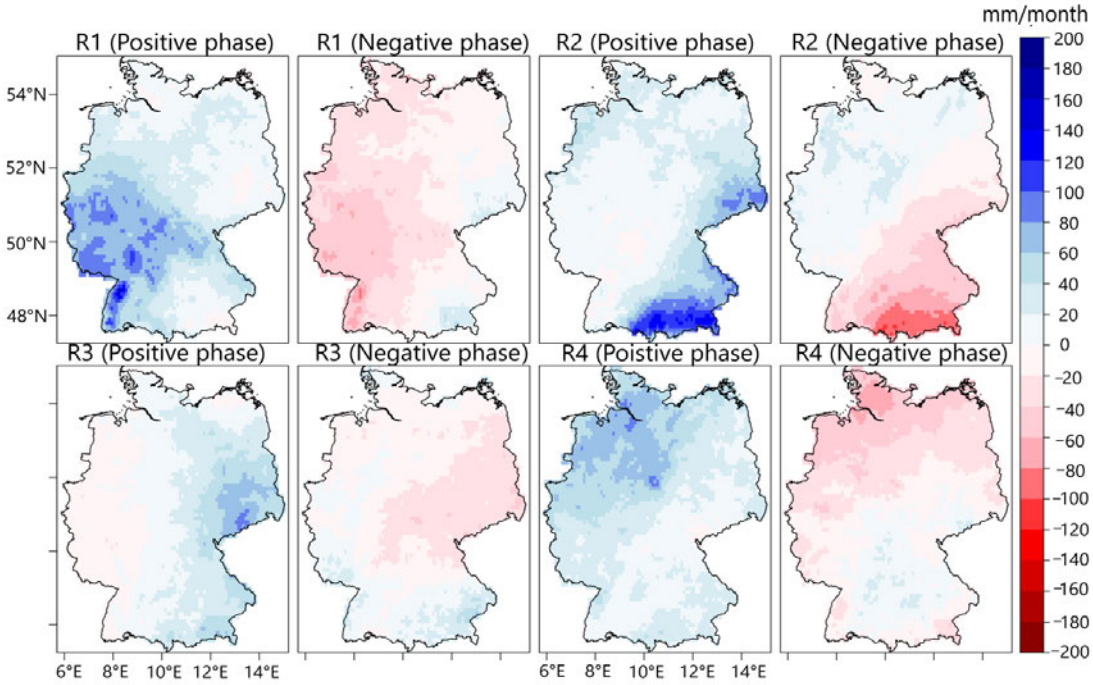

Figure 5.4: Precipitation composite anomaly patterns of the positive and negative phases of the variability patterns of MJJA precipitation anomalies in Germany in Figure 5.2

The positive and negative phases of all considered modes are mostly asymmetric. Also, there seems to be asymmetry in the contribution to the precipitation composites. This can be a consequence of the fuzzy and overlapping nature of the large-scale meteorological processes that cause precipitation: the synoptic-scale processes associated with the formation of precipitation at a given region, modified by local geographical effects such as orography, can extend to influence precipitation at other regions equally. In principle, the regions are not hard with step boundaries, especially when it comes to advective flow.

5.3 Impact of the linear scaling technique on the simulated meteorological patterns

From Figure 5.5, it is exemplified from the CCLM4 model that the observed precipitation regions from the E-OBS data can be replicated in the RCMs, though with biases (that is, spatial mismatch in the pattern configurations). As a spatial mode depends on the precise geographical location with the largest PC loadings and gradient of the pattern, the agreement

in geographical overlap and magnitude at each location, which is measured by the congruence matches, is the arbiter of success for the climate model in replicating the reference modes. Based on Table 5.3, the southeastern region is robustly captured by the RCM regardless of the data that provides the lateral boundary conditions. Also, from Table 5.3, the bias in representation of the observed pattern is higher under the northern/northwestern region. Moreover, unlike in chapter 4**,** where the representation of the CTs (created from the SLP field) is improved when reanalysis data provides the boundary conditions, there is no guarantee of such improvement (that is, when reanalysis is used as the driving data) for the precipitation variability patterns shown in Figure 5.5. For example, from Table 5.3, the representations of R3 and R4 were better when MPI-ESM provides the lateral boundary conditions. A possible reason for the results is that, unlike SLP, precipitation is a highly variable parameter and due to observational uncertainty, the model physics, and limited model resolution, the variability of precipitation cannot be fully captured in models. Moreover, differences in the variability of precipitation due to small differences in the variance structure arising from spatiotemporal interpolation errors, data handling, and so forth can lead to differences in the structure of the PCs.

The impact of the LS technique on the simulated meteorological patterns can be equally assessed in Table 5.3 and Figure 5.5. Interestingly, all the individual variability patterns were reproduced after the BC which at least suggests that the LS technique does not constrain the reproducibility of the simulated meteorological patterns from the CCLM4 model. Based on the congruence matches in Table 5.3 and cursory investigation of the maps in Figure 5.5, there is no robust indication that (at a larger scale) the LS technique impacted the overall structure of the simulated meteorological patterns from the CCLM4 model. However, a close cursory investigation of the variability patterns, for example in R2, shows that the isopleths were changed by the LS technique, relative to the patterns from the raw RCM. This is an

indication that at smaller spatial scales (for example, mesoscale or less), there is the possibility that the LS technique can change the co-variability of the regions and the simulated (local) governing mechanisms.

Table 5.3: Congruence coefficient between the variability patterns of MJJA precipitation anomalies in Germany classified from E-OBS and their counterparts from the CCLM4 RCM with different forcing for the 1979 to 2005 period.

Data	**R1**	**R2**	**R3**	**R4**
MPI-ESM (RAW)	0.90	0.93	0.94	0.85
MPI-ESM (BC)	0.91	0.92	0.94	0.85
ERA-Interim	0.95	0.96	0.87	0.79

The PC scores are used to find the dates when the variability patterns occurred, either in the observed or simulated climate depending on the data that was spatially decomposed. Hence it is necessary that to preserve the physical (temporal) consistency of the spatially decomposed precipitation data, the PC scores after BC should be comparable with the PC scores before the BC, otherwise, the dates in the simulated data when a variability pattern occurred will be inconsistent after the BC. In the simplest explanation, it is a sufficient achievement that if on a given date, and due to misrepresentation of weather patterns, the date exhibits wet biases in the RCM, but after the BC, the wet biases are reduced, but not to the extent of misrepresenting the variability patterns that occurred at that date. In principle, it should be documented that the variability pattern occurred at that date but the BC improved the “actual” resulting precipitation amount that should have been simulated on that date, assuming the climatology of the variability patterns is comparable with observations. This is the idea behind requiring that the univariate BC does not notably change the PC scores (both the sign and magnitude) compared to the raw RCM. In chapter 4, it was concluded that climate models (that is, RCMs driven by GCM) have no skill to simulate the temporal sequence of the

reference CTs. Thus, it is not even a worthy goal to require that the simulated PC scores of the variability patterns from the RCM driven by MPI-ESM, in Figure 5.5, are adjusted towards observations after the BC. Also, in chapter 4, it was found that the RCMs have the skill to reproduce the climatological mean of atmospheric circulations. Hence if the BC improved the geographical overlap between the simulated and reference patterns, that is an added value, but the temporal consistency before and after BC should be maintained, though this is not guaranteed because any changes in the PC loadings are propagated into the PC scores.

The PC loadings and the standardized field are used to create the PC scores, as shown in Equation (3.9). Further, Table 5.4 indicates that the spatiotemporal configuration of the simulated meteorological pattern from the bias-corrected data is more or less the same as the same patterns from the raw RCM. The congruence matches of the PC loadings (and PC scores) from the LS output are in the excellent range with the same PC loadings (and PC scores) from the raw CCLM4 RCM (Table 5.4). Despite the scaling of the precipitation at each grid box, following the BC, the PC scores, are comparable in the corrected and raw data. This is because there are no large changes in the magnitude and configuration of the PC loadings after the BC (Table 5.4). Figure 5.6 shows the inter-annual time series of the PC scores before and after the BC, indeed there are small disparities in the absolute value of the PC scores from the raw and bias-corrected data. This is promising because it suggests that though there are some changes in the amplitude of the variability patterns, generally the changes are not so large and the temporal pattern matches, in the (un)corrected CCLM4 model, are in the excellent range (Table 5.4).

Table 5.4: Congruence match between the same respective PC scores, and PC loadings of the variability patterns of MJJA precipitation anomalies in Germany from the raw and bias-corrected CCLM4 RCM for the 1979 to 2005 period

PC	**R1**	**R2**	**R3**	**R4**
Scores	0.99	0.99	0.99	0.99
Loadings	1.00	0.99	1.00	1.00

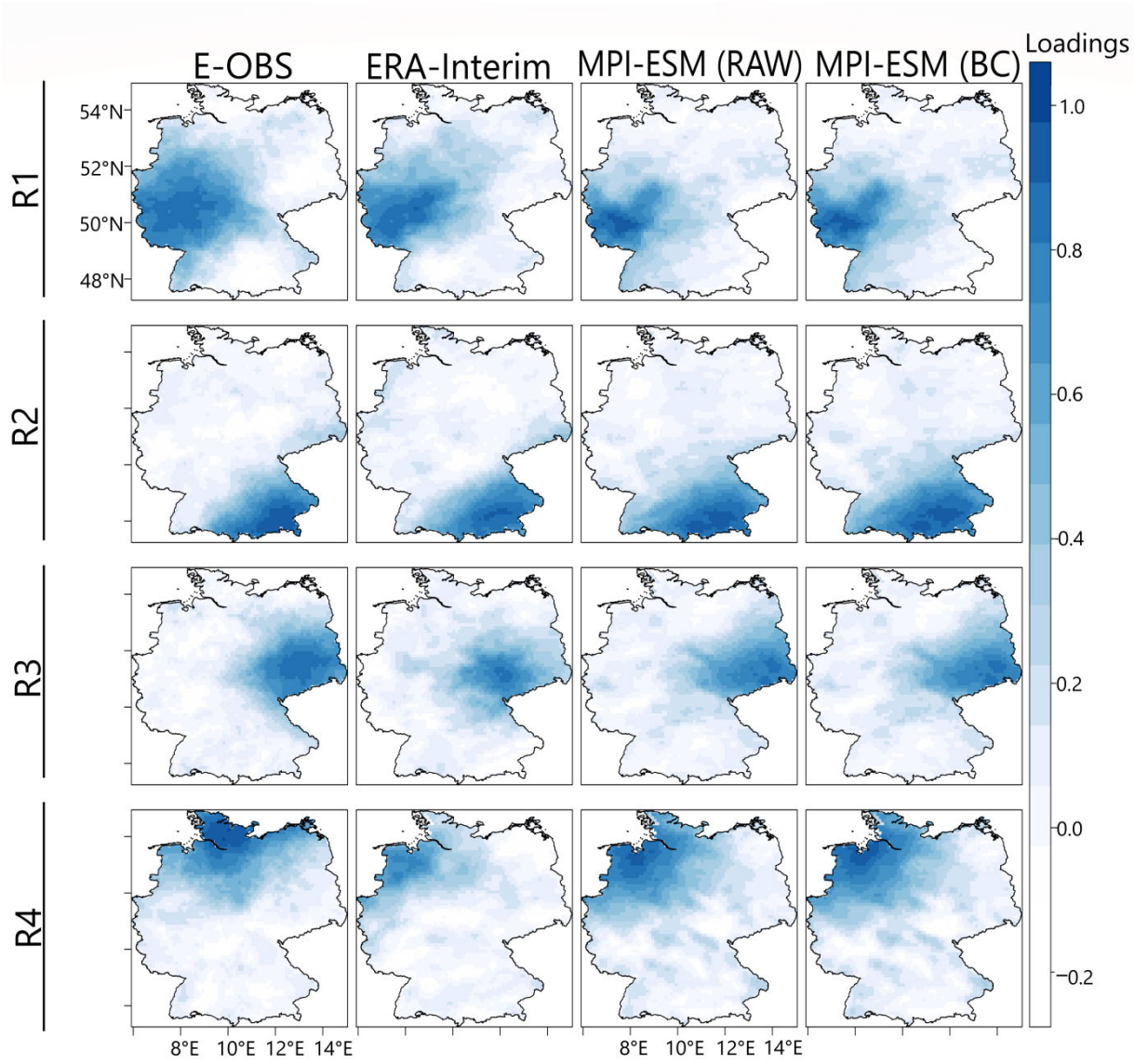

Figure 5.5: Variability patterns of MJJA precipitation anomalies in Germany from E-OBS and as simulated in the CCLM4 RCM for the 1979 to 2005 period. The simulations are for the ERA-Interim driven RCMs, MPI-ESM-LR driven RCMs for raw and bias-corrected data.

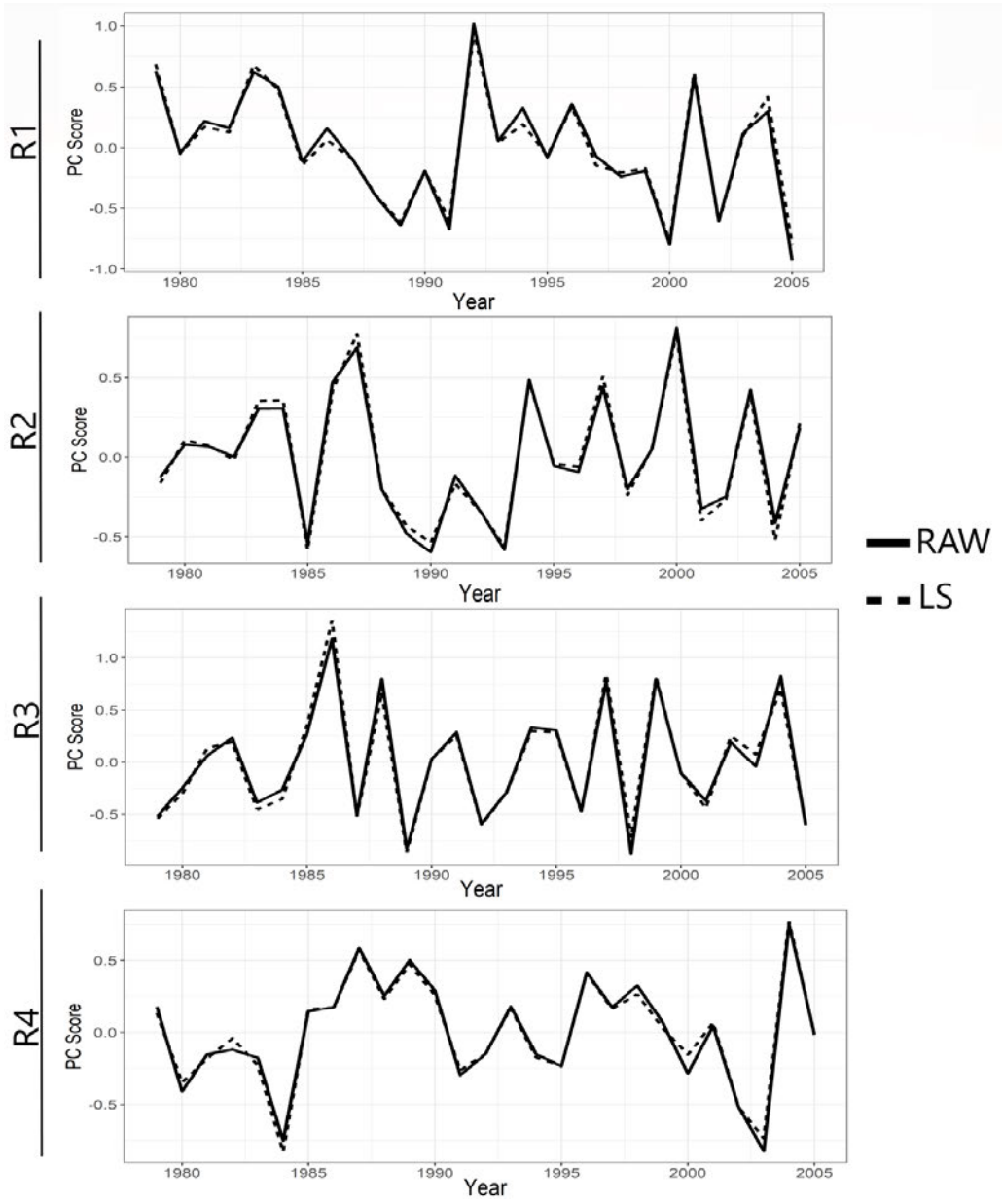

Figure 5.6: PC scores of the variability patterns of MJJA precipitation anomalies in Germany from the CCLM4 RCM driven by MPI-ESM-LR before and after bias-correction with the linear scaling technique for the 1979 to 2005 period.

From Figure 5.7, even after the BC with the LS technique, similar to Figure 5.4, the asymmetries of the precipitation composites associated with the individual meteorological patterns were replicated using the corrected CCLM4 precipitation data. Since the PC scores from the corrected CCLM4 precipitation data (that is, the LS output) can still find representative dates when the positive and negative phases of a given variability pattern

in Figure 5.5 were expressed, it is a further confirmation that the bias-corrected data still have a significant extent of (temporal) consistency with the simulated governing large-scale mechanisms associated with the precipitation patterns. Nonetheless, compared to observations (that is, Figure 5.4) Figure 5.7 reproduced the precipitation composite anomaly patterns with biases, especially for the dry phase of the western region (R1). Also like Figure 5.3, the simulated composite anomaly maps of the dates assigned to a given variability pattern (that is, the simulated wind and SLP anomaly patterns) were comparable with observations mostly for the wet phases of the variability patterns (Figure A5). The pattern configurations for the dry phases of the variability patterns were mostly misrepresented given that the SLP and wind vector composite anomaly patterns are not much comparable with the observed patterns in Figure 5.3, and at the synoptic scale, this can be a reason for the wet bias in the precipitation field: the models do not sufficiently simulate portions of large-scale anticyclonic circulations and the resulting dry regimes over Germany. For the CCLM4 model and within the analysis constraints in this study, the exception to the deficiency in simulating the dry regimes of the variability patterns is the eastern region (R3) which has the highest congruence match with the observed pattern (Table 5.3). Figure 5.7 and Figure 5.8 shows that the observed precipitation composite anomaly pattern, SLP, and wind vector composite anomaly patterns during the dry and wet phase of R3 are simulated by the CCLM4 model and reproduced with the PC scores from the LS approach. As observed from Figure 5.3, the CCLM4 model reproduced in Figure 5.8 that in the climatology of R3, northeast winds from the Baltic Sea bring wet conditions to the eastern region during summer, and dry continental easterly winds bring dry conditions to the eastern region. The PC scores from the LS output also reproduced composite anomaly patterns of the wet phases of the western region (R1), southeastern region (R2), and northern/northwestern region (R4) that are also consistent with observations (Figure A5). Thus, for the analyzed RCM, while the LS does not improve the misrepresentation of processes related to precipitation variability in Germany, when the large-scale processes that

govern the precipitation variability are sufficiently simulated, the LS output (that is, the bias-corrected precipitation field) can be expected to be consistent with the large-scale governing mechanisms to a significant extent. However, depending on the grid boxes and how much the LS changed the precipitation amounts, some inconsistency between the precipitation field and other smaller scale variability can be introduced, which can equally be deduced from the localized changes in the co-variability of the grids in Figure 5.5.

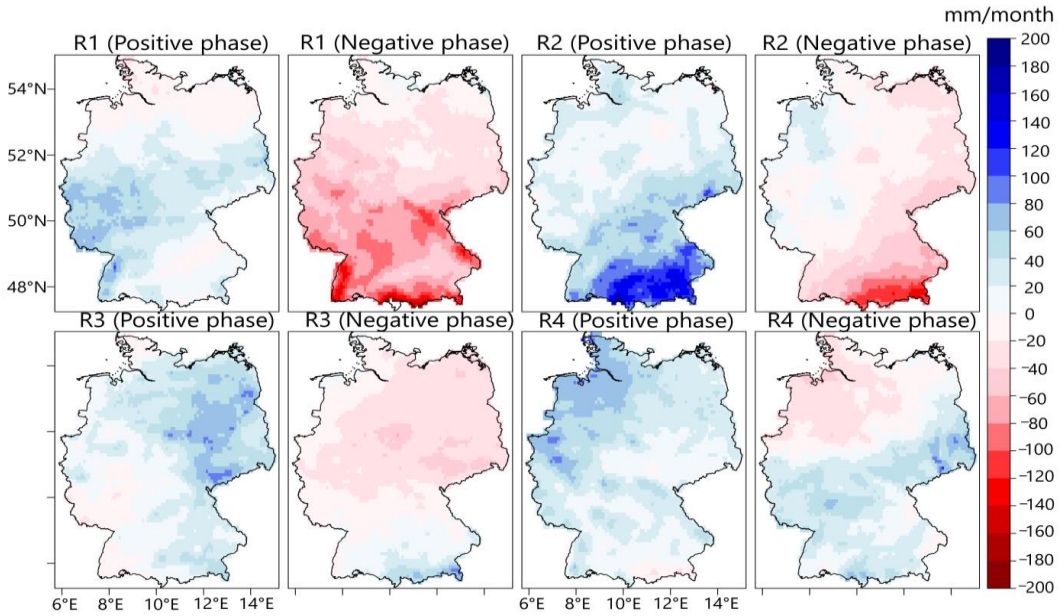

Figure 5.7: Precipitation composite anomaly patterns of the positive and negative phases of the variability patterns of MJJA precipitation anomalies in Germany from the bias-corrected CCLM4 RCM driven by MPI-ESM-LR

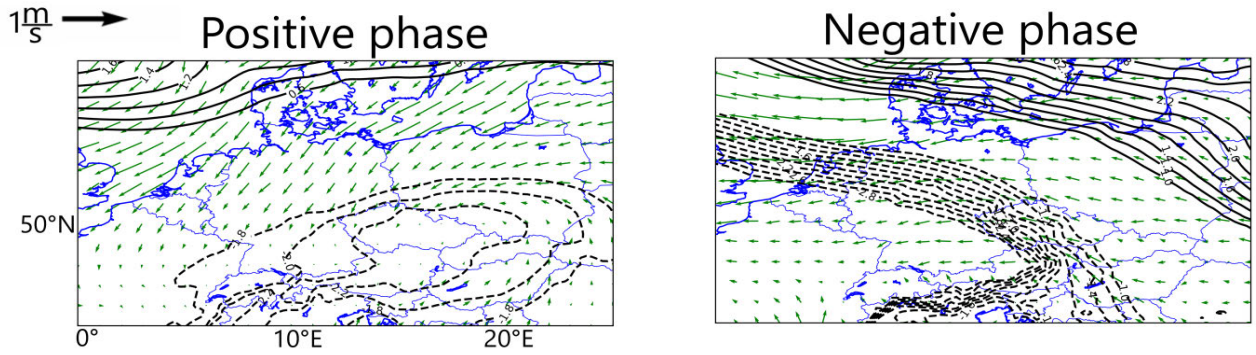

Figure 5.8: SLP (black contour) and 10-meter wind (green vectors) composite anomaly patterns of the eastern region (R3) variability pattern of MJJA precipitation anomalies from the bias-corrected CCLM4 RCM driven by MPI-ESM-LR. Dashed (thick) contour lines indicate negative (positive) SLP anomalies

Further, the LS technique is based on the assumption of a time-invariant or stationary correction factor. Under future climate change, strong climate change signals might imply that the correction factor obtained in the historical period becomes inapplicable in adjusting the future precipitation biases and might equally constrain the simulated meteorological patterns. Therefore, it is investigated if the assumption of a stationary correction factor constrains the reproducibility of the precipitation variability patterns under future climate change. Hence, the correction factor was obtained during the historical period and following the assumption of stationarity, was then applied to bias-correct the future precipitation under the highest warming scenario. Figure 5.9 suggests that the assumption of a time-invariant correction factor might not constrain the reproducibility of the simulated meteorological pattern of the bias-corrected future precipitation data. Under future climate change, Figure 5.9 shows that the patterns of the homogeneous precipitation regions were all reproduced, but with at least a borderline congruence match with the historical patterns. Since the congruence match between the patterns from the historical and the RCP8.5 scenario are not in an excellent range, some dissimilarity in the spatial configuration of the patterns can be inferred. Thus, three inferences can be made (1) since the patterns were reproduced under the RCP8.5 scenario, the basic meteorological processes that govern wet or dry conditions in Germany remain the same and lead to more or less the same homogeneous MJJA rainfall regions across the country as observed under present-day conditions, (2) the differences between the spatial structure of the historical and the RCP8.5 scenario patterns, suggest that while the meteorological processes associated with the development of the regions remain the same, climate change might be expected to impact some aspects of the governing meteorological processes, which translates to the future changes in the patterns, (3) model error in the different experiments, or assumption of a time-invariant correction factor, or the post-processing of the future data using LS, might also contribute to some of the differences between the spatial structure of the historical and the RCP8.5 scenario patterns.

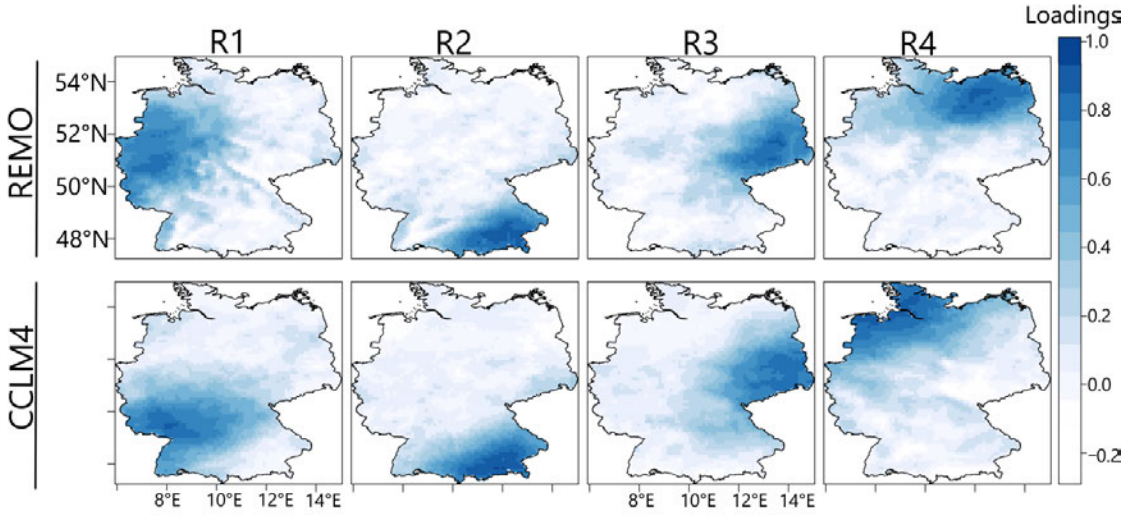

Figure 5.9: Variability patterns of MJJA precipitation anomalies in Germany as simulated by the REMO and CCLM4 RCMs, driven by MPI-ESM-LR, for the 2070 to 2100 period under the RCP8.5 emission scenario.

6. Evaluations of bias correction techniques in reducing the biases in the daily statistics of simulated precipitation and temperature

6.1 Performance of bias correction techniques in reducing simulated precipitation biases

Compared to when reanalysis data provides the lateral boundary condition, the daily precipitation amount is inflated when the RCMs are driven by MPI-ESM, increasing wet day biases (Table 6.1). Hence, like the precipitation data at the monthly resolution, at a daily resolution, the MPI-ESM model introduces more (wet) biases in the RCMs when it provides the initial and lateral boundary conditions. Figure A6 to Figure A7 show that for other RCMs in Table 3.1 and when the driving data is either MPI-ESM or CNRM, the models are characterized by wet biases, which is more notable under MPI-ESM in all calendar months.

Table 6.1: Mean absolute error in the temporal series, spatial series, and annual frequency of wet days from the REMO and CCLM4 RCMs against E-OBS for the 1989 to 2005 period.

Data set	Time (mm/day)	Spatial (mm/day)	Wet day bias (day/year)
CCLM4 (ERA-Interim)	1.18	0.26	12
CCLM4 (MPI-ESM)	2.95	0.47	58
REMO (ERA-Interim)	1.40	0.62	18
REMO (MPI-ESM)	2.79	0.81	44

The performances of three BC techniques in adjusting the biases in the statistics of daily simulated precipitation in Germany are assessed. The techniques are LS, EQM, and MQDM. Table 6.2 and Table 6.3 contain the MAE in the spatial mean and standard deviation of precipitation, before and after BC techniques are applied to the REMO and CCLM4 RCMs. Figure 6.1 and Figure 6.2 show the biases in the spatial mean and standard deviation of precipitation, respectively, exemplified from the REMO model.

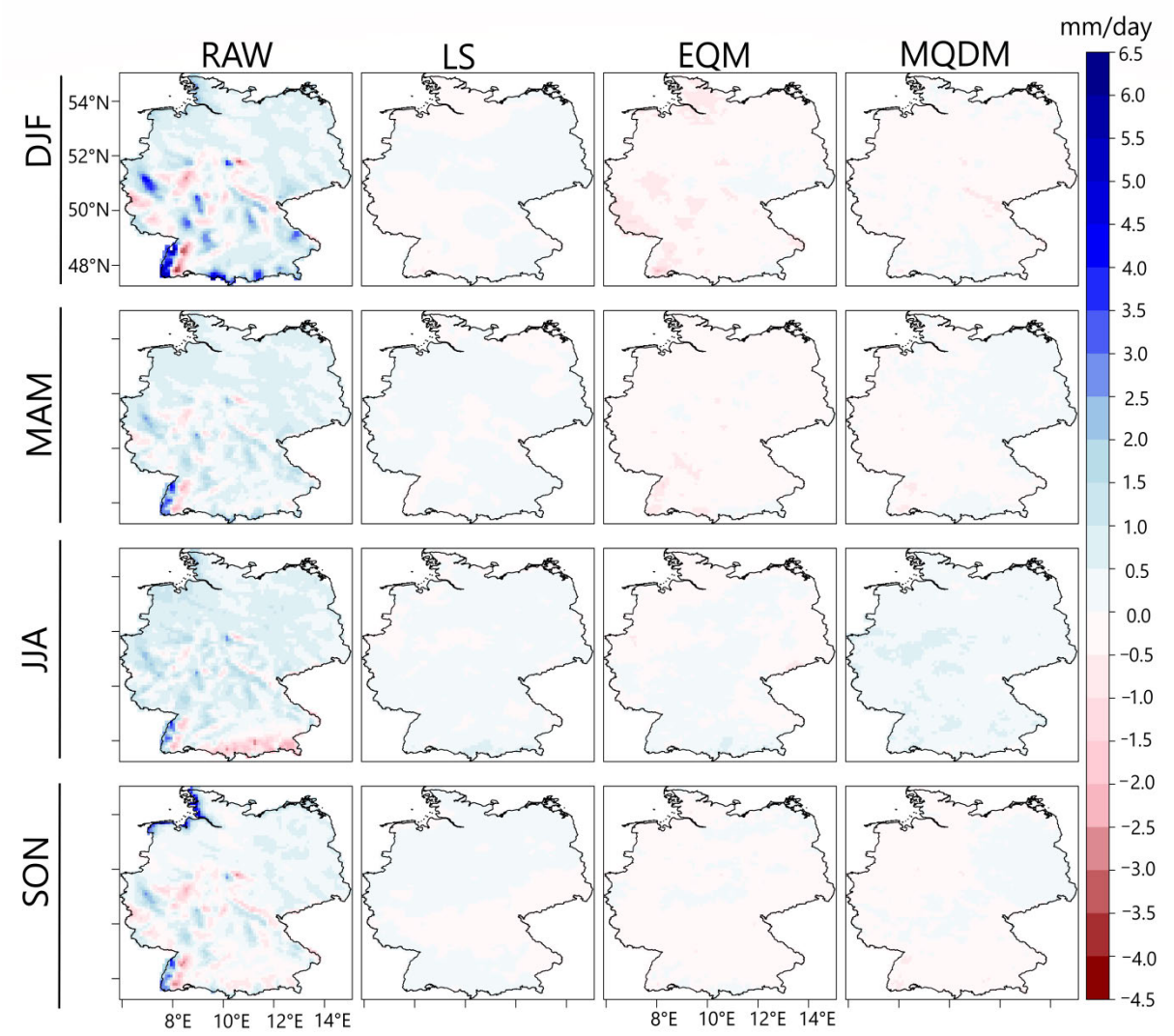

Figure 6.1: Validation of the added value of the bias correction techniques on the spatial mean of daily precipitation as simulated in the REMO RCM, driven by MPI-ESM-LR, during the 1978 to 2005 validation period. Biases are computed as the difference between the simulated seasonal mean precipitation and the observed seasonal mean precipitation (RCM minus E-OBS).

From Table 6.2, all BC techniques added value in reducing the biases in the simulated mean precipitation at the grid boxes in Germany. The relative performances of the respective BC techniques depend on the RCM and season that is considered. The dipole precipitation pattern over the southwestern part of Germany and the local biases in the REMO model were significantly reduced by all the BC techniques (Figure 6.1). For the REMO model, the LS technique performs best for all seasons in reducing the biases in the simulated mean precipitation at the grid boxes (Table 6.2). Considering that the LS algorithm focuses on

scaling the mean precipitation at each grid box to be closer to the observed, its good performance in adjusting the biases in the mean statistic is not surprising. Nonetheless, the distribution-based techniques, that is, EQM and MQDM, also added value in reducing the biases in the simulated mean precipitation at most grid boxes.

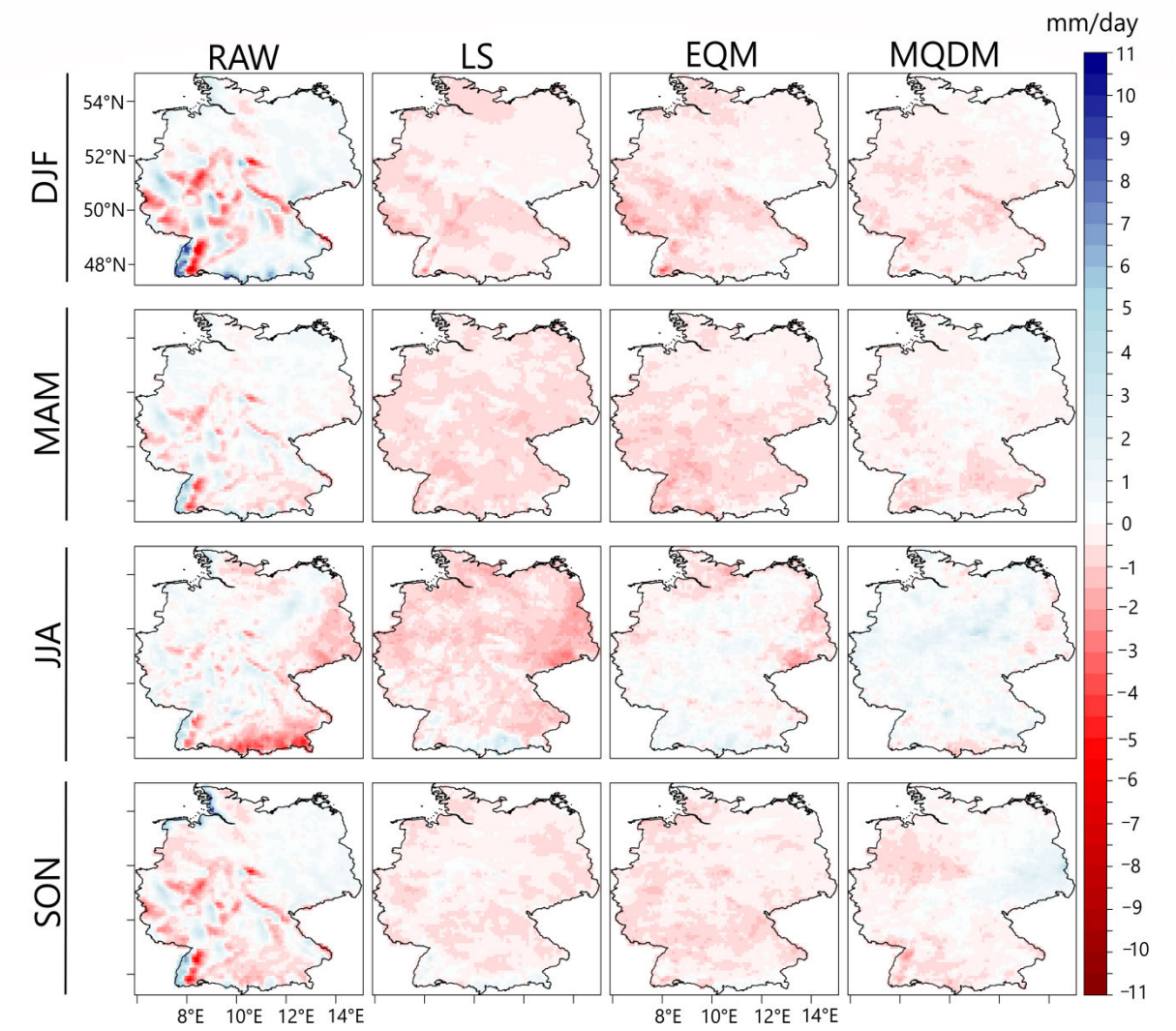

Figure 6.2: Validation of the added value of the bias correction techniques on the spatial standard deviation of daily precipitation as simulated in the REMO RCM, driven by MPI-ESM-LR, during the 1978 to 2005 validation period. Biases are computed as the difference between the simulated seasonal variability of precipitation and the observed seasonal variability of precipitation (RCM minus E-OBS).

Table 6.3 contains that the added value of the BC techniques in improving the spatial standard deviation of precipitation is slim compared to the performance of the same BC techniques on the simulated mean precipitation. Moreover, depending on the season and RCM, the LS

technique indicates the tendency of increasing the biases in the spatial standard deviation of precipitation. This is more pronounced in the CCLM4 model (Table 6.3). During DJF, the MQDM technique performs well in reducing the biases in the standard deviation and on average, did not increase the biases over Germany, for any of the seasons, relative to the raw RCM. Overall, the distribution-based BC techniques perform better in reducing the biases in the spatial variability of precipitation over Germany compared to the LS technique. The time (or seasonal) dependency of the biases can be partly due to the transient nature of the processes associated with rainfall formation in the study region. Different processes can be associated with precipitation formation at different periods. Therefore, the systematic bias in the simulated precipitation during the distinct seasons differs (Figure 6.1 and Figure 6.2).

Table 6.2: Mean absolute error (mm/day) in spatial mean of daily precipitation estimates from the RCMs, driven by MPI-ESM-LR, relative to E-OBS during the 1978 to 2005 validation period. (*) indicates the best performing BC technique with the lowest error for a given season.

RAW	**LS**	**EQM**	**MQDM**
	CCLM4		
	DJF		
0.64	0.10*	0.39	0.10*
	MAM		
0.63	0.13*	0.14	0.14
	JJA		
1.03	0.24	0.30	0.17*
	SON		
0.62	0.19	0.10*	0.21
	REMO		
	DJF		
0.82	0.08*	0.27	0.14
	MAM		
0.59	0.08*	0.20	0.13
	JJA		
0.70	0.11*	0.15	0.22
	SON		
0.51	0.09*	0.14	0.15

Table 6.3: Mean absolute error (mm/day) in the spatial standard deviation of daily precipitation estimates from the RCMs, driven by MPI-ESM-LR, relative to E-OBS during the 1978 to 2005 validation period. (*) indicates the best performing BC technique with the lowest error for a given season. (**) indicates where the BC technique increased the biases.

RAW	**LS**	**EQM**	**MQDM**
	CCLM4		
	DJF		
0.41	0.87**	0.55**	0.25*
	MAM		
0.43	0.57**	0.41*	0.42
	JJA		
0.72	0.73**	0.42*	0.44
	SON		
0.48	0.49**	0.39*	0.39*
	REMO		
	DJF		
1.04	0.44	0.45	0.32*
	MAM		
0.56	0.59**	0.55	0.33*
	JJA		
0.74	0.80**	0.42*	0.56
	SON		
0.70	0.39*	0.40	0.41

Next, the added value of BC techniques in terms of the first to fourth statistical moments of the distribution of daily precipitation time series, averaged over Germany is evaluated. Regardless of the driving data and the RCM, BC adds value in reducing the wet biases of the RCMs (Figure A6 and Figure A7). For CCLM4 and REMO, respectively, Table 6.4 and Table 6.5 contain the biases in the first to fourth statistical moments, as major statistical characteristics of the empirical distributions, before and after BC. Overall, the relative performances of the BC techniques depend on the season and RCM. However, the distribution-based BC techniques outperform the LS approach which in some cases increased the biases in the third and fourth moments (that is, skewness and kurtosis). The MQDM generally performs best in reducing the biases in the third and fourth moments. The EQM increased the biases in the third and fourth moments during SON in the REMO model. The good performance of the LS approach in reducing the biases in mean precipitation at the grid

box level, especially in the REMO model, is also replicated in Table 6.5 where for most seasons the LS technique outperforms other techniques in adjusting the temporal simulated mean value to the observed.

Table 6.4: Errors in the first to fourth moments, in mm/day, for the raw and bias-corrected precipitation estimates from the CCLM4 model driven by MPI-ESM-LR against observed precipitation values from E-OBS, during the 1978 to 2005 validation period. Error is calculated as the absolute value of the observed minus simulated statistic. (*) indicates the best performing (or no) BC technique with the lowest error for a given season, and (**) indicates the third to the fourth moment where the BC technique increased the biases.

Statistic	**RAW**	**LS**	**EQM**	**MQDM**
	DJF			
Mean	0.64	0.08	0.39	0.02*
SD	0.03*	0.68	0.56	0.18
Skewness	0.42	0.43**	0.08	0.05*
Kurtosis	1.77	1.73	0.85	0.44*
	MAM			
Mean	0.63	0.13	0.12	0.10*
SD	0.17*	0.37	0.32	0.25
Skewness	0.49	0.36	0.10*	0.22
Kurtosis	2.27	1.50	0.56*	1.31
	JJA			
Mean	1.03	0.33	0.23	0.14*
SD	0.43	0.38	0.02*	0.06
Skewness	0.43	0.49**	0.20	0.07*
Kurtosis	2.17	2.42**	1.43	0.59*
	SON			
Mean	0.59	0.18	0.01*	0.19
SD	0.12*	0.34	0.23	0.37
Skewness	0.48	0.58**	0.30	0.08*
Kurtosis	2.45	3.15**	1.88	0.36*

For the CCLM4 model, the MQDM performs best in improving the first moment. The second-moment quantity that is represented by the standard deviation poses a challenge to the BC techniques. Mostly, the raw RCMs capture the temporal variability better than the corrected precipitation time series. Nonetheless, there are some relative improvements in the simulated standard deviation under the MQDM technique. The relatively better performance of the MQDM in improving the higher moments can be attributed to the change-preserving

attribute of the QDM over the entire distribution, and the incorporation of the spatial dependency of precipitation during the BC, which enhanced the inter-site correlations. The tendency of the LS technique to increase the biases in the higher moments of daily precipitation was not replicated when the same LS is applied to precipitation data from the same RCMs but at monthly resolution (Table 5.1). This suggests that the performance of the BC technique depends also on the temporal resolution of the data.

Table 6.5: Same as Table 6.4 but for the REMO model. Copyright © [2022a] [Ibebuchi et al.].

Statistic	**RAW**	**LS**	**EQM**	**MQDM**
	DJF			
Mean	0.58	0.00*	0.25	0.11
SD	0.07*	0.44	0.46	0.43
Skewness	0.37	0.36	0.19*	0.22
Kurtosis	1.52	1.92**	1.19	0.93*
	MAM			
Mean	0.50	0.04*	0.19	0.04*
SD	0.05*	0.46	0.32	0.21
Skewness	0.23	0.42	0.27	0.08*
Kurtosis	1.45	1.86**	1.50**	1.44*
	JJA			
Mean	0.51	0.09	0.00*	0.30
SD	0.14	0.40	0.13	0.00*
Skewness	0.46	0.26	0.03*	0.26
Kurtosis	2.06	0.98	0.23*	0.98
	SON			
Mean	0.24	0.04**	0.13	0.10
SD	0.06*	0.33	0.39	0.20
Skewness	0.20	0.38**	0.38**	0.02*
Kurtosis	0.57	2.08**	2.22**	0.45*

To examine the performance of the BC techniques in capturing extreme values of precipitation, return value calculations during JJA are used. First, a generalized extreme value distribution is fitted to the annual maximum JJA values of (un)corrected simulated

precipitation during the validation period and the results are compared to the observed return values from E-OBS (Figure 6.3). Second, to assess the sensitivity of the results in Figure 6.3, the analysis is repeated using the peak-over-threshold approach with the Gumbel distribution (Figure 6.4). The peak-over-threshold approach helps to optimize the calculations given that the sample size can be larger compared to the annual maxima approach. To accommodate more values, the 90th percentile precipitation threshold from E-OBS was used in defining extreme precipitation in Germany. Observed daily precipitation, raw, as well as bias-corrected (precipitation) outputs that exceed this threshold, are used for the return value estimates depicted in Figure 6.4.

Figure 6.3 shows that based on the GEV distribution, the observed return values of precipitation are best represented by the MQDM approach. Based on the MAE, MQDM outperforms other BC techniques by a large margin in both RCMs. For the peak-over-threshold approach, the results are slightly different compared to the annual maxima approach. Fischer and Schumann (2014) reported that in terms of extreme events, the peak-over-threshold approach can be relatively more robust. This is also confirmed in this study based on the Gumbel model fit. Figure 6.4 shows that similar to the annual maxima approach, the MQDM output is closest to observations in the CCLM4 model, whereas in REMO, the EQM outperforms the MQDM by a slim margin (that is, based on the MAE). In all cases, the LS approach increases the biases in the simulated return values of precipitation. Generally, the MQDM outperforms the other BC techniques in adjusting the simulated summer extreme precipitation characteristics across Germany to the observed values. Moreover, Cannon et al. (2015) noted that compared to the EQM, the QDM, which is implemented in the MQDM algorithm performs better in correcting precipitation extremes. Since the change signal is incorporated in the MQDM, it is reasonable that it performs well in capturing precipitation extremes during JJA in Germany. Moreover, the MQDM has the skill to reduce the biases in

other statistical aspects of precipitation such as the annual cycle and the frequency statistics (Figure A6 to Figure A9). The MQDM also has skill in adjusting the inter-site temporal correlations of the precipitation field towards observations. However, it is a univariate BC technique in the sense that it is applied to only one variable and is not designed to adjust inter-variable dependencies towards observations.

a)

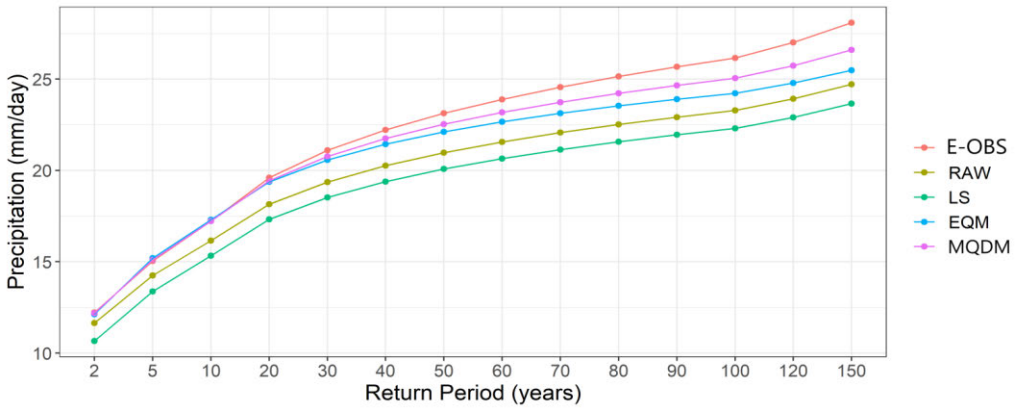

b)

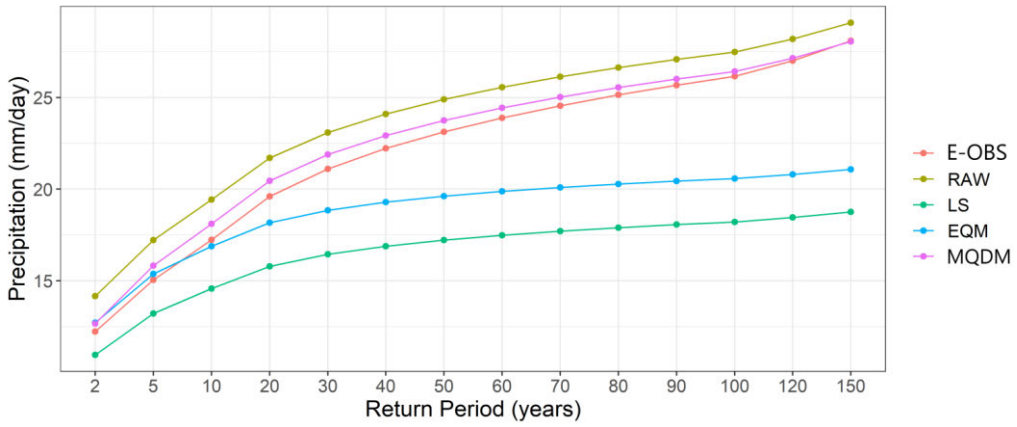

Figure 6.3: Return level plot of precipitation averaged over Germany from (a) REMO and (b) CCLM4, driven by MPI-ESM-LR, before and after bias correction, during JJA in the 1978 to 2005 validation period, using the annual maxima approach and generalized extreme value distribution.

a)

b)

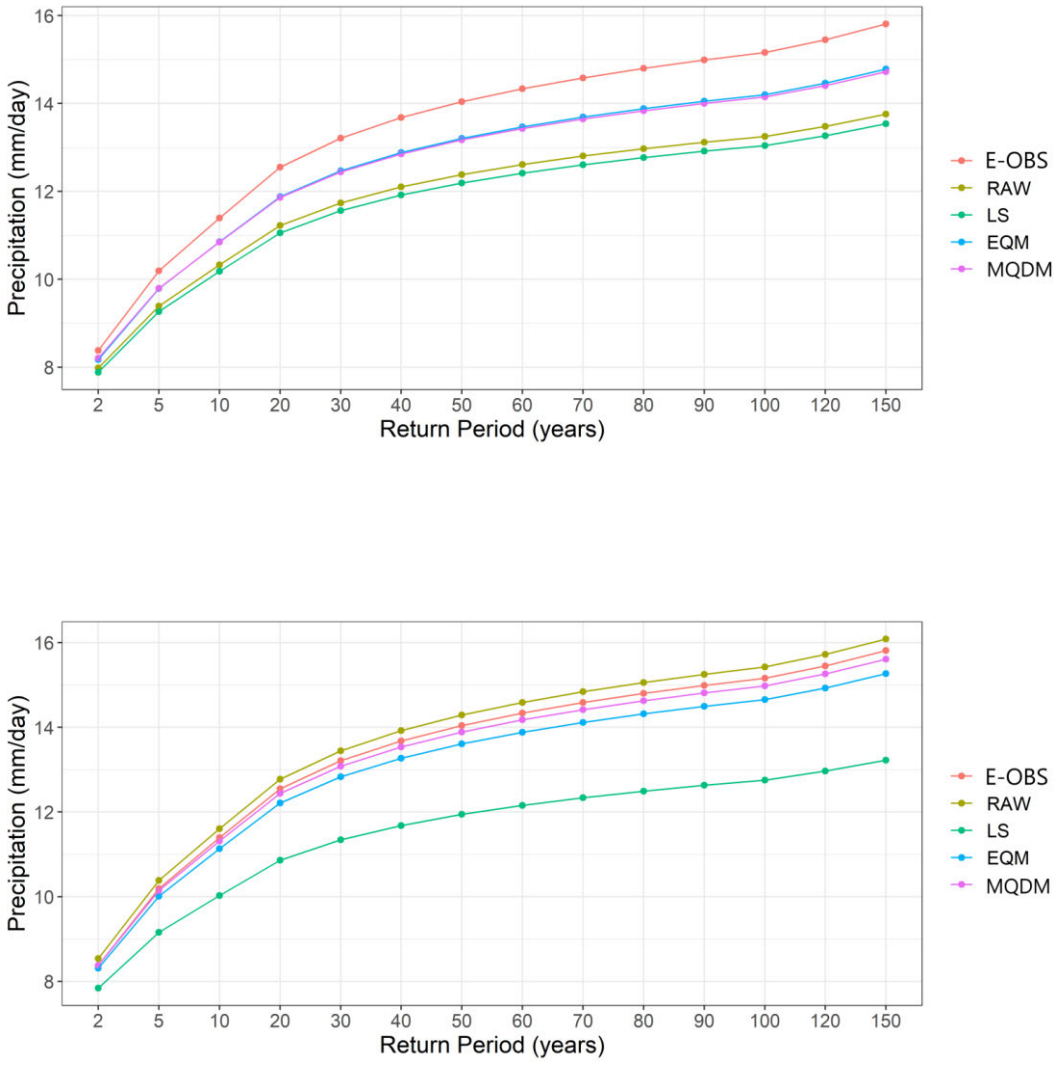

Figure 6.4: Return level plot of precipitation averaged over Germany from (a) REMO and (b) CCLM4, driven by MPI-ESM-LR, before and after bias correction, during JJA in the 1978 to 2005 validation period, using the peak over threshold approach and Gumbel distribution.

6.2 Performance of bias correction techniques in reducing simulated temperature biases

For temperature that is mostly well simulated by the RCMs and does not exhibit high spatial heterogeneity compared to precipitation, using the MQDM did not indicate any clear added value, both in improving the inter-site correlations (that were already comparable with observations) and the basic statistics. The BC output was almost the same as using the QDM that is used in matching the multivariate distributions. Therefore, for temperature, the traditional QDM is applied in adjusting the systematic biases.

Figure 6.5 and Figure 6.6 show the performance of the BC techniques for the mean and standard deviation of simulated temperature values from the REMO model. Accordingly, the MAE before and after bias correcting the CCLM4 and REMO RCMs is contained in Table 6.6 and Table 6.7. The added value of the BC in adjusting the simulated mean temperature towards the observed is highest during JJA when the CCLM4 is characterized by a notable cold bias (Figure A10). During JJA, for the CCLM4 model, ~ 77.8% of the errors in the spatial mean statistic of temperature were reduced by the LS and QDM, while ~ 68.3% of the errors were reduced by the EQM. Similarly, Figure 6.5 shows that the REMO model has the highest bias in simulating mean temperature over Germany during the SON season. The EQM reduces the errors during SON by ~ 76.6%; the LS and QDM reduced the errors by ~ 73.4%. Seasons when the error magnitude is small, that is, when the raw RCM performs well in simulating the mean temperature values during the validation period, for example, JJA from the REMO model (Table 6.7); DJF and SON for the CCLM4 model (Table 6.6), the BC techniques did not add value but rather increased the biases (in the mean statistic), especially for CCLM4. Thus, when there is little or no room for improvement in the temperature estimates during the validation period, the need for applying BC or an optimal BC approach to adopt might as well be assessed.

The relative performances of the BC techniques in adjusting the simulated mean temperature values show dependency on the season, RCM, and region. Unlike in precipitation where the BC techniques mostly perform differently, visual inspection of the spatial maps in Figure 6.5 and Figure A10 shows that the added value from the BC techniques is quite similar for temperature.

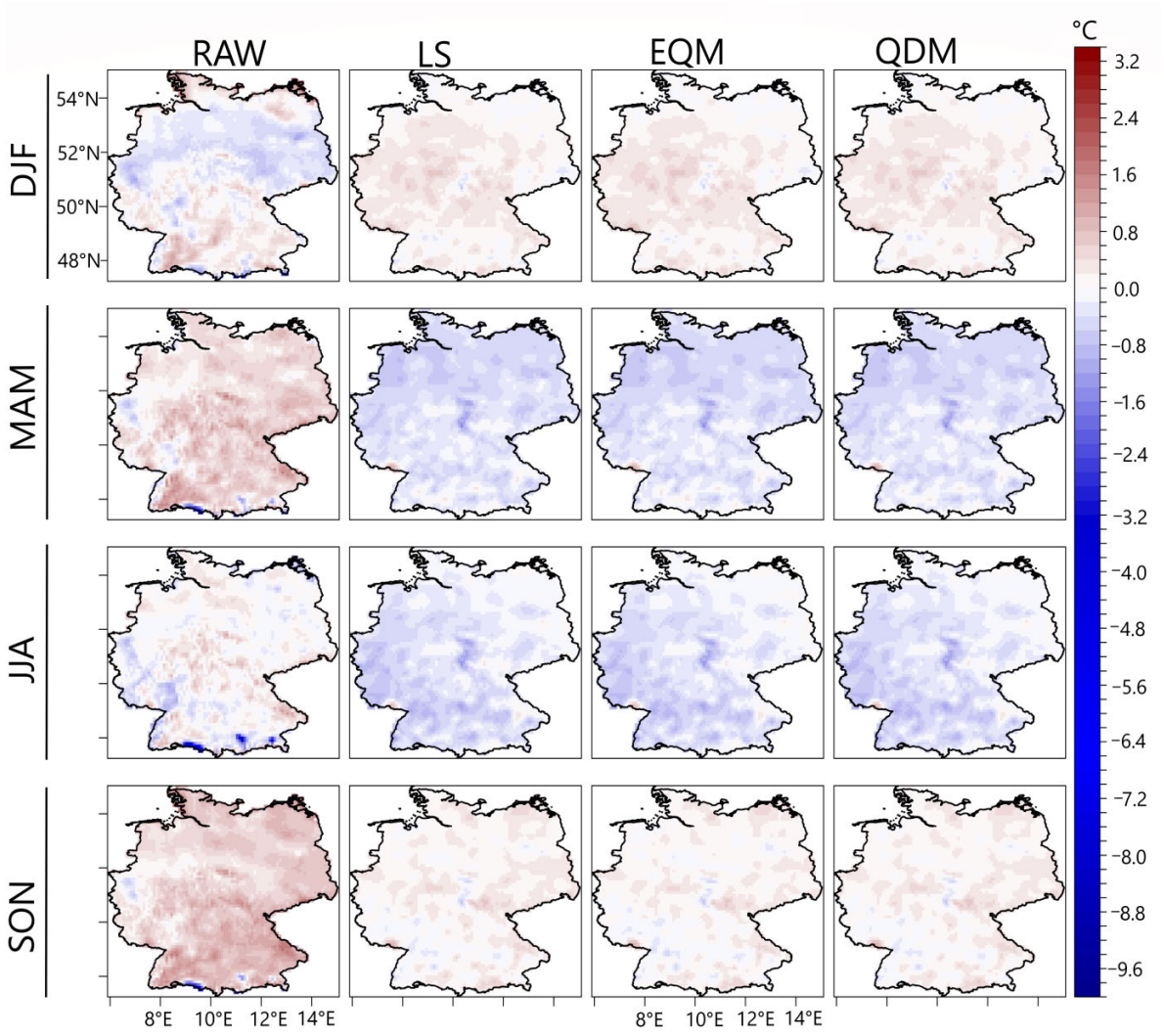

Figure 6.5: Validation of the added value of the bias correction techniques on the spatial mean of daily temperature as simulated in the REMO RCM, driven by MPI-ESM-LR, during the 1978 to 2005 validation period. Biases are computed as the difference between the simulated seasonal mean temperature and the observed seasonal mean temperature (RCM minus E-OBS)

The same inferences on the added value of the BC techniques also hold when the standard deviation of temperature is considered. When the error magnitude in simulating the standard deviation of temperature over Germany is large in the validation period, the (distribution-

based) BC techniques add value by reducing the errors; but when the errors are small the BC techniques increased the biases (Table 6.6 and Table 6.7; Figure 6.6 and Figure A11). Also, the LS technique has no significant effect on changing the variability of temperature.

Table 6.6: Mean absolute error (in °C) for the spatial mean and standard deviation of the daily temperature values from the CCLM4 RCM, driven by MPI-ESM-LR, relative to E-OBS during the 1978 to 2005 validation period. (*) indicates the best performing (or no) BC technique with the lowest error for a given season.

RAW	**LS**	**EQM**	**QDM**
	Mean		
	DJF		
0.33*	0.86	0.95	0.84
	MAM		
0.48	0.36	0.33*	0.36
	JJA		
1.26	0.28*	0.40	0.28*
	SON		
0.39*	0.83	0.72	0.81
	SD		
	DJF		
0.19*	0.19*	0.28	0.34
	MAM		
0.41	0.41	0.17	0.16*
	JJA		
0.64	0.64	0.18	0.10*
	SON		
0.32*	0.32*	0.60	0.72

Further, as exemplified in Table 6.8 with the CCLM4 model, during the DJF and JJA seasons, when the averages were considered (that is, average temperature over Germany), the inferences from the spatial statistical analysis still hold. For the first to fourth statistical moments, the larger the error magnitude in simulating the statistical moments, during the validation periods, the higher the added value of the BC techniques. Thus, unlike simulated precipitation, which is usually characterized by notable biases, the added value of the BC techniques for temperature seems to be more controlled by the magnitude of the biases. Overall, the more sophisticated BC techniques do not outperform the simple LS approach in

adjusting daily temperature biases over Germany, especially when the biases in the statistical moments of the raw RCM outputs are closer to zero.

Table 6.7: Mean absolute error (in °C) for the spatial mean and standard deviation of daily temperature values from the REMO RCM, driven by MPI-ESM-LR, relative to E-OBS during the 1978 to 2005 validation period. (*) indicates the best performing (or no) BC technique with the lowest error for a given season.

RAW	**LS**	**EQM**	**QDM**
	Mean		
	DJF		
0.33	0.19*	0.20	0.19*
	MAM		
0.49	0.40*	0.40*	0.40*
	JJA		
0.26*	0.33	0.32	0.33
	SON		
0.64	0.17	0.15*	0.17
	SD		
	DJF		
0.63	0.63	0.43*	0.47
	MAM		
0.19*	0.19*	0.28	0.29
	JJA		
0.31*	0.31*	0.32	0.32
	SON		
0.19*	0.19*	0.37	0.41

Table 6.8: Errors in the first to fourth moments, in °C, for the raw and bias-corrected temperature values from the CCLM4 model driven by MPI-ESM-LR against observed temperature values from E-OBS, during the 1978 to 2005 validation period. Error is calculated as the absolute value of the observed minus simulated statistical moment. (*) indicates the best performing (or no) BC technique with the lowest error for a given season.

Statistic	**RAW**	**LS**	**EQM**	**QDM**
	DJF			
Mean	0.03*	0.86	0.95	0.86
SD	0.65	0.65	0.41*	0.42
Skewness	0.25	0.25	0.17	0.15*
Kurtosis	0.50	0.50	0.29*	0.41
	JJA			
Mean	1.26	0.25*	0.38	0.25*
SD	0.59	0.59	0.17	0.08*
Skewness	0.49	0.49	0.18*	0.22
Kurtosis	0.90	0.90	0.39*	0.47

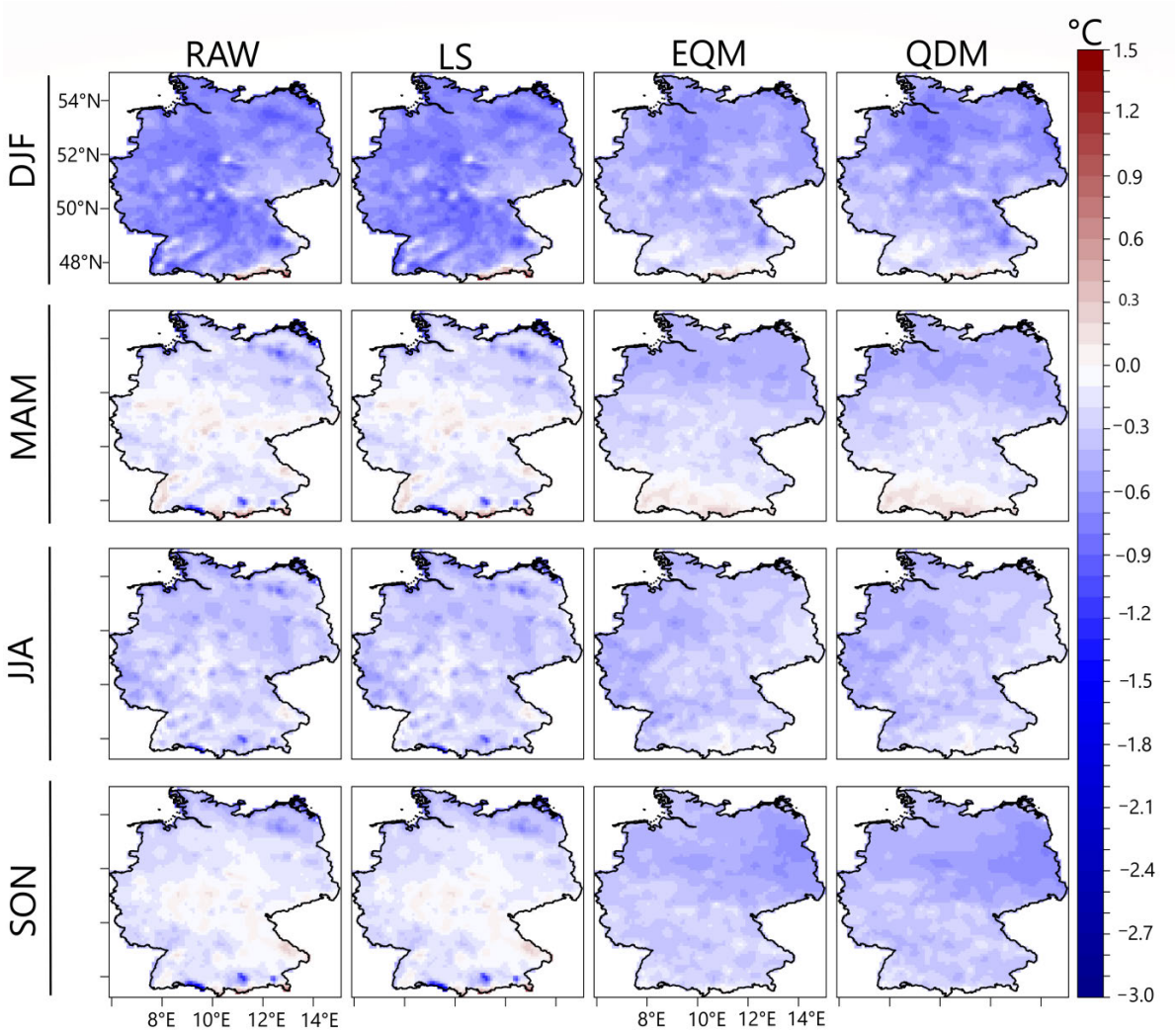

Figure 6.6: Validation of the added value of the bias correction techniques on the spatial standard deviation of temperature as simulated in the REMO RCM, driven by MPI-ESM-LR, during the 1978 to 2005 validation period. Biases are computed as the difference between the simulated standard deviation of temperature and the observed standard deviation of temperature (RCM minus E-OBS)

7. Impact of distinct bias correction techniques on the simulated meteorological patterns of temperature and precipitation at a daily temporal resolution

In chapter 5, the impact of the LS technique on the statistics and simulated meteorological patterns of precipitation, at a monthly resolution was examined; it was found that the LS technique can be sufficient to adjust the basic statistics of monthly precipitation towards observations; also, the spatiotemporal configurations of the simulated meteorological patterns of precipitation were reproduced after the bias correction with LS. However, from chapter 6, for the same set of RCMs, the LS technique indicates the tendency to increase the biases in the higher moments of daily precipitation. This suggests that there can be further uncertainty on how the BC techniques impact the simulated meteorological patterns as a function of the temporal resolution at which the BC is applied and the temporal resolution at which the meteorological patterns were classified. Hence in this chapter, three BC techniques (LS, EQM, and QDM) are applied to reduce the biases in simulated precipitation and temperature on a daily scale. The impact of the distinct BC techniques on the individual and coupled simulated meteorological patterns of precipitation and temperature, classified at daily and monthly time scales are examined during the 1978 to 2005 validation period.

Figures 7.1 to Figure 7.3 show the summer variability patterns of precipitation and temperature, in Germany. Following the same criterion of analyzing only PC patterns that match well with correlation vectors that they are indexed to with at least a congruence coefficient of 0.92, four variability patterns were classified for precipitation, and two variability patterns for temperature. The rotated S-MD PCA algorithm was applied to daily data during the summer season. Figure 7.1 and Figure 7.2 show that as obtained from the monthly precipitation data (Figure 5.2), the summer homogeneous precipitation regions are also the western, southeastern, eastern, and northern/north-western regions when daily data is

used for the classification. However, based on congruence matches, the simulated meteorological patterns based on monthly data have more errors (relative to observations from E-OBS) compared to the simulated meteorological patterns that are based on daily data. Perhaps the daily simulated data relatively captures better than the monthly simulated data, some spatiotemporal variability of the meteorological patterns. Thus, for the precipitation data at a daily scale, the co-variability of the grids (and the governing processes driving the correlations) is well simulated and quite close to observations from E-OBS. The congruence matches between the observed and simulated meteorological patterns in Figure 7.1 were all greater than 0.99 (that is, an excellent match in the overall spatial structure) both before and after BC. Therefore, the BC techniques do not notably change the simulated co-variability of the grids and the large-scale governing mechanisms, since the overall spatial configuration of the PC loadings patterns remains more or less the same before and after BC. Based on the congruence matches between the same PC scores from the corrected and uncorrected RCM, which were in the excellent range, no notable changes were equally found in the amplitude (that is, temporal structure) of the summer variability patterns.

A cursory inspection of Figure 7.1 shows that the isopleths were slightly altered by the BC techniques. Therefore, similar to the conclusions in chapter 5 that were based on only the LS technique applied to monthly data: while in at least the synoptic scale, no notable changes in the spatiotemporal structure of the simulated meteorological patterns were found at a more localized scale, the BC changed the co-variability of the grids and so the underlying local mechanisms. Thus, the basic inference from Figure 7.1 is that the effect of the BC on the simulated meteorological patterns depends on the spatial scale considered. At a larger scale (that is, at least the synoptic scale), since the simulated meteorological patterns were all reproduced before and after the BC with a congruence match with the reference (greater than 0.99 in all cases) the BC techniques have little or no effect on the simulated meteorological

patterns at a larger spatial scale. However, at a more localized spatial scale, depending on the region, and specifically where strong spatial correlation exists among the grids as can be seen in Figure 7.1, the BC changes the localized spatial configuration of the simulated meteorological patterns.

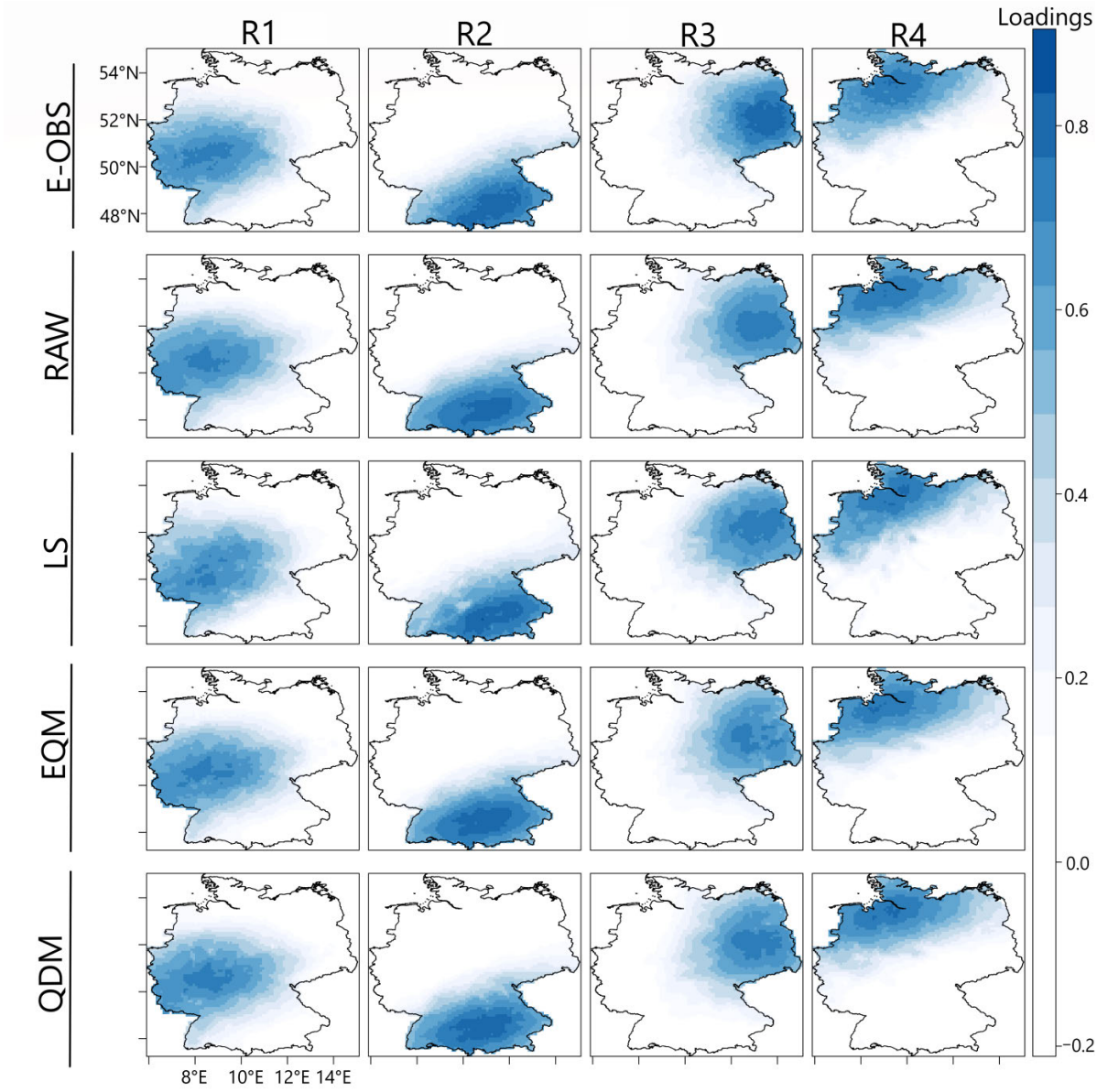

Figure 7.1: Variability patterns of daily boreal summer precipitation anomalies from E-OBS and as simulated by the REMO RCM driven by MPI-ESM-LR for the for the 1978 to 2005 validation period. The simulations are for the raw RCM and bias-corrected outputs from the three BC techniques. The similarity matrix used in the rotated S-MD PCA is based on the temporal correlations between the daily precipitation values at the grid boxes.

From Table 7.1, for the meteorological patterns of precipitation based on the daily data accumulated on a monthly scale, the RCMs all perform well (congruence match greater than 0.90 in all cases) in producing the observed patterns (Figure 7.2). Also, relatively, the LS technique did not significantly affect the co-variability of the grids (Table 7.1). The EQM and QDM techniques appear to slightly impact the spatial configuration of the patterns, based on the congruence matches in Table 7.1, but the effect is slim (or more localized) and not notable at a larger scale. Thus, the distinct BC techniques can impact the spatial structure of the simulated meteorological patterns differently, at more localized spatial scales (Figure 7.1 and Figure 7.2). Further, it can be inferred from Figure 7.1 and Figure 7.2 that regardless of the temporal resolution at which the meteorological patterns are classified, they are reproduced after the BC.

Table 7.1: Congruence coefficient between the simulated variability patterns of boreal summer precipitation from E-OBS, and for the raw and bias-corrected precipitation model output for the 1978 to 2005 validation period

Output	**R1**	**R3**	**R3**	**R4**
		REMO		
RAW	0.94	0.92	0.95	0.93
LS	0.94	0.92	0.95	0.93
EQM	0.95	0.92	0.94	0.92
QDM	0.95	0.92	0.95	0.92
		CCLM4		
RAW	0.94	0.95	0.96	0.91
LS	0.94	0.95	0.96	0.91
EQM	0.93	0.96	0.95	0.90
QDM	0.93	0.96	0.95	0.91

Figure 7.3 show that the summer temperature variability patterns comprise the northern region and southern region with an overlap in the central regions. The co-variability of the grids is highest in each case at the southernmost and northernmost domains. Both the REMO and CCLM4 RCMs reproduced the temperature regions as observed (both with daily and monthly data) with congruence matches greater than 0.98 in all cases (Figure 7.3, only shown for

REMO). Thus, the RCMs simulate the temperature regimes better than the precipitation regimes, regardless of the time scale at which the classification is done. Moreover, it is promising that overall, none of the BC techniques (clearly) modified the spatial structure and reproducibility of the simulated meteorological patterns, both for temperature and precipitation. The same result holds for meteorological patterns from other adjacent seasons other than the summer season.

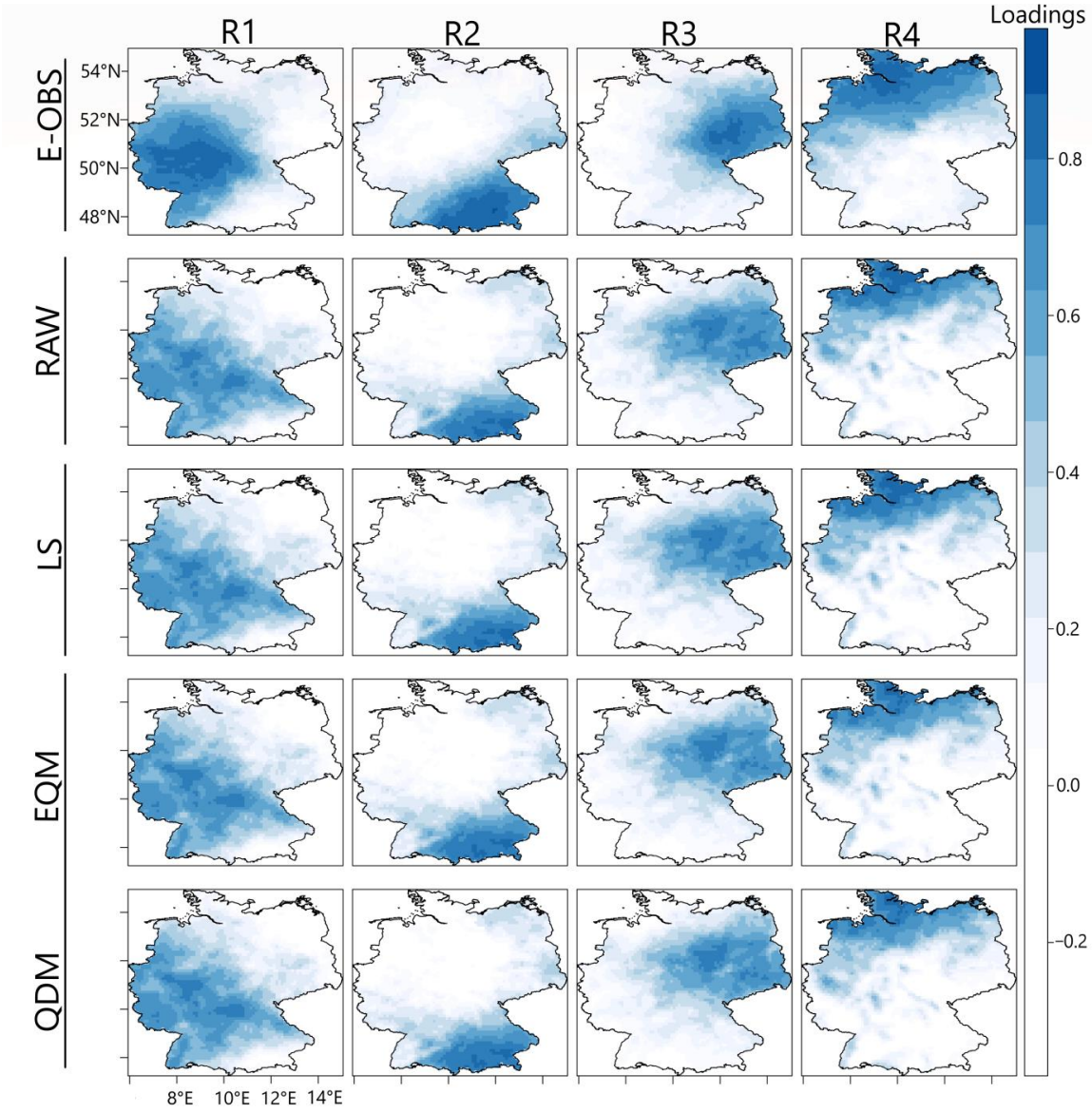

Figure 7.2: Variability patterns of monthly boreal summer precipitation anomalies from E-OBS and as simulated by the REMO RCM driven by MPI-ESM-LR for the 1978 to 2005 validation period. The simulations are for the raw RCM and bias-corrected outputs from the three BC techniques. The similarity matrix used in the rotated S-MD PCA is based on the correlation between the daily precipitation values accumulated to monthly precipitation totals.

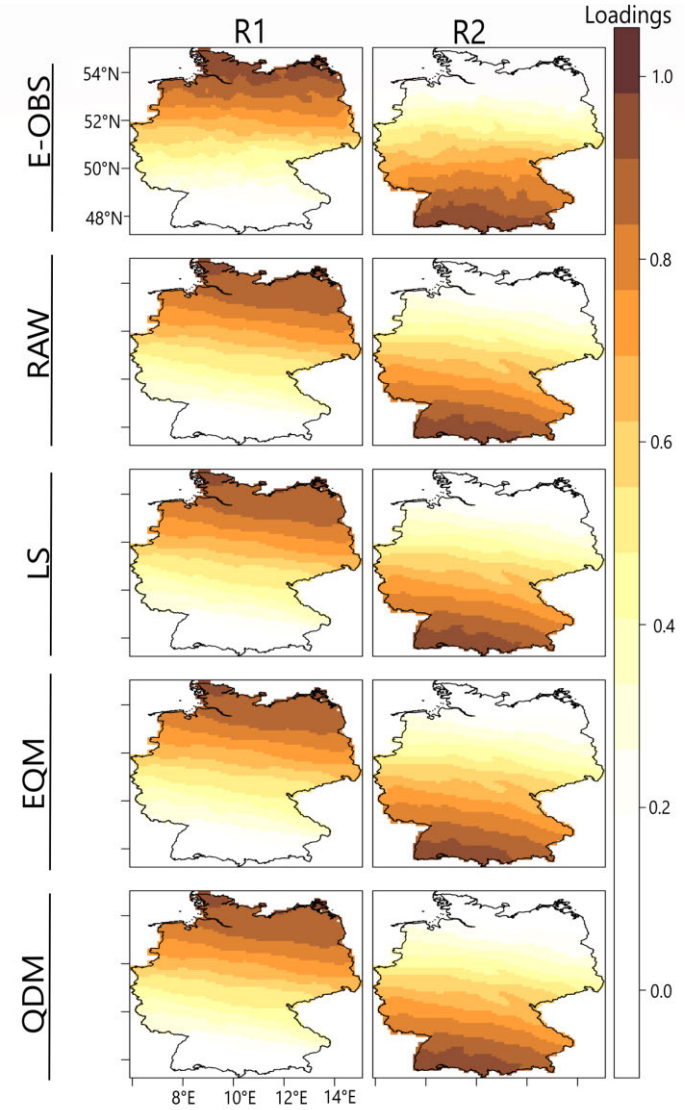

Figure 7.3: Variability patterns of daily boreal summer temperature anomalies from E-OBS and as simulated by the REMO RCM driven by MPI-ESM-LR for the1978 to 2005 validation period. The simulations are for the raw RCM and bias-corrected outputs from the three BC techniques.

Based on the suggestion of Cherry (1997), an optimal way to investigate the coupling between atmospheric modes is to apply rotated PCA to the individual fields, ensure that the individual patterns can be physically interpretable, and then apply correlations between the PC patterns from the respective fields; therefore, the rotated S-MD PC patterns between precipitation and temperature obtained from the respective seasons of the year were correlated. Correlation with

a magnitude of ~0.5 (that is, the correlation coefficient) was found between two respective PC patterns from precipitation and temperature during the DJF season. Given that the PC scores (that is, the time series) that were correlated, were not notably changed after the BC, there was equally no robust indication that the simulated coupling between the PC patterns was constrained or improved by the BC techniques, based on the statistical significance of the correlations.

8. Impact of bias correction on inter-variable dependencies

8.1 Seasonal correlations between temperature and precipitation before and after bias correction

Table 8.1 contains the correlations between the daily time series of temperature and precipitation averaged over Germany, during the 1978 to 2005 validation period. A statistically significant correlation was obtained only during DJF from the observational data. Interestingly, the raw RCM outputs simulate the coherency of temperature and precipitation averaged over Germany during DJF with the same correlation sign and a quite similar magnitude of the correlation coefficient as observed from E-OBS (Table 8.1). The positive correlation implies that during winter, higher temperatures can be related to enhanced precipitation over Germany; to physically justify the statistical correlations, recall that the DJF temperature averaged over Germany relates to the NAO with a statistically significant correlation coefficient of 0.64 (Figure 2.4). Further, it can be recalled from Figure 2.4 to Figure 2.6 that during DJF, the fingerprint of the positive (negative) NAO on the dominant atmospheric circulation mode over Western Europe implies enhanced moist westerly advective flow from the North Atlantic (dry northerly advective flow from the anticyclone over the high latitude) towards western Europe, resulting in higher temperatures and enhanced precipitation (lower temperature and dry conditions) over Germany. Therefore, it is concluded that the observed statistical correlations in Table 8.1 between DJF temperature and precipitation, averaged over Germany, can be physically interpreted. Since the raw RCMs capture the statistical correlations as observed, it is an indication that large portions of the mechanisms behind the relationship between winter temperature and precipitation over Germany are simulated by the models.

Table 8.1: The correlation coefficient between the seasonal time series of daily temperature and daily precipitation averaged over Germany, from E-OBS, the raw REMO and CCLM4 RCMs driven by the MPI-ESM-LR. (*) indicates correlations that are statistically significant at a 95% confidence level based on the Kendall Tau-b. The correlations are for the 1978 to 2005 validation period

E-OBS	**RCM**
	REMO
DJF	
0.37*	0.39*
MAM	
−0.01	−0.09
JJA	
−0.19	−0.20
SON	
0.08	−0.01
	CCLM4
DJF	
0.37*	0.36*
MAM	
−0.01	−0.01
JJA	
−0.19	−0.01
SON	
0.08	0.06

Further, to examine if the RCMs simulate the observed correlations between the NAO and DJF temperature, averaged over Germany (that is, the relationship shown in Figure 2.4), the RCMs driven by ERA-Interim are used for the analysis. This is because as mentioned earlier, the simulations are more consistent with observations when reanalysis provides the boundary condition. Indeed, the RCMs captured the observed correlation between average DJF temperature in Germany and the NAO index, and based on the statistical significance of the correlations, the BC techniques did not notably alter the simulated correlations, at least for most grid boxes and on average (Table 8.2). This is a further confirmation that when the models simulate the signals of large-scale climate drivers such as the NAO, BC does not destroy the imprint of the climate driver that is represented in the simulated variable. Therefore, averaged over Germany, Table 8.2 contains that the climate models are still physically consistent with the NAO variability before and after BC.

Table 8.2: Correlation coefficients between simulated temperatures, averaged over Germany, from the RCMs driven by ERA-Interim, and the NAO index, during DJF, for the 1978 to 2005 validation period. (*) indicates correlations that are statistically significant at a 95% confidence level based on the Kendall Tau-b

RCM	**RAW**	**LS**	**EQM**	**QDM**
REMO	0.77*	0.77*	0.76*	0.72*
CCLM4	0.73*	0.72*	0.76*	0.75*

Next, the correlations between temperature and precipitation at the grid box level are examined for both observed data and (un)corrected RCMs. Table 8.3 contains the summary statistics of the 4840 correlation coefficients, that is, the number of grid boxes in the study domain at which daily temperature and precipitation time series are related during DJF. The values for each statistic are comparable across the data sets (that is, observational data, bias-corrected, and raw RCMs), though the values are not the same in most cases, especially between the observed and simulated values. This suggests that while the simulated and observed correlations at some grid boxes are distinct, on average the magnitude and sign of the correlations are comparable. Nonetheless, under the REMO model, the minimum values indicate that some grid(s) has a negative correlation coefficient, and the LS technique inflates the magnitude of that negative correlation.

The comparison of the correlations between temperature and precipitation at each grid box, across the data sets is investigated further using the KS test. First, the KS test indicated that the data values (that is, the 4840 correlation coefficients) from the observed and simulated data sets (both corrected and uncorrected) are from different continuous distributions (pvalue < 0.05, so the null hypothesis is rejected). This further indicates that there is no robust indication that the univariate BC techniques improved the simulated correlations towards observation. Table 8.4 contains the KS D statistics for each simulated data value compared to the observed. It can be seen that the simulated empirical distribution function from the raw

RCMs is closest to observation. Also, from Table 8.4, depending on the RCM, the univariate BC techniques can increase that distance, in other words, degrade the simulated correlations at specific grid boxes.

Table 8.3: Summary statistics of the empirical distribution of the correlation coefficients between temperature and precipitation time series at the 4840 grid boxes in the study domain during DJF 1978 to 2005 validation period

Statistic	**E-OBS**	**RAW**	**LS**	**EQM**	**QDM**
		R**EMO**			
minimum	0.00	−0.06	−0.21	−0.07	−0.09
5 percentile	0.17	0.10	0.09	0.09	0.09
First quartile	0.24	0.20	0.20	0.20	0.20
Median	0.28	0.26	0.26	0.25	0.26
mean	0.27	0.26	0.25	0.25	0.25
Third quartile	0.31	0.33	0.32	0.31	0.32
95 percentile	0.34	0.39	0.39	0.37	0.38
Maximum	0.38	0.47	0.47	0.45	0.45
		CCLM4			
minimum	0.00	0.11	0.11	0.12	0.11
5 percentile	0.17	0.18	0.18	0.17	0.17
First quartile	0.24	0.23	0.23	0.21	0.21
Median	0.28	0.27	0.27	0.25	0.26
mean	0.27	0.26	0.26	0.25	0.25
Third quartile	0.31	0.30	0.30	0.28	0.29
95 percentile	0.38	0.33	0.33	0.31	0.31
Maximum	0.38	0.35	0.34	0.33	0.33

In Table 8.4, The KS D statistic from the LS approach is mostly close to that from the raw RCM. A plausible reason is that the LS approach applied to daily data, mostly corrects the biases in the mean statistic, while other simulated statistics, for example, the higher moments, still have biases that are comparable with the raw RCM. Considering the REMO model, the QDM performs well for both temperature and precipitation, but the same QDM technique increased the DJF spatial mean and variability temperature biases under CCLM4 (Table 6.6).

As a result, the distance between the empirical distribution function from the simulated and observed data values is further increased in the CCLM4 model by the QDM approach (Table 8.4). This suggests that the choice of the RCM and the performance of distribution-based univariate BC techniques on the individual variables also play major roles in how the BC affects the correlations at the grid box level.

Table 8.4: KS D statistic between the observed empirical distribution functions and that of the simulated data values before and after bias correction, during DJF 1978 to 2005 validation period. The distribution is based on the correlation coefficients between temperature and precipitation time series at the 4840 grid boxes.

RAW	**LS**	**EQM**	**QDM**
	REMO		
0.16	0.17	0.19	0.16
	CCLM4		
0.10	0.10	0.24	0.21

To examine further, Figure 8.1 shows the spatial map of the correlations between the daily DJF temperature and precipitation for observations, and for the CCLM4 model before and after BC with QDM. By visual examination of the correlation maps, the spatial patterns of the correlations were captured by the raw RCM with modest bias (spatial match with Pearson's correlation is 0.83). From both observed and simulated data, the relationship between DJF precipitation and temperature in Germany is weakest over the northeastern parts of Germany and the southeastern parts of Germany. Based on synoptic circulations, a plausible reason can be because, for the northeastern region, dry easterly continental air masses make the boundary layer drier (R3 in Figure 5.3 and Figure 5.4). From Figure 8.1, it can be inferred that (1) for most grid boxes, the simulated correlations between temperature and precipitation in Germany, were not notably changed by the BC; and on the assumption that the correlations (on average) can be physically interpreted based on the NAO variability, this strengthens previous results that univariate BC techniques do not notably change the simulated large-scale

processes, (2) the information from Table 8.3 and Table 8.4 can be further strengthened that while on average, the simulated correlations before and after BC are comparable, at specific grid boxes the BC techniques changed the simulated correlations. For example, in the western part of Germany, Figure 8.1 shows that the magnitude of the simulated correlations was weakened in some regions after the QDM was applied to the individual variables. Indeed, from Figure 8.2a and Figure 8.2b, compared to E-OBS, there are biases in the magnitude of the simulated correlations from the (un)corrected CCLM4 model that is comparable in some domains, but distinct in other domains. Figure 8.2c confirms further that the QDM (slightly) weakened the magnitude of the simulated correlations at some grid boxes, except for the southern parts that have positive biases relative to the raw CCLM4 model.

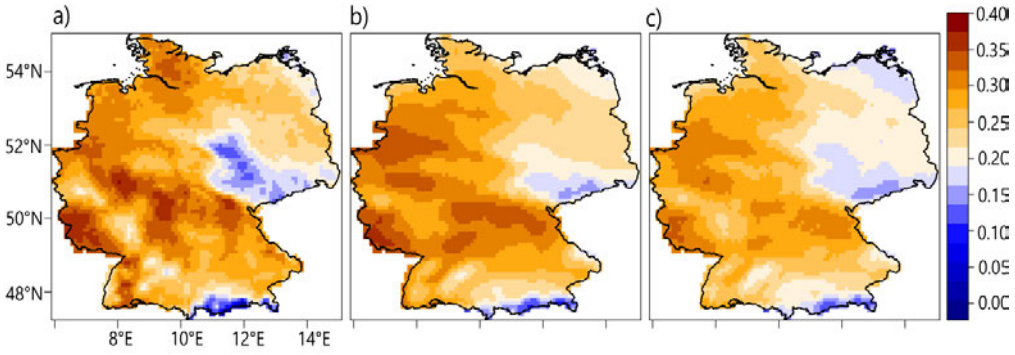

Figure 8.1: Correlation maps between temperature and precipitation from (a) E-OBS, (b) raw CCLM4 RCM output driven by MPI-ESM-LR, and (c) bias-corrected CCLM4 RCM with the QDM technique. The Colour bar is Pearson's correlation coefficient. The correlations are for the daily data for the DJF season, from 1978 to 2005 validation period.

8.1 - Seasonal correlations between temperature and precipitation before and after bias correction

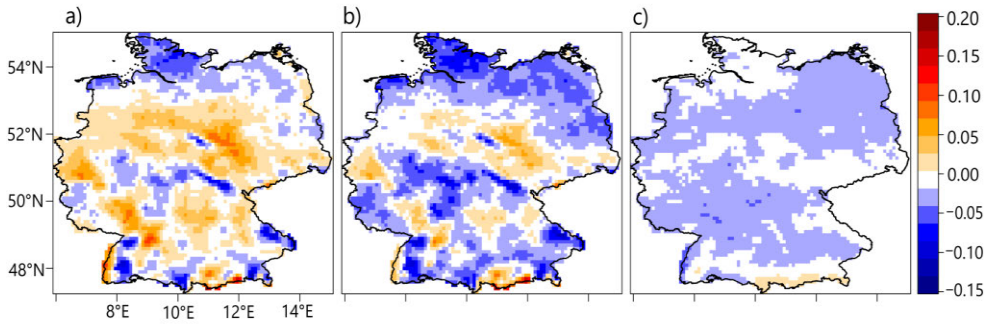

Figure 8.2: Difference between (a) simulated correlation coefficients from raw CCLM4 RCM and that from E-OBS, (b) simulated correlation coefficients from the bias-corrected CCLM4 RCM using the QDM and that from EOBS, (c) simulated correlation coefficients from the bias-corrected CCLM4 RCM using the QDM and that from the raw CCLM4 RCM. The correlation is for the daily temperature and precipitation data for the DJF season, from 1978 to 2005 validation period. The Colour bar is Pearson's correlation coefficient.

8.2 Added value of inter-variable multivariate bias correction on the coherency between climate variables

Recall that the QDM as presented in this study has the flexibility to be used as a univariate BC technique; or as a multivariate BC technique but applied to a single variable and using homogeneous grid boxes as related variables to improve inter-site correlations (that is, MQDM); or as a multivariate BC technique applied to more than one variable at the same time and grid box to improve inter-variable dependencies (that is, MBCn). Further, it is plausible that at specific grid boxes where the QDM degraded the simulated statistical correlations, the bias-corrected variables are no longer physically consistent. For hydrological modeling that relies on consistency between both temperature and precipitation, it will be necessary to ensure that the BC techniques do not degrade the simulated correlations or even improves the correlations among the corrected variables towards observations. Therefore, during the 1978 to 2005 evaluation period for the DJF season when significant correlation was obtained between temperature and precipitation (Table 8.1), the performance of the MBCn in adjusting the biases in the simulated correlations, as well as in the statistics of the

simulated variables is examined further. Given that the MBCn is computationally intensive, randomly selected grid points where the QDM output (that is, QDM applied to CCLM4 model) and the raw CCLM4 model failed to capture a comparable magnitude of the observed correlations are used to investigate the added value of the MBCn. For that reason, two grid points (further referred to as G1 and G2) are used to exemplify the results as documented in Table 8.5 and Table 8.6.

Table 8.5: Correlations coefficients between temperature and precipitation as observed from E-OBS and as simulated by the CCLM4 RCM at the two randomly selected grid boxes before and after univariate and multivariate bias corrections during the 1978 to 2005 validation period for the DJF season. (*) indicates the best performing BC technique with the lowest error.

Grid box	**E-OBS**	**RAW**	**QDM**	**MBCn**
G1	0.25	0.14	0.13	0.25*
G2	0.24	0.15	0.16	0.25*

From Table 8.5, it is obvious that unlike QDM (and the other univariate BC techniques), the MBCn adds clear value in improving the inter-variable correlations towards observations. Nonetheless, the marginal distribution of the MBCn output is supposed to be comparable with that from QDM. Therefore, the bias in the statistics of the corrected individual variables after using QDM and MBCn should be comparable (Table 8.6). From Table 8.6, both QDM and MBCn add more value in reducing the precipitation biases at the grid boxes, but the QDM slightly outperforms the MBCn in adjusting the statistics of the individual variables towards observation. For temperature, the tendency of increasing the biases can be seen under G1 (that is, the 95-percentile value) because the bias from the raw RCM is closer to zero in the validation period - leaving no room for improvement by the BC. As the evaluations in this study is based on the historical climate, the possibility of the BC techniques to increase the biases in the simulated statistic might not be a challenge when the BC techniques are applied to projected values under future emission scenarios. This is because for simulated temperature, warm biases are common in the projected temperature values, especially under

the higher emission scenarios, relative to the historical temperature values. Thus, the BC will be of added value in reducing the warm biases. Further, a reason for the slightly better performance of the QDM in improving the statistics of temperature and precipitation, respectively, at the randomly selected grid boxes (Table 8.6) can be because MBCn reorders the time series of ranks, therefore, possible change in the temporal structure of the data is possible (Vrac 2018).

Table 8.6: Errors in the basic statistics of the time series of simulated temperature and precipitation from CCLM4 RCM at the two randomly selected grid boxes before and after univariate and multivariate bias corrections during the 1978 to 2005 validation period for the DJF season. (*) indicates the best performing (or no) BC technique with the lowest error

Statistic	**RAW**	**QDM**	**MBCn**
Precipitation (mm/day)			
	G1		
Mean	1.77	0.30*	0.35
Standard deviation	0.66	0.44*	0.47
5 percentile	0.00	0.00	0.00
95 percentile	3.61	1.86*	1.89
	G2		
Mean	3.66	0.41*	0.46
Standard deviation	2.89	0.48*	0.51
5 percentile	0.00	0.00	0.00
95 percentile	8.45	1.91*	2.00
Temperature (°C)			
	G1		
Mean	1.72	0.01*	0.12
Standard deviation	0.71	0.11*	0.22
5 percentile	2.47	0.28*	0.30
95 percentile	0.03*	0.68	0.69
	G2		
Mean	0.20	0.18*	0.19
Standard deviation	0.50	0.11*	0.15
5 percentile	1.08	0.38*	0.41
95 percentile	0.49	0.33*	0.38

9. Discussion and recommendations

Several previous studies have highlighted the added value of BC in improving the usability of RCMs for climate impact studies (Paeth et al. 2005; Hagemann et al. 2011; Cannon 2016, 2017; Maraun et al. 2019). Nonetheless, a more comprehensive evaluation of the strengths and weaknesses of RCMs in simulating meteorological processes, and the assessment of the impact of distinct BC techniques on both the statistical and physical aspects of the bias-corrected data sets are necessary (Maraun 2016). The reasons are because (1) current BC techniques do not correct circulation biases and biases associated with the misrepresentation of processes (Maraun et al. 2021), therefore the raw RCMs need to capture large portions of the observed meteorological processes, (2) commonly applied BC techniques do not improve all the statistical characteristics of the RCM output (Ibebuchi et al. 2022a), (3) BC might alter the simulated meteorological patterns and the corresponding meteorological processes (Rocheta et al. 2014), (4) possible modification of the statistical moments and the simulated meteorological patterns might imply that the coherency between the bias-corrected variable and other climate variables is equally altered (Cannon 2017).

Ehret et al. (2012) have suggested that BC may hide the simulated biases because while it appears to improve some statistical aspects of the RCM, the BC output might no longer be physically consistent, and the GCM-RCM model chain might equally be modified. Nonetheless, BC can indeed be a viable technique for impact studies that have targeted requirements on the (statistical) aspect of the RCMs that need to be improved for a specific set of simulated climate variables. The need for hindcast evaluation of distinct BC techniques, to determine the most optimal technique for a targeted study is crucial to avoid further uncertainties in interpreting future change signals (Figure A12). Also, in model selection and evaluations, the selected climate models need to simulate meteorological processes because

deficiencies in simulating processes are major causes of model error and are not corrected by BC but can be improved as part of model development.

Prein et al. (2019) reported that biases from GCMs can significantly impact the representation of weather types in RCMs and the credibility of climate impact assessment with RCMs. One of the major challenges in characterizing circulation biases in climate models is the method used in classifying the atmospheric circulation modes. For example, Landgren et al. (2013) found that the choice of the classification method used, constrained the capability of the RCMs to replicate the reference atmospheric circulation modes over Scandinavia. Addor et al. (2016) stressed the need to decompose GCM-RCM time series using CTs to enable evaluation of process misrepresentation in the RCMs. This study applied a new fuzzy time decomposition technique (that is, the rotated T-MD PCA applied in a fuzzy manner), which has been successfully tested for climate research in several studies (Ibebuchi and Paeth 2021; Ibebuchi 2022a, 2022b, 2022c). The classification method was used to obtain physically interpretable CTs over Western Europe that were easily reproduced from climate model data sets. Using the classified CTs, the representation of atmospheric circulation modes in the RCMs, based on the quality of the RCMs and the data providing the lateral boundary condition was evaluated. Interestingly, the analyzed RCMs replicated portions of the reference circulation patterns and the temporal sequence of circulation patterns when reanalysis data provides the lateral boundary conditions. Further, the results indicated that the GCM-RCM chain can only reproduce the climatological mean of the reference circulation patterns but does not have the skill in reproducing the temporal sequence of the reference circulation patterns. The results agree with Herrara-Lormendez et al. (2022) that in Europe, there is a better agreement in the representation of synoptic circulations among reanalysis products compared to GCMs. Also, the models indicated deficiency in simulating anticyclonic circulations over Western Europe. A major conclusion in the capability of the RCMs to

replicate the reference circulation patterns is that the forcing model was found to be the main factor in reproducing atmospheric circulation (Ibebuchi 2022b).

Several studies have reported that the added value of BC techniques on the statistical aspect of the RCM can be constrained by (1) the choice of RCM and reference data (Gampe et al. 2019), (2) the climate variable considered and the region of inquiry (Luo et al. 2018), (3) the time considered (Haerter et al. 2010; Teng et al. 2015), (4) the choice of the BC technique (Gudmundsson et al. 2012), (5) the temporal resolution of the underlying data (Shreshtha et al. 2017), and (5) the statistical metric of interest: often statistical mean against standard deviation in addition to simulated trends (Hempel et al. 2013). An important finding in this study is that the choice of the appropriate BC technique highly depends on the variable of interest, computation resources, and the aspect of the RCM which is needed to be improved for a targeted study. This implies that no BC technique might be ranked the best, without reservations in relative performances or computation time and resources.

The performances of the BC techniques are evaluated based on the added value to the statistical characterization of the RCMs, and in maintaining the physical consistency of the RCM. Physical consistency was defined in this study as consistency with the meteorological processes associated with the climate variable, and consistency between the bias-corrected variable and other climate variables. For monthly data, simple bias correction techniques such as LS can be sufficient to adjust the biases in the statistics of the simulated climate variable (Shreshtha et al. 2017; Ibebuchi et al. 2022b). However, for precipitation data at the daily resolution, the LS technique adjusts only biases in the first moment but tends to increase the biases in the higher moments. A similar result was reported by Berg et al. (2012) that scaling BC techniques applied to daily simulated precipitation increase the biases in the higher statistical moments. Thus, another important finding in this study is that the temporal resolution, at which the BC technique is applied, is a significant factor in the performance of

the BC technique (Ibebuchi et al. 2022a, 2022b). Adjusting the biases in the statistical moments of daily simulated data is more challenging compared to monthly data, especially for precipitation.

For hydrological impact assessments that require a better representation of the statistics of precipitation (including extreme values), and inter-site correlations that are comparable with observations, the MQDM was developed in this study to produce bias-corrected precipitation data that can fulfil such requirements (Ibebuchi et al. 2022a). For temperature that is mostly well simulated in the raw RCMs, the added value of the distinct BC techniques is relatively slim, compared to when the same techniques are applied to precipitation data for the same suite of RCMs. The results are in agreement with Tong et al. (2021) that for temperature data, there is mostly consistency among the BC techniques, so it is difficult to decide the overall best performing technique. Moreover, it was found that the LS technique did not improve the higher moments of temperature towards observations when they are simulated with biases. The results in this study on the performance of the BC techniques in reducing the biases in the statistics of temperature and precipitation are equally valid if a different data is considered as a reference if its resolution is comparable to the model data (Adakudlu et al. 2022).

Maraun and Widmann (2018) reported that BC techniques might introduce inconsistencies with the driving model. In this study, and for the first time, physically interpretable homogenous regions of summer precipitation and temperature anomalies in Germany were classified using the rotated S-MD PCA applied in a fuzzy manner (Ibebuchi et al. 2022b). No robust indication was found that the BC techniques applied to the analyzed RCMs changed (at a larger scale) the simulated meteorological patterns of temperature and precipitation and the consistency with between the simulated patterns and the synoptic scale mechanisms associated with the pattern variability. Generally, the spatiotemporal configuration of the variability patterns (at a larger scale) was barely affected by all the BC techniques.

Nonetheless, at a relatively more localized spatial scale, the simulated co-variability of the grids was changed by the BC. Thus, while the simulated meteorological patterns are reproduced after the BC, at more localized spatial scales, the simulated co-variability of the grids and the (localized) governing process might be changed by the BC techniques.

Further, univariate BC techniques do not consider inter-variable dependency. According to Rocheta et al. (2014), the application of univariate BC techniques at each grid box in the study region can alter the spatial variability of the simulated variable, which might modify the underlying spatial atmospheric modes and physics. Since BC corrects how much precipitation and temperature that are allowed in each grid box, it is plausible that some aspects of the physical consistency in the fields can be altered, for example, the effects of microphysical and dynamical cloud processes on precipitation, depending on the grid box. Hence, it is arguable that univariate BC techniques might negatively impact the simulated correlations between different climate variables (Maraun 2016). This can imply also that the agreement between aspects of model dynamics might become inconsistent (Bürger et al. 2011).

In this study, a statistically significant correlation between temperature and precipitation in Germany was obtained during the DJF season. The correlation between the spatially averaged temperature and precipitation during the DJF season in Germany implies that higher temperatures can result in higher precipitation amounts (Trenberth and Shea 2005). Further, this relationship can be modified by elevation, continentality and other local-scale processes (Rebetez 1996) so that the correlations are not homogeneous across the grid boxes. To understand the dynamics linking temperature and precipitation in Germany during DJF, and to justify the statistical correlations it was found that during DJF, positive (negative) NAO can imply synoptic circulations associated with wet and warmer (dry and colder) winter conditions over Germany. Thus, the observed and simulated statistical correlation between temperature and precipitation is subject to a well-founded physical explanation.

Depending on the grid box, all the univariate BC techniques tested in this study can degrade the simulated correlations between temperature and precipitation in Germany. This can be a further reason why at localized spatial scales the BC techniques changed the co-variability of the grids (that is, in the simulated meteorological patterns) because the rotated S-MD PCA applied to obtain the meteorological patterns is based on temporal correlations between values at the grid boxes. Therefore, since the correlations between temperature and precipitation can be physically interpreted, depending on the grid box, some aspects of the physical consistency in the simulated variable can be changed by the univariate BC techniques that degraded the inter-variable dependencies (Meyer et al. 2019). Given that hydrological hazards are often associated with local precipitation extremes (Olsson et al. 2012) the overreaching inference is that for hydrological modeling that relies on consistency between both temperature and precipitation, it should be examined if the relevant grid boxes have simulated correlation between the variables that are comparable with observation, and if the grid boxes are negatively affected by the univariate BC technique applied.

Commonly, a copula theory (Nelson 2006) that considers the joint dependency of variables in the course of the BC is used in multivariate bias correction. The implementation of multivariate BC usually relies on univariate BC algorithms to match the simulated multivariate distribution to the observed multivariate distribution (Cannon et al. 2015). The MBCn is the multivariate aspect of the QDM that is designed to improve inter-variable dependencies. Unlike the QDM and MQDM, the MBCn improved the simulated correlations between temperature and precipitation towards observations. Also, at some boxes, the MBCn slightly improved the inter-site correlations of precipitation, but not better than the MQDM. Nonetheless, as reported by François et al. (2020), multivariate BC techniques designed to improve inter-variable dependencies have their deficiencies which were fairly reproduced in this work. François et al. (2020) explained that due to the instability of some multivariate BC

techniques, there is the possibility that the statistical features (for example, simulated temporal structures compared to observations) of the corrected RCMs are degraded. There is also the open question if the coherency between the variables is time-invariant because the non-stationarity of the copula under future climate change is plausible (Zscheischler et al. 2017). Further, increasing the number of variables to be corrected can result in the deterioration of spatial properties of the corrected outputs (François et al. 2020).

In summary, for the study region, it is recommended that simple BC techniques such as LS have the advantage of not being computationally intensive and can be applied to adjust biases in the statistics of monthly temperature and precipitation when incorporating change signal is not of interest. The MQDM that incorporates the spatial dependency structure of precipitation (that has complex spatial interactions) during the BC can be recommended to adjust the biases in the statistics of daily precipitation. For daily temperature, any of the univariate distribution-based BC techniques (that is, EQM or QDM) can be used to adjust the biases in the statistics of temperature, but to incorporate the change signal, QDM might be preferred. The univariate BC techniques tested in this study do not improve the correlations between climate variables. Hence while relative to QDM, the MBCn can be computationally intensive, the MBCn is highly recommended for impact studies that require physical consistency or coherency among climate variables that is comparable with observations. Nonetheless, depending on factors such as nonstationary copula, the MBCn might not always be superior to the QDM, and so its superiority over univariate BC techniques can be problem dependent. Given these trade-offs, the most recommended BC technique depends on the targeted applications of the bias-corrected RCM outputs. Given that depending on the grid box, the QDM that is less computationally intensive does not notably change the simulated inter-variable correlations, a combination of both univariate and multivariate techniques might be considered when the model simulates the observed inter-variable and inter-site dependencies well. This implies

that after applying the univariate BC technique, the few relevant grid boxes where the coherency of the climate variables was significantly misrepresented can be noted, and the multivariate BC technique that considers inter-variable dependency can be applied to adjust the biases at those grid boxes.

Finally, it is recommended that regardless of the BC technique applied, the simulated portions of the meteorological processes should be examined before and after the BC, to further document how the BC has impacted the physical consistency of the RCM.

10. Conclusions

This study evaluated the representation of large-scale circulation patterns in an ensemble of EURO-CORDEX CMIP5 RCMs, and the added value of distinct BC approaches to improving the usability of RCMs for impact assessments. The conclusions are:

(1) The analyzed EURO-CORDEX CMIP5 RCMs produced the reference circulation patterns in Western Europe, but with biases dependent on the choice of RCM and the data providing the lateral boundary conditions. The results further indicated that the data providing the lateral boundary conditions is the main factor in reproducing the atmospheric circulation.

(2) BC techniques added value in reducing the systematic biases in the statistics of simulated temperature and precipitation in Germany. However, the relative performances of the BC techniques can be problem dependent. Hence for a targeted study, a careful evaluation of the distinct BC techniques is necessary for deciding the most appropriate technique(s) to use.

(3) There was no robust indication that at a larger spatial scale, the BC techniques tested in this study constrained the reproducibility of the simulated meteorological patterns of the bias-corrected variables as well as the governing large-scale mechanisms. Nonetheless, at more localized spatial scales, there is the indication that the BC techniques changed the co-variability of the grids, especially for precipitation.

(4) Univariate BC techniques improved the statistics of the RCM towards observations, but did not improve inter-variable correlations, that is, the correlation between temperature and precipitation in Germany. To improve the co-variability among bias-corrected variables, multivariate BC techniques that adjust inter-variable dependencies during the BC proved to be efficient.

Bibliography

Abiodun BJ, Pal JS, Afiesimama EA, Gutowski WJ, Adedoyin A (2008) Simulation of west African monsoon using RegCM3 Part II: impacts of deforestation and desertification. Theor Appl Climatol 93:245–261

Adakudlu M, Xoplaki E, Paeth H, Ibebuchi C, Schönbein D (2022) Providing useful local climate information through statistical bias correction. EGU General Assembly 2022, Vienna, Austria, 23-27 May 2022, EGU22–430

Addor N, Rohrer M, Furrer R, Seibert J (2016) Propagation of biases in climate models from the synoptic to the regional scale: Implications for bias adjustment. J Geophys Res Atmos 121:2075–2089

An S (2003) Conditional Maximum Covariance Analysis and Its Application to the Tropical Indian Ocean SST and Surface Wind Stress Anomalies. J Clim 16:2932–2938

Barros V, Field C, Dokken D, Mastrandrea M, Mach K, Bilir T, Chatterjee M, Ebi K, Estrada Y, Genova R, Girma B, Kissel E, Levy A, MacCracken S, Mastrandrea P, White L, (eds). Climate change (2014) impacts, adaptation, and vulnerability. Part B: regional aspects. In: Contribution of working group II to the fifth assessment report of the intergovernmental panel on climate change. Cambridge University Press, Cambridge

Behera SK, Rao SA, Saji HN, Yamagata T (2003) Comments on “A Cautionary Note on the Interpretation of EOFs.” J Clim 16:1087–1093

Benestad R (2016) Downscaling Climate Information. Oxford Research Encyclopedia of Climate Science. Retrieved 21 December 2021, from https://doi.org/10.1093/acrefore/9780190228620.013.27

Berg P, Feldmann H, Panitz H-J (2012) Bias correction of high resolution regional climate model data. J Hydrol 448–449:80–92

Bronstert A, Kolokotronis V, Schwandt D, Straub H (2007) Comparison and evaluation of regional climate scenarios for hydrological impact analysis: General scheme and application example. Int J Climatol 27:1579–1594

Bürger G, Schulla J, Werner A (2011) Estimates of future flow, including extremes, of the Columbia River headwaters. Water Resour Res 47: W10520

Cannon AJ, Sobie SR, Murdock TQ (2015) Bias Correction of GCM Precipitation by Quantile Mapping: How Well Do Methods Preserve Changes in Quantiles and Extremes? J Clim 28:6938–6959

Cannon AJ (2016) Multivariate Bias Correction of Climate Model Output: Matching Marginal Distributions and Intervariable Dependence Structure. J Clim 29:7045–7064

Cannon AJ (2017) Multivariate quantile mapping bias correction: An N-dimensional probability density function transform for climate model simulations of multiple variables. Clim Dyn 50:31–49

Cattell RB (1966) The scree test for the number of factors. Multivar Behav Res. 1:245–276

Cherry S (1996) Singular Value Decomposition Analysis and Canonical Correlation Analysis. J Clim 9:2003–2009

Cherry S (1997) Some Comments on Singular Value Decomposition Analysis. J Clim 10: 1759–1761

Clark AJ, Gallus WA, Xue M, Kong F (2010) Convection-allowing and convection-parameterizing ensemble forecasts of a mesoscale convective vortex and associated severe weather environment. WAF 25:1052–1081

Compagnucci RH, Araneo D, Canziani PO (2001) Principal sequence pattern analysis: a new approach to classifying the evolution of atmospheric systems. Int J Climatol 21:197–217

Compagnucci RH, Richman MB (2008) Can principal component analysis provide atmospheric circulation or teleconnection patterns? Int J Climatol 6:703–726

Cornes RG, van der Schrier G, van den Besselaar EJM, Jones PD (2018) An Ensemble Version of the E-OBS Temperature and Precipitation Datasets. J Geophys Res Atmos 123: 9391–9409

Craig PM, Ferreira D, Methven J (2016) The contrast between Atlantic and Pacific surface water fluxes. Tellus A: Dyn Meteorol Oceanogr 69:1

Davis RE, Hayden BP, Gay DA, Phillips WL, Jones GV (1997) The North Atlantic subtropical anticyclone. J Clim 10:728–744

Dholakia SG, Bhavsar CD (2017) Factor recovery by principal component analysis and Harris component analysis. Asian J Soc Sci Arts Humanit 7:2249–7315

Dosio A, Paruolo P (2011) Bias correction of the ENSEMBLES high resolution climate change projections for use by impact models: Evaluation on the present climate. J Geophys Res Atmos 116

Druyan LM, Fulakeza M, Lonergan P (2008) The impact of vertical resolution on regional model simulation of the west African summer monsoon. Int J Climatol 28:1293–1314

Eden JM, Widmann M, Grawe D, Rast S (2012) Skill, correction, and downscaling of GCM-simulated precipitation. J Clim 25:3970–3984

Ehret U, Zehe E, Wulfmeyer V, Warrach-Sagi K, Liebert J (2012) Should we apply bias correction to global and regional climate model data? Hydrol Earth Syst Sci Discuss 9:5355–5387

Faghih M, Brissette F, Sabeti P (2022) Impact of correcting sub-daily climate model biases for hydrological studies. Hydrol Earth Syst Sci 26:1545–1563

Feldmann H, Früh B, Schädler G, et al. (2008) Evaluation of the precipitation for South-western Germany from high resolution simulations with regional climate models. Meteorol Z 17:455–465

Fernandez-Granja JA, Casanueva A, Bedia J, Fernandez J (2021) Improved atmospheric circulation over Europe by the new generation of CMIP6 earth system models. Clim Dyn 56: 3527–3540

Fischer S, Schumann A (2014) Comparison between classical annual maxima and peak over threshold approach concerning robustness. Retrieved 21 December 2021, from https://doi.org/10.17877/DE290R-15512

Flato G, Marotzke J, Abiodun B, Braconnot P, Chou SC, Collins W, Cox P, Driouech F, Emori S, Eyring V, Forest C, Gleckler P, Guilyardi E, Jakob C, Kattsov V, Reason C, Rummukainen M (2013) Evaluation of Climate Models. In: Climate Change 2013: The Physical Science Basis. Contribution of Working Group I to the Fifth Assessment Report of the Intergovernmental Panel on Climate Change [Stocker TF, Qin D, Plattner G-K, Tignor M, Allen SK, Boschung J, Nauels A, Xia Y, Bex V, Midgley PM (eds.)]. Cambridge University Press, Cambridge, United Kingdom and New York, NY, USA

Fowler HJ, Blenkinsop S, Tebaldi C (2007) Linking climate change modelling to impacts studies: Recent advances in downscaling techniques for hydrological modelling. Int J Climatol 27:1547–1578

François B, Vrac M, Cannon AJ, Robin Y, Allard D (2020) Multivariate bias corrections of climate simulations: which benefits for which losses? Earth Sys Dynam 11:537–562

Gampe D, Schmid J, Ludwig R (2019) Impact of Reference Dataset Selection on RCM Evaluation, Bias Correction, and Resulting Climate Change Signals of Precipitation. J Hydrometeorol 20:1813-1828

Gudmundsson L, Bremnes J, Haugen J, Engen-Skaugen T (2012) Technical note: Downscaling RCM precipitation to the station scale using statistical transformations—A comparison of methods. Hydrol Earth Syst Sci 16:3383–3390

Haerter J, Hagemann S, Moseley C, Piani C (2010) Climate model bias correction and the role of timescales. Hydrol Earth Syst Sci Discuss 15:1065–1079

Hagemann S, Chen C, Haerter J, Heinke J, Gerten D, Piani C (2011) Impact of a statistical bias correction on the projected hydrological changes obtained from three GCMs and two hydrology models. J Hydrometeorol 12:556–578

Hempel S, Frieler K, Warszawski L, Schewe J, Piontek F (2013) A trend-preserving bias correction—The ISI-MIP approach. Earth System Dyn 4:219–236

Hendrickson AE, White PO (1964) Promax: a quick method to oblique simple structure. Br J Stat Psychol 17:65

Henley J, Chrisafis A, Jones S (2019) France records all-time highest temperature of 45.9C. The Guardian. Retrieved 14 April 2021, from

https://www.theguardian.com/world/2019/jun/28/france-on-red-alert-as-heatwave-forecast-to-reach-record-45c

Herrara-Lormendez P, Mastrantonas N, Douville H, Hoy A, Matschullat J (2022) Synoptic circulation changes over Central Europe from 1900 to 2100: Reanalyses and Coupled Model Intercomparison Project phase 6. Int J Climatol 42:4062–4077

Hersbach H, Bell B, Berrisford P, Hirahara S, et al. (2020) The ERA5 global reanalysis. Q J R Meteorol Soc 730:1999–2049

Hurrell JW (1995) Decadal trends in the North Atlantic Oscillation: Regional temperatures and precipitation. Science 269:676–679

Huth R, Beck C, Philipp A, Demuzere M, Ustrnul Z, Cahynová M, Kysely J, Tveito OE (2008) Classifications of atmospheric circulation patterns: recent advances and applications. Ann N Y Acad Sci 1146:105–152

Ibebuchi CC, Paeth H (2021) The Imprint of the Southern Annular Mode on Black Carbon AOD in the Western Cape Province. Atmosphere 12:1287

Ibebuchi and Richman (2022) Optimized classification of atmospheric modes of variability using rotated principal component analysis. Personal discussion

Ibebuchi CC (2022a) Patterns of atmospheric circulation in Western Europe linked to heavy rainfall in Germany: preliminary analysis into the 2021 heavy rainfall episode. Theor Appl Climatol 148:269–283

Ibebuchi CC (2022b) On the representation of atmospheric circulation modes in regional climate models over Western Europe. Int J Climatol 43:668–682

Ibebuchi CC (2022c) Circulation patterns linked to the positive sub-tropical Indian Ocean dipole. Adv Atmos Sci 40:110–128

Ibebuchi CC, Schönbein D, Adakudlu M, Xoplaki E, Paeth H (2022a) Comparison of three techniques to adjust daily precipitation biases from regional climate models over Germany. Water 14:600

Ibebuchi CC, Schönbein D, Paeth H (2022b) On the added value of statistical post-processing of regional climate models to identify homogeneous patterns of summer rainfall anomalies in Germany. Clim Dyn 59:2769–2783

Jacob D, Petersen J, Eggert B, Alias A, et al. (2014) EURO-CORDEX: new high-resolution climate change projections for European impact research. Reg Environ Change 14:563–578

Janjic T, Bormann N, Bocquet M, Carton J, Cohn S, Dance S, Losa S, Nichols N, Potthast R, Waller J, Weston P (2017) On the representation error in data assimilation. Q J R Meteorol 144:1257–1278

Jones PW (1999) First- and Second-Order Conservative Remapping Schemes for Grids in Spherical Coordinates. Mon Wea Rev 127:2204–2210

Karl TR, Koscielny AJ (1982) Drought in the United States: 1895–1981. J Climatology 2:313-329

Kendall M (1938) A new measure of rank correlation. Biometrika 30:81–89

Kidson JW (1997) The utility of surface and upper air data in synoptic climatological specification of surface climatic variables. Int J Climatol 17:399–413

Landgren OA, Skaugen TE, Haugen JE (2013) Evaluation of circulation patterns over Scandinavia from ENSEMBLES regional climate models. In: Report no. 4/2013 Climate

Lenderink G, van Ulden A, van den Hurk B, et al. (2007) A study on combining global and regional climate model results for generating climate scenarios of temperature and precipitation for the Netherlands. Clim Dyn 29:157–176

Lorenzo-Seva U, ten Berge JMF (2006) Tucker's congruence coefficient as a meaningful index of factor similarity. Methodology 2:57–64

Luo M, Liu T, Meng F, Duan Y, Frankl A, Bao A, De Maeyer P (2018) Comparing Bias Correction Methods Used in Downscaling Precipitation and Temperature from Regional Climate Models: A Case Study from the Kaidu River Basin in Western China. Water 10:1046

Maraun D, Wetterhall F, Ireson AM, Chandler RE, et al. (2010) Precipitation downscaling under climate change: Recent developments to bridge the gap between dynamical models and the end user. Rev Geophys 48:RG3003

Maraun D (2016) Bias Correcting Climate Change Simulations - a Critical Review. Curr Clim Change Rep 2:211–220

Maraun D, Shepherd T, Widmann M, Zappa G, Walton D, Gutierrez JM, Mearns L (2017) Towards process-informed bias correction of climate change simulations. Nat Clim Change 7:764–773

Maraun D, Widmann M (2018) Statistical Downscaling and Bias Correction for Climate Research. Cambridge: Cambridge University Press

Maraun D, Huth R, Gutiérrez J, San Martín D et al. (2019) The VALUE perfect predictor experiment: Evaluation of temporal variability. Int J Climatol 39:3786–3818

Maraun D, Truhetz H, Schaffer A (2021) Regional Climate Model Biases, Their Dependence on Synoptic Circulation Biases and the Potential for Bias Adjustment: A Process-Oriented

Evaluation of the Austrian Regional Climate Projections. J Geophys Res Atmos 126:e2020JD032824

Massey FJ (1951) The Kolmogorov-Smirnov Test for Goodness of Fit. J Am Stat Assoc 46: 68

Mehta V, Suarez M, Manganello J, Delworth T (2000) Oceanic influence on the North Atlantic Oscillation and associated Northern Hemisphere climate variations: 1959–1993. Geophys Res Lett 27:121–124

Merkenschlager C, Hertig E (2020) Seasonal assessments of future daily precipitation extremes in the Mediterranean area under consideration of non-stationarities within the predictor-predictand relationships. Clim Res 80

Meyer J, Kohn I, Stahl K, Hakala K, Seibert J, Cannon AJ (2019) Effects of univariate and multivariate bias correction on hydrological impact projections in alpine catchments. HESS 23:339–1354

Müller WA, Jungclaus JH, Mauritsen T, Baehr J, Bittner M, et al. (2018) A Higher-resolution Version of the Max Planck Institute Earth System Model (MPI-ESM1.2-HR). J Adv Model Earth Syst 10:383–1413

Nelsen RB (2006) An Introduction to Copulas. 2nd ed. Springer, 218 pp

Olsson J, Willén U, Kawamura A (2012) Downscaling extreme short-term regional climate model precipitation for urban hydrological applications. Hydrol Res 43:341–351

Osborn TJ, Briffa KR, Tett SFB, Jones PD, Trigo RM (1999) Evaluation of the North Atlantic Oscillation as simulated by a climate model. Clim Dyn 15:685–702

Paeth H, Born K, Podzun R, Jacob D (2005) Regional dynamical downscaling over West Africa: Model evaluation and comparison of wet and dry years. Meteorol Z 14:349–367

Paeth H, Born K, Girmes R, Podzun R, Jacob D (2009) Regional Climate Change in Tropical and Northern Africa due to Greenhouse Forcing and Land Use Changes. J Clim 22:114–132

Paeth H (2011) Postprocessing of simulated precipitation for impact research in West Africa. Part I: Model output statistics for monthly data. Clim Dyn 36:1321–1336

Paeth H, Diederich M (2011) Postprocessing of simulated precipitation for impact studies in West Africa – part II: a weather generator for daily data. Clim Dyn 36:1337–1348

Panofsky HW, Brier GW (1968) Some Applications of Statistics to Meteorology. The Pennsylvania State University Press, Philadelphia, 6186

Prein AF, Bukovsky MS, Mearns LO, Bruyère CL, Done JM (2019) Simulating North American weather types with regional climate models. Front Environ Sci 7:36

Prohaska J (1976) A technique for analyzing the linear relationships between two meteorological fields. Mon Wea Rev 104:1345–1353

Rebetez M (1996) Seasonal relationship between temperature, precipitation and snow cover in a mountainous region. Theor Appl Climatol 54:99–106

Rencher AC (1992) Interpretation of Canonical Discriminant Functions, Canonical Variates, and Principal Components. Am Stat 46:217–225

Ricardo T, Osborn T, Corte-Real J (2002) The North Atlantic Oscillation influence on Europe: climate impacts and associated physical mechanisms. Clim Res 20:9–17

Richman MB (1981) Obliquely rotated principal components: an improved meteorological map typing technique? J Appl Meteorol 20:1145–1159

Richman MB, Lamb PJ (1985) Climatic pattern analysis of three and seven-day summer rainfall in the Central United States: some methodological considerations and regionalization. J Clim Appl Meteorol 12:1325–1343

Richman MB (1986) Rotation of principal components. J Climatol 6:293–335

Richman MB, Easterling W (1988) Procrustes Target Analysis: A Multivariate Tool for Identification of Climate Fluctuations. J Geophys Res 93:10989–11003

Richman MB, Gong X (1999) Relationships between the definition of the hyperplane width to the fidelity of principal component loadings patterns. J Clim 6:1557–1576

Rocheta E, Evans JP, Sharma A (2014) Assessing atmospheric bias correction for dynamical consistency using potential vorticity. Environ Res Lett 9:124010

Rosen C (2010) Mexican climate reports under fire. Nature. Retrieved 21 October 2021, from https://doi.org/10.1038/news.2010.640

Scaife AA, Folland CK, Alexande LV, Moberg A, Knight JR (2008) European Climate Extremes and the North Atlantic Oscillation. J Clim 21:72–83

Shrestha M, Acharya S, Shrestha P (2017) Bias correction of climate models for hydrological modeling – are simple methods still useful? Meteorol Appl 24:531–539

Sillmann J, Kharin V, Zhang X, Zwiers F, Bronaugh D (2013) Climate extremes indices in the CMIP5 multimodel ensemble: Part 1. Model evaluation in the present climate. J Geophys Res Atmos 118:1716–1733

Skliris N, Zika JD, Herold L, et al. (2018) Mediterranean sea water budget long-term trend inferred from salinity observations. Clim Dyn 51:2857–2876

Teichmann C, Eggert B, Elizalde A, Haensler A, Jacob D, et al. (2013) How Does a Regional Climate Model Modify the Projected Climate Change Signal of the Driving GCM: A Study over Different CORDEX Regions Using REMO. Atmosphere 4:214–236

Teng J, Potter N, Chiew F, Zhang L, Wang B, Vaze J, Evans J (2015) How does bias correction of regional climate model precipitation affect modelled runoff? Hydrol Earth Syst Sci 19:711–728

Tong Y, Gao X, Han Z, et al. (2021) Bias correction of temperature and precipitation over China for RCM simulations using the QM and QDM methods. Clim Dyn 57:1425–1443

Trenberth KE, Shea DJ (2005) Relationships between precipitation and surface temperature. Geophys Res Lett 32

Trenberth KE (2007) Warmer oceans, stronger hurricanes. Scientific American 45−51. Retrieved 21 April 2021, from https://www.scientificamerican.com/article/warmer-oceans-stronger-hurricanes/

Vaittinada Ayar P, Vrac M, Mailhot A (2021) Ensemble bias correction of climate simulations: preserving internal variability. Sci Rep 11:3098

Vazquez M, Ferreira F, Nieto R, Liberato M, Gimeno L (2020) Moisture transport toward Europe and extreme precipitation events, in Proceedings of the 3rd International Electronic Conference on Atmospheric Sciences, 16–30 November 2020, MDPI: Basel, Switzerland

Volosciuk C, Maraun D, Semenov V, et al. (2016) Rising Mediterranean Sea surface temperatures amplify extreme summer precipitation in Central Europe. Sci Rep 6:32450

Vrac M (2018) Multivariate bias adjustment of high-dimensional climate simulations: the Rank Resampling for Distributions and Dependences (R2D2) bias correction. Hydrol Earth Syst Sci 22:3175–3196

Walker G (1904) Walker: Identifying the Southern Oscillation. Retrieved 21 June 2022, from https://iridl.ldeo.columbia.edu/maproom/ENSO/New/walker.html

White D, Richman MB, Yarnal B (1991) Climate regionalization and rotation of principal components. Int J Climatol 11:1–25

Widmann M, Bedia J, Gutiérrez J, Bosshard T, Hertig E, Maraun D, et al. (2019) Validation of spatial variability in downscaling results from the VALUE perfect predictor experiment. Int J Climatol 39:3819–3845

Wilby RL, Wigley TML (1997) Downscaling general circulation model output: a review of methods and limitations. Prog Phys Geogr 21:530–548

Wu J, Gao X (2020) Present day bias and future change signal of temperature over China in a series of multi-GCM driven RCM simulations. Clim Dyn 54:1113–1130

Zhang B, Soden BJ (2019) Constraining climate model projections of regional precipitation change. Geophys Res Lett 46:10522–10531

Zscheischler J, Fischer EM, Lange S (2017) The effect of univariate bias adjustment on multivariate hazard estimates. Earth Syst Dynam 10:31–43

List of Publications

Ibebuchi CC (2022a) Patterns of atmospheric circulation in Western Europe linked to heavy rainfall in Germany: preliminary analysis into the 2021 heavy rainfall episode. Theor Appl Climatol 148:269–283. **Author contribution:** study was designed and executed by I.C.C.

Ibebuchi CC (2022b) On the representation of atmospheric circulation modes in regional climate models over Western Europe. Int J Climatol 43:668–682. **Author contribution:** study was designed and executed by I.C.C.

Ibebuchi CC (2022c) Circulation patterns linked to the positive sub-tropical Indian Ocean dipole. Adv Atmos Sci 40:110–128. **Author contribution:** study was designed and executed by I.C.C.

Ibebuchi CC, Schönbein D, Adakudlu M, Xoplaki E, Paeth H (2022a) Comparison of three techniques to adjust daily precipitation biases from regional climate models over Germany. Water 14:600. **Author contribution:** Conceptualization; methodology; software; validation; formal analysis; investigation; data curation; writing—original draft preparation; writing—reviewing and editing; visualization.

Ibebuchi CC, Schönbein D, Paeth H (2022b) On the added value of statistical post-processing of regional climate models to identify homogeneous patterns of summer rainfall anomalies in Germany. Clim Dyn 59:2769–2783. **Author contribution:** Conceptualization; methodology; software; validation; formal analysis; investigation; data curation; writing—original draft preparation; writing—reviewing and editing; visualization.

Appendix

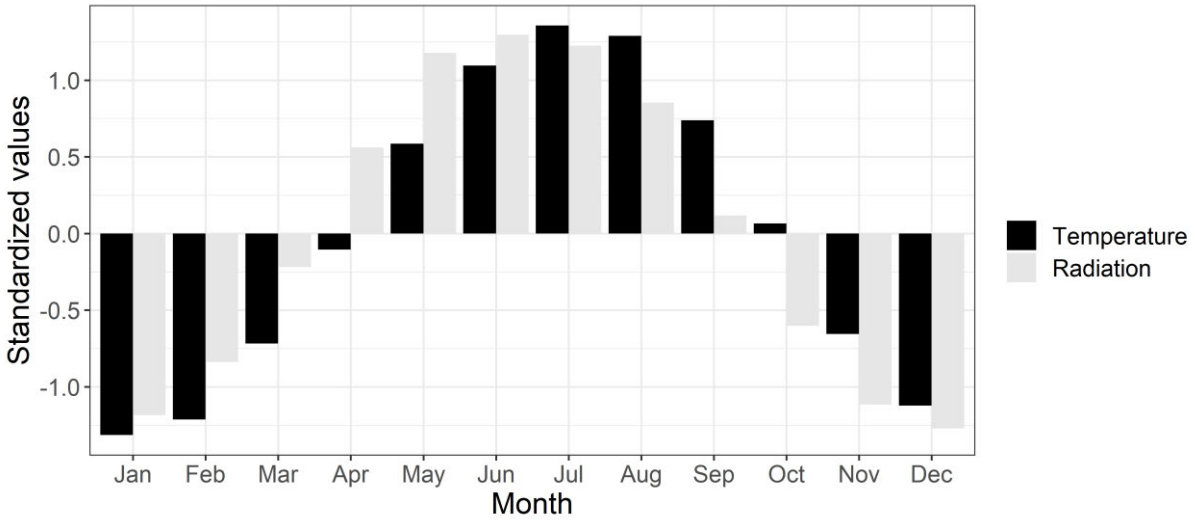

Figure A1: Standardized values of temperature and solar radiation, averaged over Germany. The data source is E-OBS from 1981 to 2010

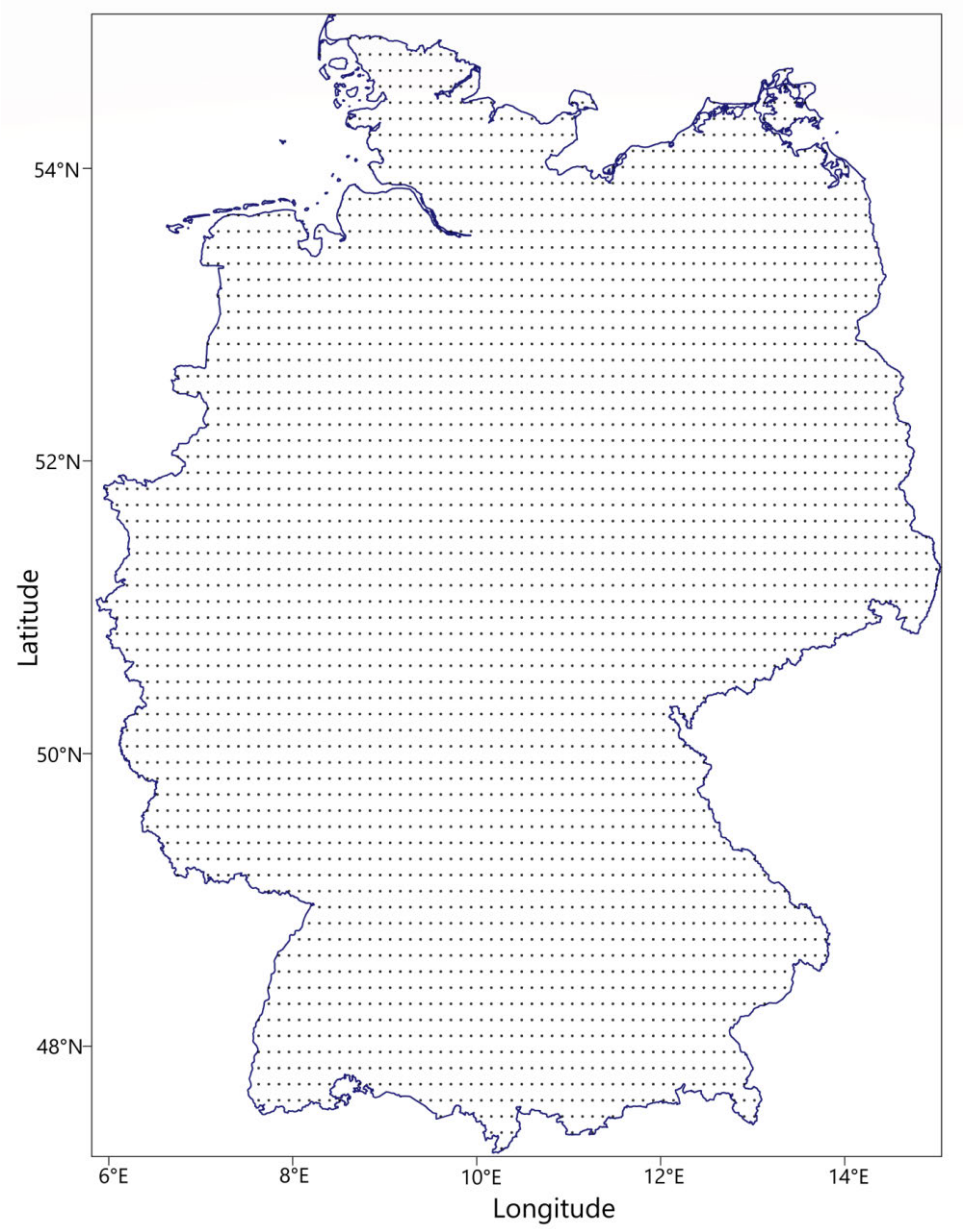

Figure A2: Horizontal resolution of the RCM data in the study domain

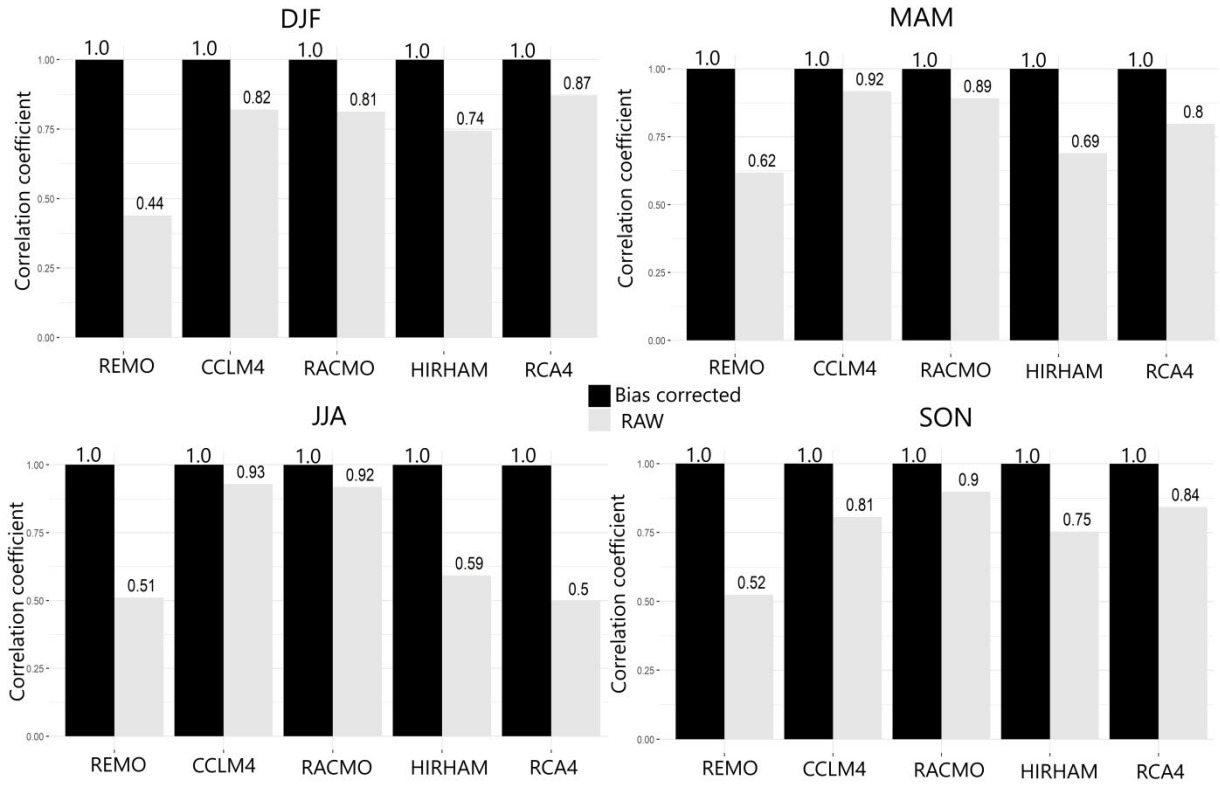

Figure A3: Performance of linear scaling on the spatial correlation between observed and simulated precipitation data from five distinct RCMs driven by MPI-ESM-LR. The validation period is 1979 to 2005.

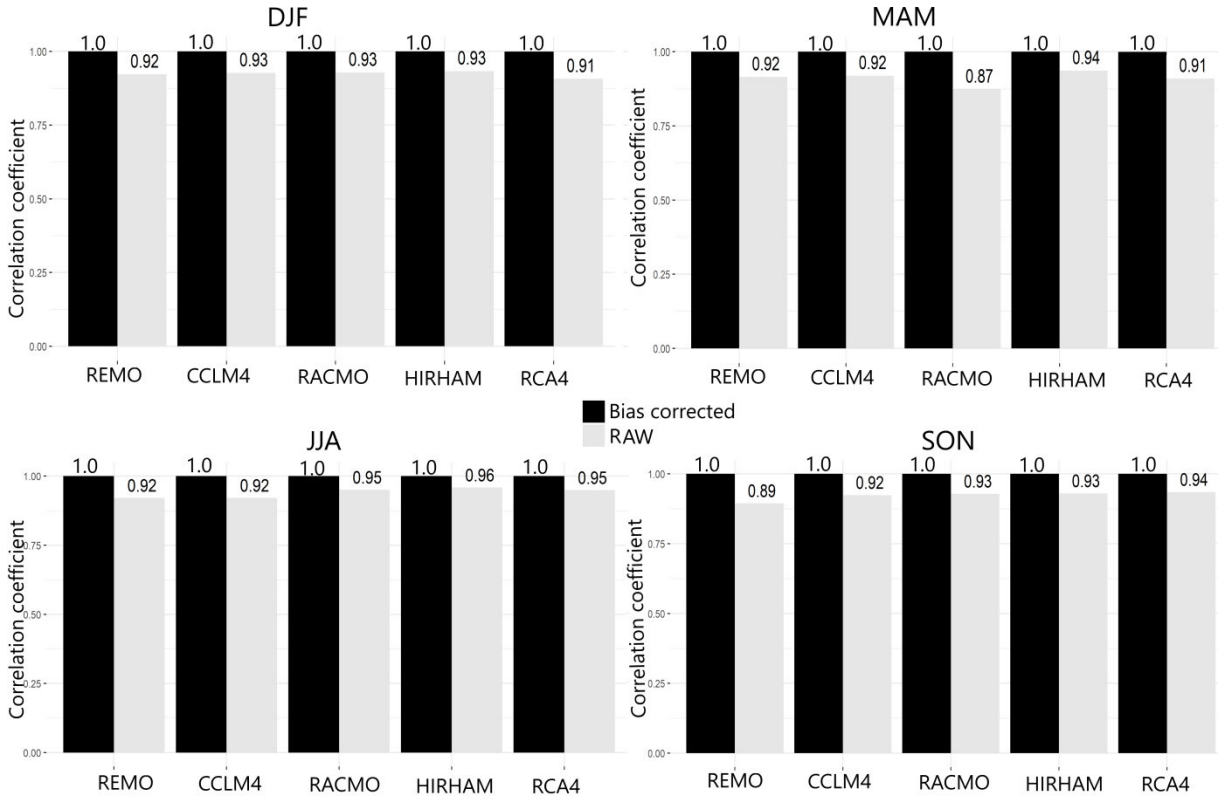

Figure A4: Performance of linear scaling on the spatial correlation between observed and simulated temperature data from five distinct RCMs driven by MPI-ESM-LR. The validation period is 1979 to 2005.

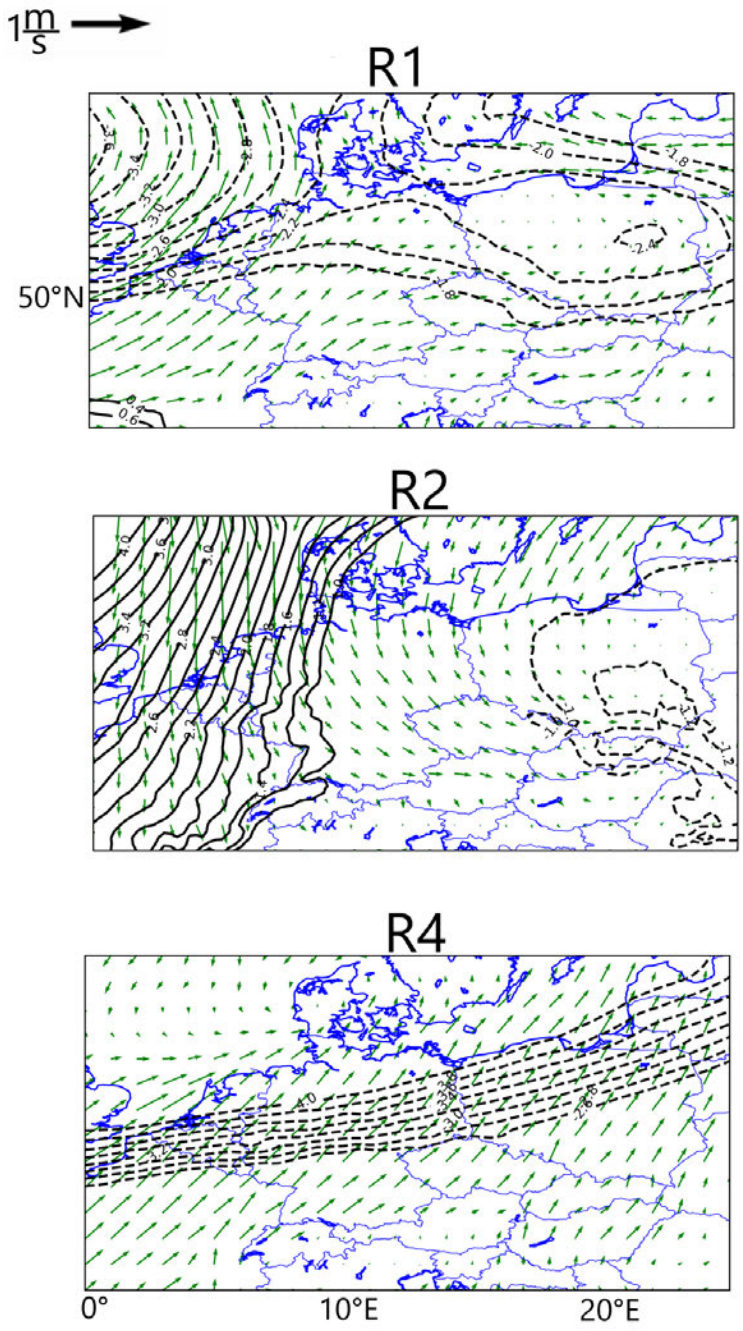

Figure A5: SLP (black contour) and 10-meter wind (green vectors) composite anomaly patterns of the positive phase of some MJJA precipitation variability patterns from the CCLM4 RCM driven by MPI-ESM-LR. The composite patterns are created with the PC scores from the linear scaling output applied to the CCLM4 RCM. Dashed (thick) contours indicate negative (positive) SLP anomaly.

a)

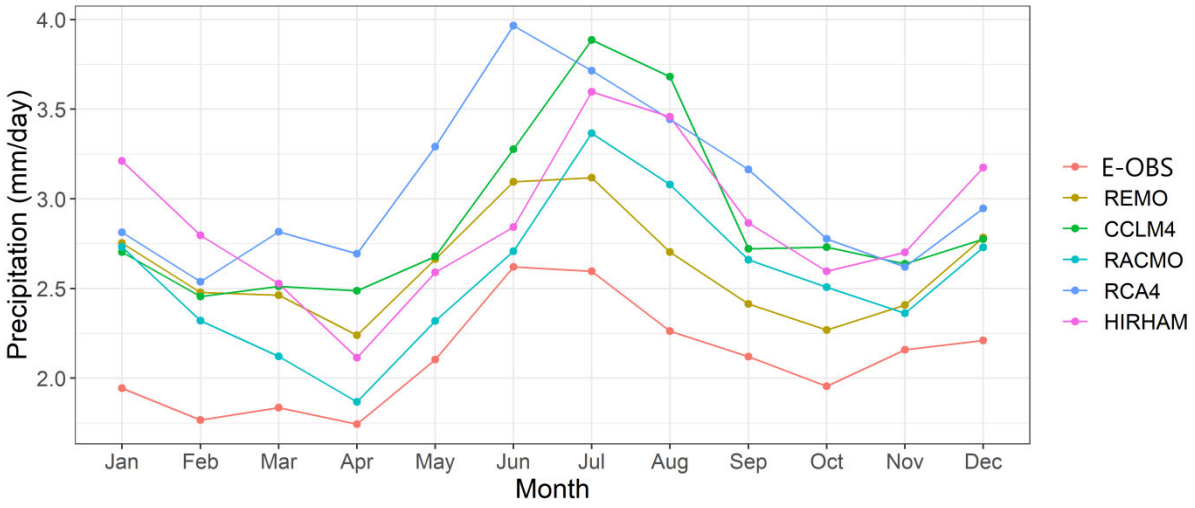

b)

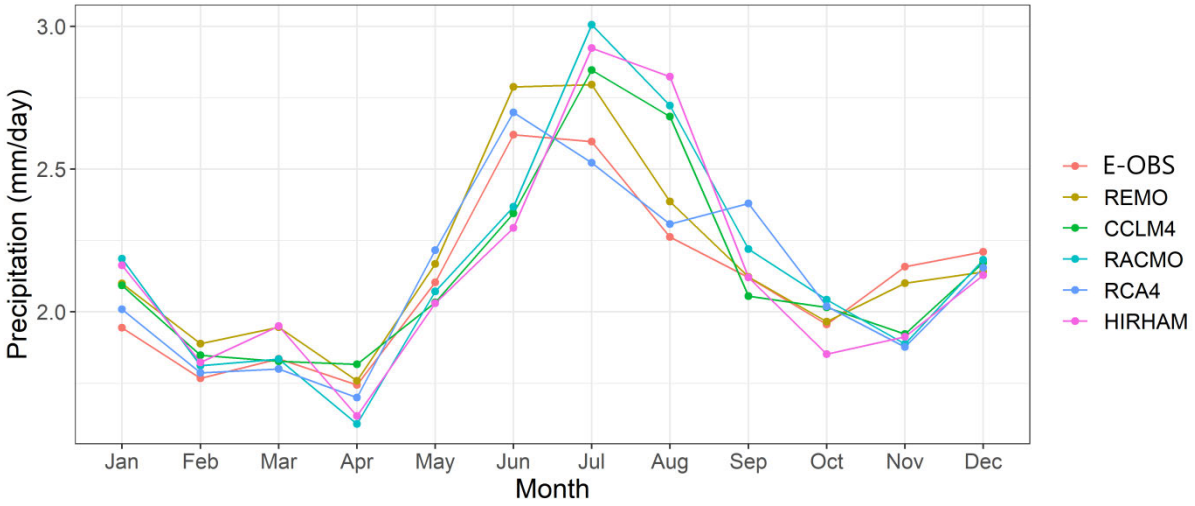

Figure A6: Annual cycle of daily precipitation data from the raw RCMs driven by the MPI-ESM-LR (a) and after bias correction with MQDM (b)

a)

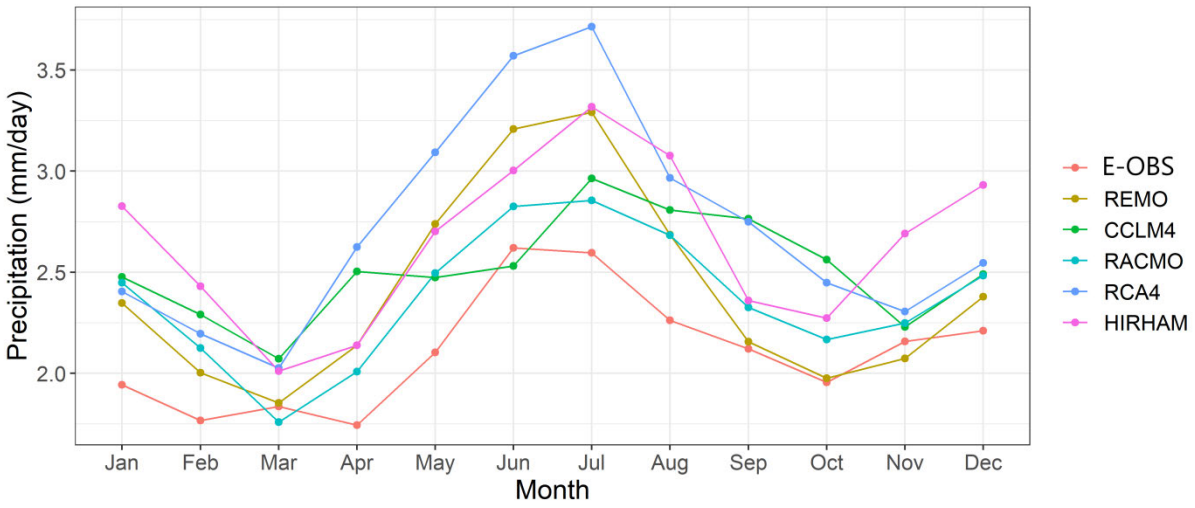

b)

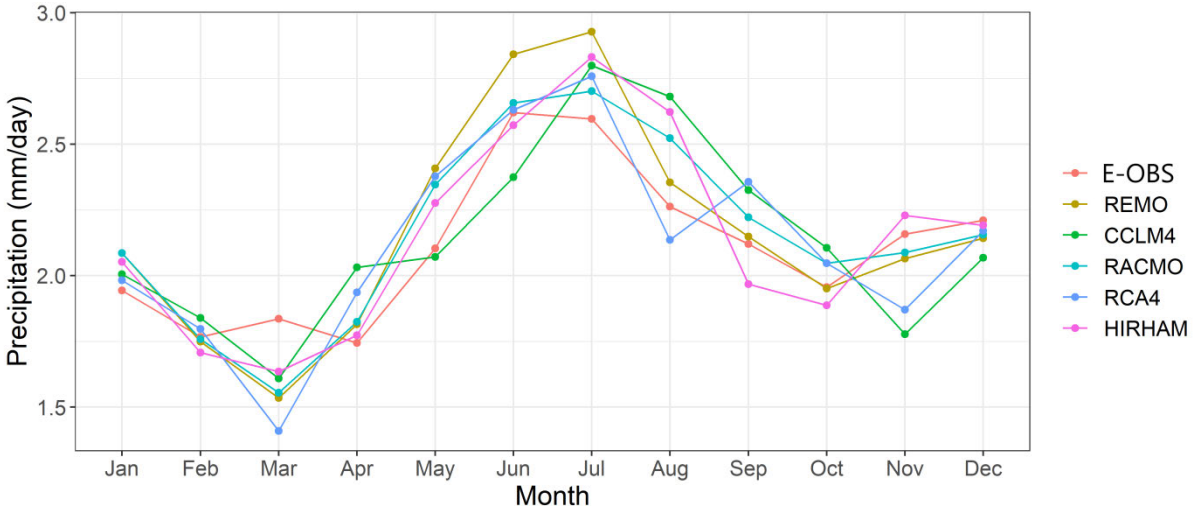

Figure A7: Annual cycle of daily precipitation data from the raw RCMs driven by the CNRM (a) and after bias correction with MQDM (b)

a)

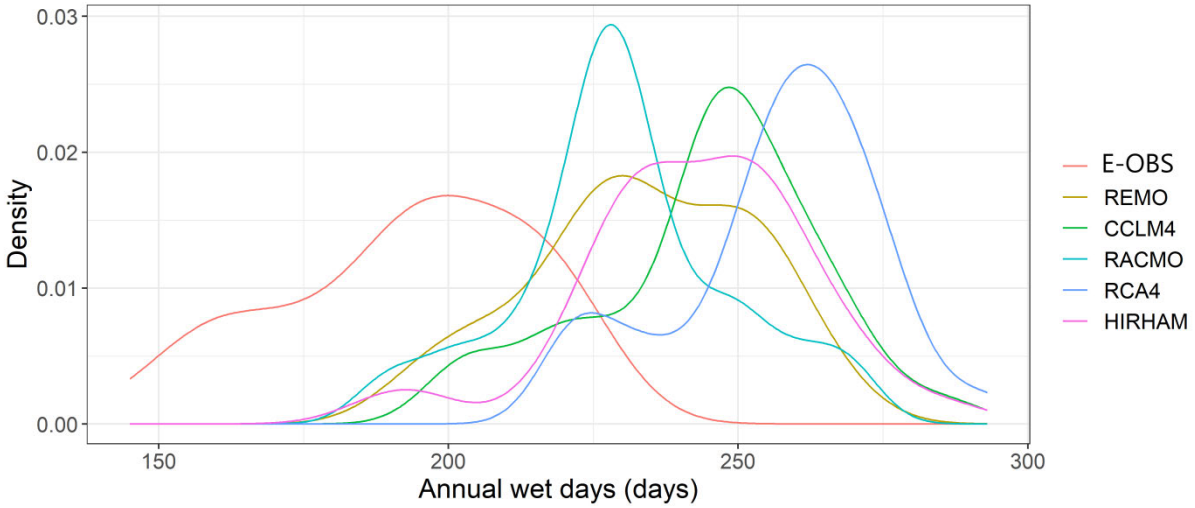

b)

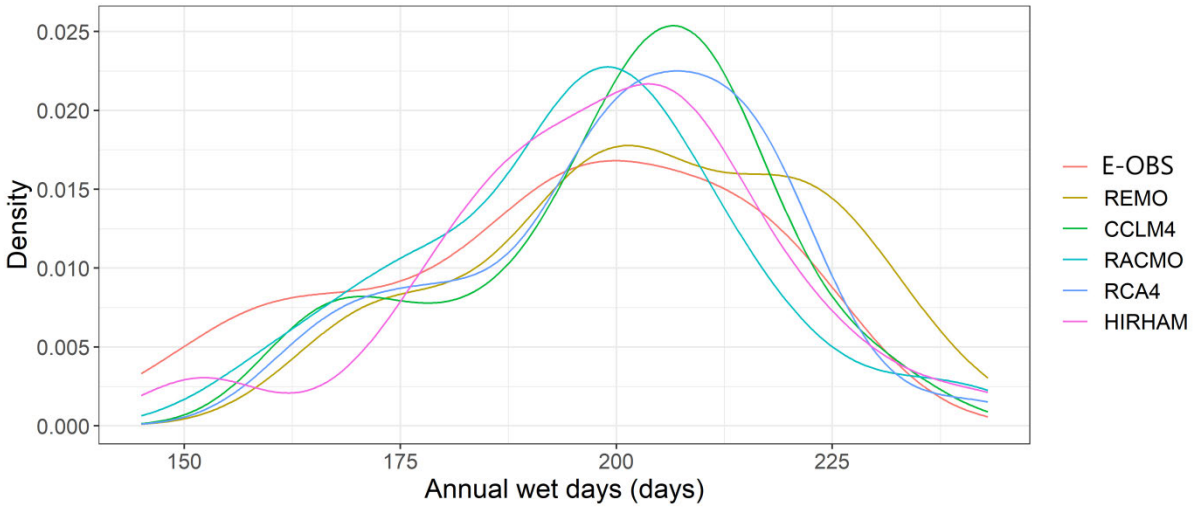

Figure A8: Annual wet day frequency of daily precipitation data from the raw RCMs driven by the MPI-ESM-LR (a) and after bias correction with MQDM (b)

a)

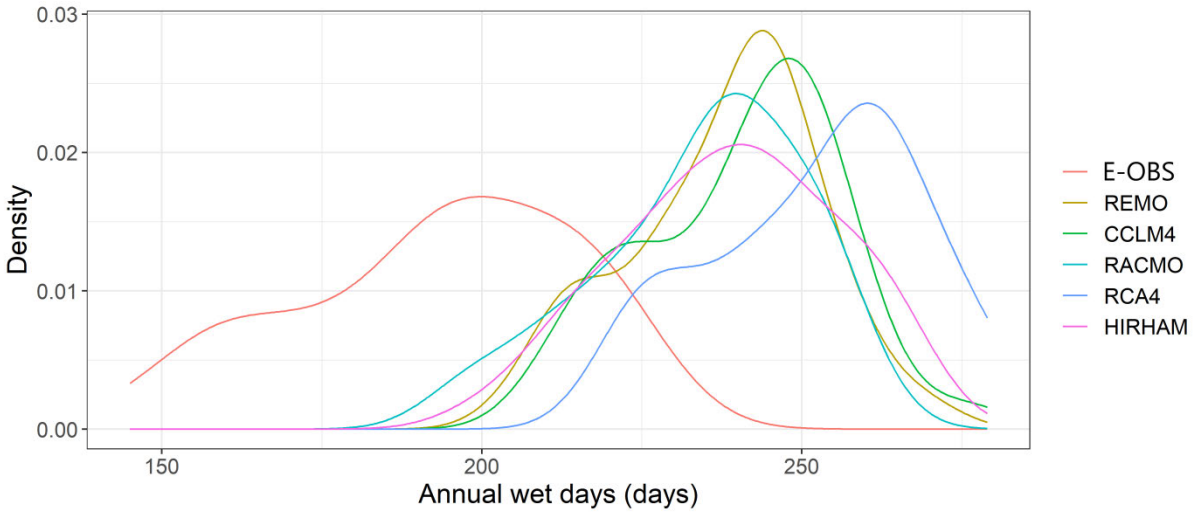

b)

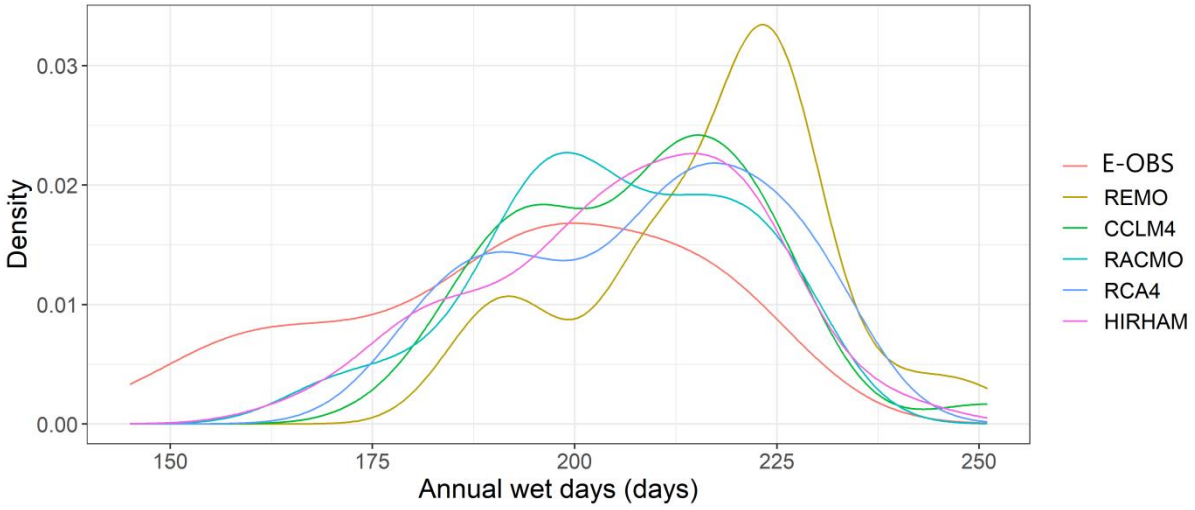

Figure A9: Annual wet day frequency of daily precipitation data from the raw RCMs driven by the CNRM (a) and after bias correction with MQDM (b)

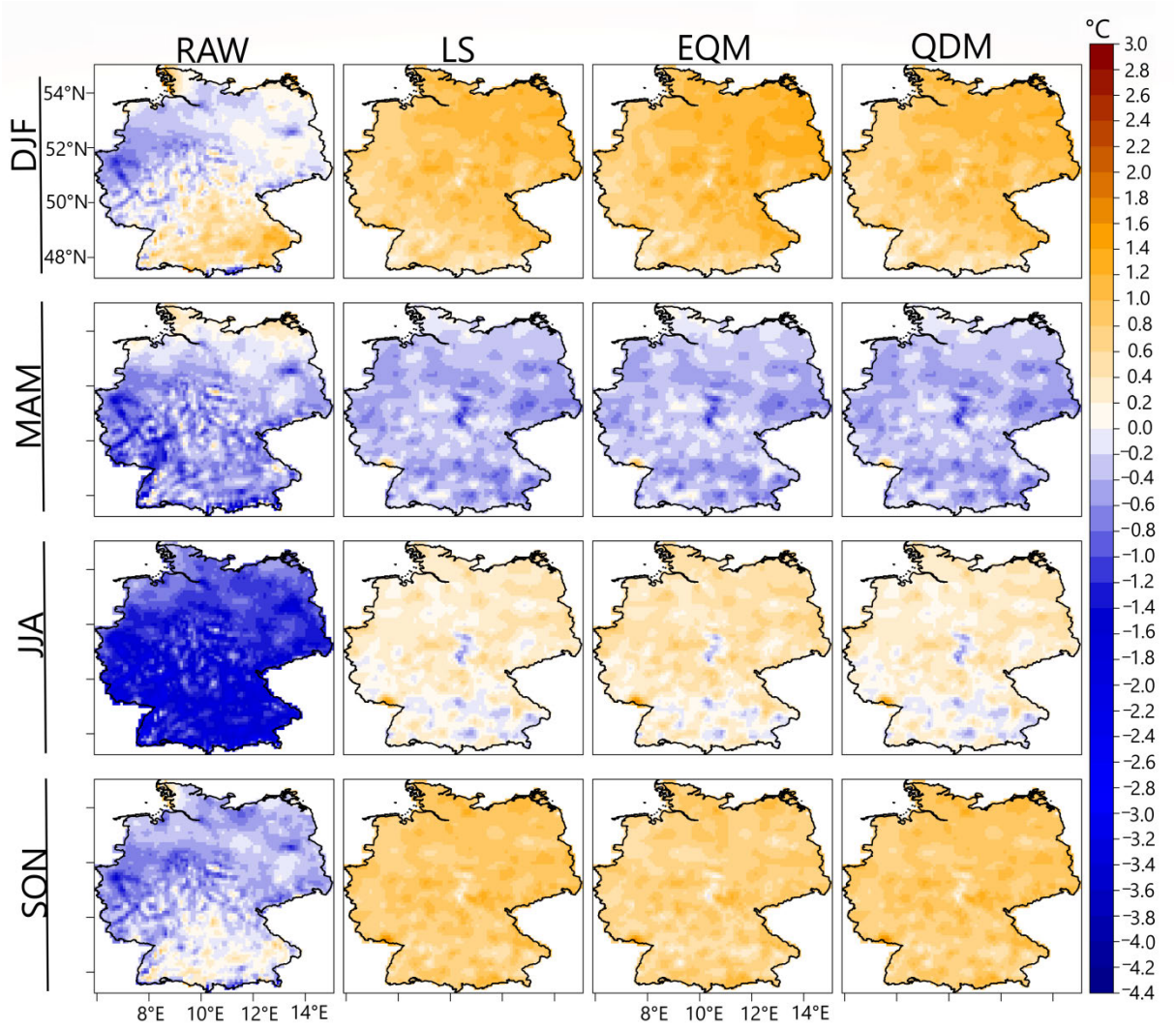

Figure A10: Validation of the added value of the bias correction techniques on the spatial mean of daily temperature as simulated in the CCLM4 RCM, driven by MPI-ESM-LR, during the 1978 to 2005 validation period. Biases are computed as the difference between the simulated seasonal mean temperature and the observed seasonal mean temperature (RCM minus E-OBS)

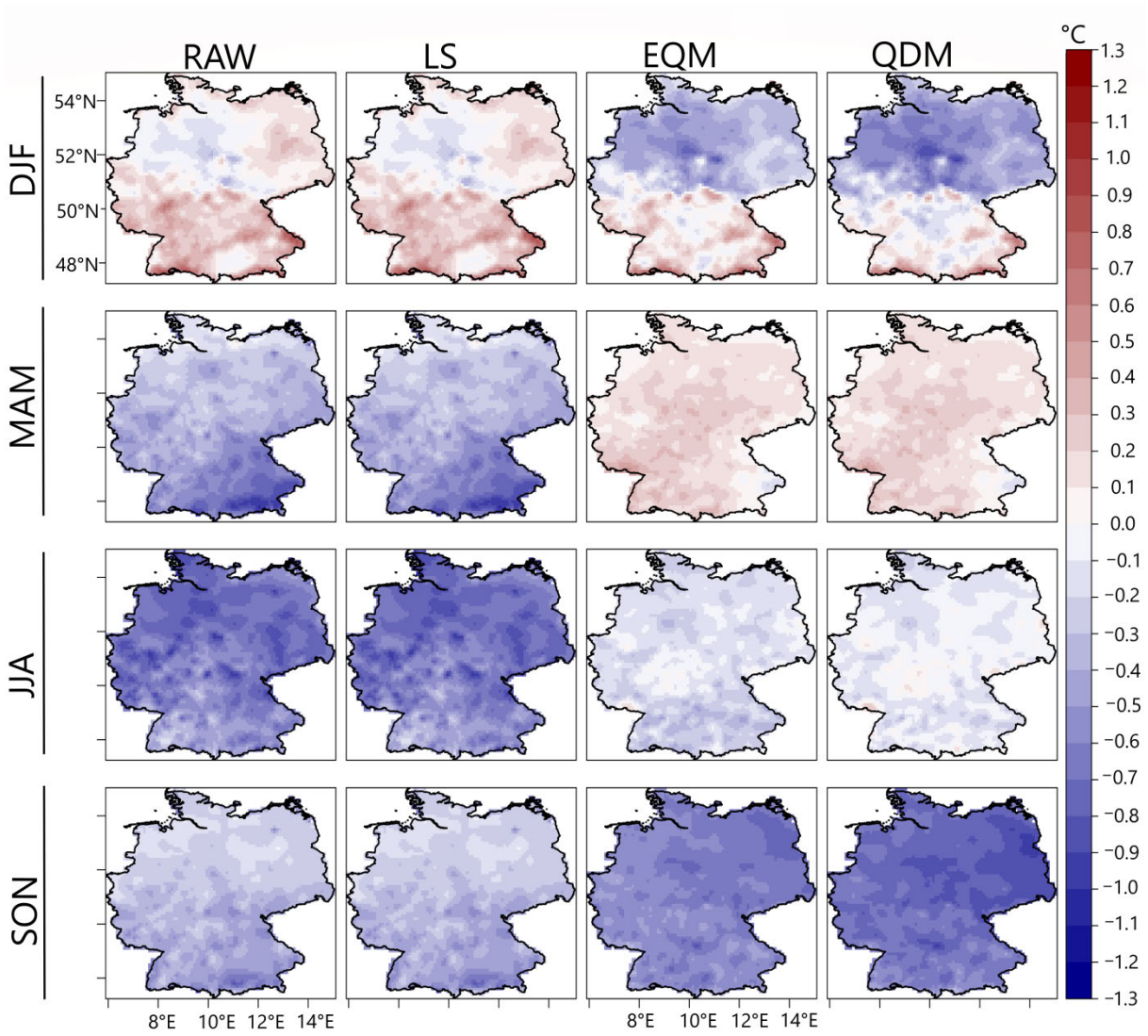

Figure A11: Validation of the added value of the bias correction techniques on the spatial standard deviation of daily temperature as simulated in the CCLM4 RCM, driven by MPI-ESM-LR, during the 1978 to 2005 validation period. Biases are computed as the difference between the simulated standard deviation of temperature and the observed standard deviation of temperature (RCM minus E-OBS)

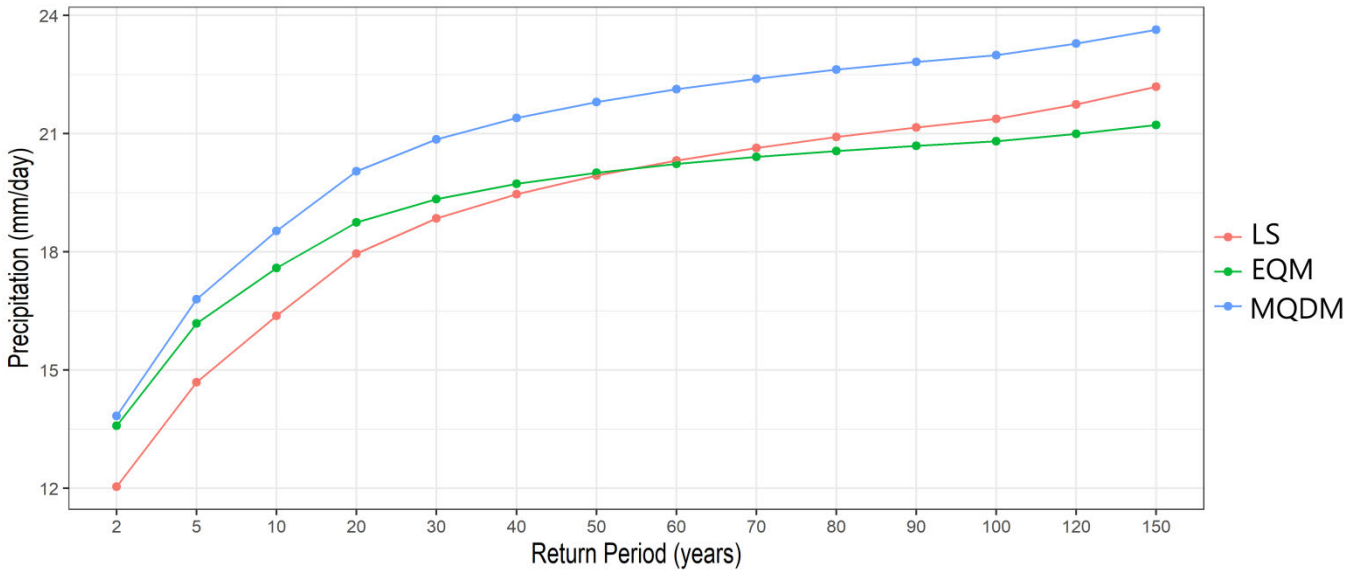

Figure A12: Return level plot of daily precipitation averaged over Germany under the RCP8.5 scenario (2070-2100). The precipitation values are from BC outputs using LS; EQM and MQDM techniques.

Acknowledgment

The study has been funded by the RegIKlim project of the German Ministry of Education and Research under grant 01LR2002D. I thank my parents, my wife and my siblings for the support, encouragement, and prayers. I thank my mentors, Prof. Heiko Paeth, Prof. Barbara Sponholz, and Prof. Hartwig Frimmel for their mentorship. Most important, I am very thankful to Jesus Christ, for HIS constant inspiration, guidance, and leadership in my academic life and beyond.

Eidesstattliche Erklärung

Hiermit erkläre ich an Eides statt, die Dissertation eigenständig, d.h. insbesondere selbständig und ohne Hilfe eines kommerziellen Promotionsberaters, angefertigt und keine anderen als die von mir angegebenen Quellen und Hilfsmittel verwendet zu haben.

Ich erkläre außerdem, dass die Dissertation weder in gleicher noch in ähnlicher Form bereits in einem anderen Prüfungsverfahren vorgelegen hat.

Würzburg, 07-03-2023

Ort, Datum Unterschrift